INTERNATIONAL COUNCIL FOR SCIENCE

INTERGOVERNMENTAL OCEANOGRAPHIC COMMISSION

WORLD METEOROLOGICAL ORGANIZATION

**WORLD CLIMATE RESEARCH PROGRAMME**

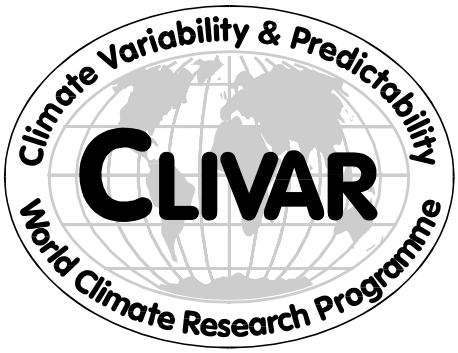


# JSC/CLIVAR Workshop on Decadal Predictability

**Scripps Institution of Oceanography**
**La Jolla, CA, USA**
**October 4-6, 2000**

March 2001

**WCRP Informal Report No 1/2001**
ICPO No. 39

CLIVAR is a component of the World Climate Research Programme (WCRP), which was established by WMO and ICSU, and is carried out in association with IOC and SCOR. The scientific planning and development of CLIVAR is under the guidance of the JSC Scientific Steering Group for CLIVAR assisted by the CLIVAR International Project Office. The Joint Scientific Committee (JSC) is the main body of WMO-ICSU-IOC formulating overall WCRP scientific concepts.

Bibliographic Citation

INTERNATIONAL CLIVAR PROJECT OFFICE, 2001: JSC/CLIVAR Workshop on Decadal Predictability, October 2000. International CLIVAR Project Office, CLIVAR Publication Series No. 39. (Unpublished manuscript).

# TABLE OF CONTENTS

# Workshop on Decadal Climate Predictability

# Executive Summary

## Scripps Institution of Oceanography, La Jolla, CA, USA, 4-6 October 2000

**George Boer**
**Canadian Centre f. Climate Modelling & Analysis, University of Victoria**
**Victoria, Canada**
**George.Boer@ec.gc.ca**

**Mojib Latif, Max-Planck-Institute for Meteorology, Hamburg, Germany**

**Roger Newson, Joint Planning Staff for WCRP, WMO, Geneva, Switzerland**

The joint WGCM/WGSIP Workshop on Decadal Climate Predictability took place at the Scripps Institution of Oceanography, La Jolla, CA, USA, from 4-6 October 2000. There were over 30 participants from 18 different scientific institutions, groups and organizations. The objective of the workshop was to form an overall sense of the "state of the art" in decadal predictability. Since this area of study is in its infancy, the intent was a true "workshop" which would explore observed and simulated decadal variability, decadal predictability, and such practical attempts to produce decadal forecasts as were available. The Workshop was organized into a series of presentations in these broad areas followed, on the final morning, by three break-out working groups. The groups summarised the status of observations and observed variability, simulations and simulated variability, and prediction/predictability and made recommendations and suggestions.

Most presentations on observations and simulations focused on interdecadal variability in the Pacific and North Atlantic. Several talks highlighted the multi-decadal variability in the Atlantic Ocean. This type of variability has typical time scales of 60-80 years, and it can be described from direct temperature observations and from indirect data for the last millennium. The multi-decadal variability involves an interhemispheric dipole in the Atlantic sea surface temperature, and there is some evidence that it may be predictable several years in advance, based on a perfect-model predictability study made with a coupled ocean-atmosphere general circulation model. Other regions of relatively high "potential" decadal predictability, identified in the control runs of 11 coupled models in the CMIP1 database, are the North Pacific, the tropical Pacific and the Southern Ocean. Decadal predictability of surface temperature over land appears to be very modest in these results.

In sum, the workshop considered long time-scale phenomena in the coupled system and the evidence for decadal predictability. There was some indication of predictability, mainly at higher latitudes and associated with long timescales in the ocean, obtained from prognostic perfect model and diagnostic potential predictability studies. The utility and practical achievement of decadal forecasts, nevertheless remains an open question which requires directed attention and active research.

### Observations and simulations of decadal variability

Considerable attention was paid to the North Atlantic Oscillation, although no clear consensus emerged as to its preferred time-scale. To first order, it appears that the atmosphere forces the sea surface temperature via heat fluxes and Ekman currents. A secondary effect is due to changes in the Atlantic gyre or thermohaline circulations responsible for anomalies. As well as uncertainties in the underlying mechanism for the North Atlantic Oscillation, simulations of response/feedback to the associated sea surface temperature anomalies differed among models.

The understanding of the North Pacific Oscillation (or Interdecadal Pacific Oscillation), is also comparatively rudimentary, although there has recently been progress in modelling decadal changes in the North Pacific. In the tropical Pacific, coupling to mid-latitudes does not appear to explain much of the variance (temperature/salinity anomalies may be the key, but these anomalies are small). The role of the Southern Hemisphere oceans, if any, is unknown. Decadal variability could also not be clearly separated from global warming which might itself be responsible for some decadal variability. How global warming might interact with "natural" decadal variability is not yet clear.

As a basis for further progress, much longer time series of data and model runs were seen as essential (i.e. from reanalyses, paleoclimatic data, and extended coupled model integrations). The requirement was also expressed for a multi-decadal ocean and/or coupled ocean/atmosphere reanalysis for hypothesis testing, for initialising simulations and decadal forecasts.

**Predictability and prediction**

Some predictability at decadal timescales of the ocean circulation at higher latitudes (particularly the thermohaline circulation) was inferred from potential predictability studies and perfect model experiments. Associated variations over land might be predictable also, but only explain a small fraction of the total variance. In the tropical Pacific, some weak evidence of decadal predictability was noted. The question of how decadal and interannual variability interact is unanswered. There are large areas where there is yet no firm understanding, namely those concerning the tropical Atlantic dipole, the Interdecadal Pacific Oscillation, and the North Atlantic and the predictability of the North Atlantic Oscillation.

There was some consensus that the thermohaline circulation may be predictable at decadal time scales provided that initial oceanic conditions could be satisfactorily specified. However, the impact of the North Atlantic Oscillation on the export of freshwater from the Arctic remained to be clarified. Improved simulations of overflows and deep (ocean) convection which affect temperature/salinity locally were also needed. The interaction between ENSO variability on decadal timescales and the thermohaline circulation was not well understood. A pioneering attempt at practical decadal forecasting (by the Hadley Centre) is underway but has achieved only modest results to date.

**Future directions**

It was considered that a vital step in making progress from the current rather elementary position was work on understanding the mechanisms that might underlie predictability (including the study of particular modes). The understanding of the dynamics involved in these mechanisms is limited. Time-scale interactions (e.g. the Interdecadal Pacific Oscillation with ENSO) also needs study.

The possibility of a "Historical Decadal Forecast Project" was raised, which would include efforts toward an improved understanding of mechanisms, use of initial conditions from atmospheric and oceanic reanalyses (based on data from merging all available observations and model simulations), model development (in particular sub-grid scale ocean features such as overflow, convection), and ensemble approaches (forecasts from sequential analyses and from different models, estimates of skill, statistical treatments, probabilistic forecasts). Other areas where work was needed was better international co-ordination of ocean analysis as a basis for initializing decadal forecasts (including quality control of data, obtaining more salinity observations), and the study of the relative roles of sea surface temperature, sea-ice, vegetation cover, and external effects. Another useful step would be to begin to document the potential societal impact of decadal predictions.

# Appendix 1: List of participants

**Mathew Barlow**
IRI International Research Institute
Lamont-Doherty Geological Observatory of Columbia University
Route 9W
Palisades, NY 10964
U. S. A.
email: mattb@iri.ldeo.columbia.edu

**George J. Boer**
Canadian Centre for Climate Modelling and Analysis
Atmospheric Environment Service
University of Victoria
P.O. Box 1700
Victoria, B.C. V8W 2Y2
Canada
email: George.Boer@ec.gc.ca

**Li Chongyin**
LASG, Institute of Atmospheric Physics
Chinese Academy of Sciences
P.O.Box 2718
Beijing 10080
China
email: lasgsgi4@iap.ac.cn

**Kim Cobb**
University of California
Scripps Institution of Oceanography
9500 Gilman Drive
La Jolla, CA 92093-0236
U.S.A.
email: kcobb@ucsd.edu

**Arnaud Czaja**
Massachusetts Institute of Technology
Department of Earth, Atmospheric, and Planetary Sciences
77 Massachusetts Avenue
Cambridge, MA 02139-4307
U.S.A.
email: czaja@ocean.mit.edu

**Gidon Eshel**
University of Chicago
Dept. of Geophysical Sciences
Ellis Avenue
Chicago, IL 60637
U. S. A.
email: geshel@uchicago.edu

**Chris Folland**
Meteorological Office, Hadley Centre for Climate Prediction and Research
London Road
Bracknell, Berkshire RG12 2SY
U.K.
email: cfolland@meto.gov.uk

**Stephen Griffies**
Princeton University
Geophysical Fluid Laboratory
Route 1, Forrestal Campus
Princeton, New Jersey 08542
U.S.A.
email: smg@gfdl.gov

**Mojib Latif**
Max-Planck-Institut für Meteorologie
Bundesstraße 55
20146 Hamburg
Germany
email: latif@dkrz.de

**Carine Laurent**
Laboratoire de Météorologie Dynamique du CNRS
UPMC, Tour 25-15, 5e etage, Boite 99
4, place Jussieu
F-75252 Paris, Cedex 05
France
email: claurent@lmd.jussieu.fr

**Peter Lemke**
Universität Kiel
Institut für Meereskunde
Düsternbrooker Weg 20
24105 Kiel
Germany
email: plemke@ifm.uni-kiel.de

**Michael E. Mann**
University of Virginia
Department of Environmental Sciences
Clark Hall
Charlottesville, VA 22903
U.S.A.
email: mann@virginia.edu

**Bryant J. McAvaney**
Bureau of Meteorology Research Centre
G.P.O. Box 1289 K
Melbourne, Victoria 3001
Australia
email: b.mcavaney@bon.gov.au

**Gerald A. Meehl**
National Center for Atmospheric Research
Climate&Global Change Division
P.O. Box 3000
Boulder, CO. 80307-3000
U.S.A.
email: meehl@ncar.ucar.edu

**Vikram M. Mehta**
NASA/NASA-Univ. of Maryland Joint Center for Earth System Science
Department of Meteorology
College Park, Maryland 20742
U.S.A.
email: mehta@climate.gsfc.nasa.gov

**Arthur J. Miller**
University of California, San Diego
Scripps Institution of Oceanography
9500 Gilman Drive
La Jolla, CA 92093-0224
U.S.A.
email: ajmiller@jedac.ucsd.edu

**Roger Newson**
World Meteorological Organization
WCRP
C.P. 2300
CH-1211 Geneva 2
Switzerland
email: newson_r@gateway.wmo.ch

**David Pierce**
Scripps Institution of Oceanography
University of California, San Diego
0224 9500 Gilman Dr.
La Jolla, CA 92093-0224
U. S. A.
email: dpierce@ucsd.edu

**Scott B. Power**
Bureau of Meteorology Research Centre
G.P.O. Box 1289 K
Melbourne, Victoria 3001
Australia
email: sbp@bom.gov.au

**Mark J. Rodwell**
Hadley Center for Climate Prediction and Research
Meteorological Office
London Road
Bracknell, Berkshire, RG12 2SY
U.K.
email: mjrodwell@meto.gov.uk

**R.A. Schiffer**
NASA Headquarters, Code Y
300 E Street, SW
Washington, DC 20456
U.S.A.
email: rschiffer@mtpe.hq.nasa.gov

**Niklas Schneider**
Scripps Institution of Oceanography
University of California, San Diego
0224 9500 Gilman Dr.
La Jolla, CA 92093-0224
U. S. A.
email: nschneider@ucsd.edu oder
niklas@moana.ucsd.edu

**Neville Smith**
Bureau of Meteorology Research Centre
P.O. Box 1289 K
Melbourne, Vic. 3001
Australia
email: nrs@bom.gov.au oder

**Ronald J. Stouffer**
Princeton University
Geophysical Fluid Laboratory/NOAA
Room 232
P.O. Box 308
Princeton, N.J. 08542
U.S.A.
email: rjs@gfdl.gov

**Geoffrey K. Vallis**
Princeton University
AOS/GFDL
Princeton, NJ 08544
USA
email: gkv@princeton.edu

Masahiro Watanabe
University of Tokyo
Center for Climate System Research (CCSR)
4-6-1 Komaba, Meguro-ku
Tokyo, 153-8904
Japan
email: hiro@ccsr.u-tokyo.ac.jp

**Tamaki Yasuda**
The Meteorological Research Institute
Climate Research Department
1-1, Nagamine, Tsukuba
Ibaraki 305-0052
Japan
email: tyasuda@mri-jma.go.jp

# Appendix 2: Extended Abstracts

## Characteristic Spatial and Temporal Structures of Pacific Sea Surface Temperature

**Mathew Barlow**
**IRI at LDEO, Columbia University, Palisades, NY, USA**
**mattb@iri.ldeo.columbia.edu**

### 1. Spatial patterns

The Pacific appears to have characteristic spatial patterns that occasionally show a strong influence in sea surface temperature (SST) anomalies for several years at a time. A well known example is the spatial pattern associated with the climate „transition“ of 1976/77 (Fig. 1a), frequently identified as a realization of the „Pacific Decadal Oscillation“ (PDO). The period from 1962 to 1966 (a time of severe drought in the northeastern U.S.) was also characterized by a stable pattern, but local to the North Pacific (Fig. 1b). Low frequency variability of the cold tongue region, with some similarity to the El Niño- Southern Oscillation (ENSO), has also been noted (Fig. 1c). In addition to the eastern equatorial centre of ENSO, two additional areas appear to be centres of action (noted by asterisks in the panels of Fig. 1): the central North Pacific and the subtropical eastern Pacific. An examination of the standard deviation of monthly SSTs (Fig. 1d) shows that these two regions are local maxima of variance (and of SST gradient, not shown). Rotated principal component analysis (RPCA) of monthly SSTs yields the basin-wide "PDO" pattern as the second mode (Fig. 1e), behind ENSO, and the North Pacific pattern as the third mode (Fig. 1f). Aside from some high frequency noise, the RPCA time series are virtually identical to the raw time series at the respective centres of action. The regressions to these unprocessed time series are shown in Figs. 1g and 1h.

*In summary, the two patterns appear to be robust and of consequence, as they 1. occasionally dominate the SST anomalies for multi-year periods, 2. are the 2nd and 3rd leading modes of RPC analysis, 3. may be regressed directly from the raw data, and 4. are physically related to the climatological distribution of variance.*

### 2. Contribution to patterns from different frequencies

Although the multi-year averages demonstrate a strong low frequency component to these modes, the details of spatial pattern and time evolution have varied considerably between studies. Here, the RPCA time series are used to analyse the time evolution; using the raw time series from the respective centres of action yields nearly identical results. The global relationship for the PDO-type pattern (RPC 2) is shown in Fig. 2a, with the contributions from 2mo-1yr periodicities shown in Fig. 2b, from 8-12yr in Fig. 2c, and 15-25yr in Fig. 2d. The same frequency breakdown is shown for the North Pacific pattern (RPC 3) in Figs. 2e-h.

*For both modes, the high (sub-annual) and low (decadal) frequency parts of the pattern look quite similar in the North Pacific, while differing greatly throughout the rest of the domain.*

### 3. Power spectrum of the PDO

The power spectrum for RPC 2 ("PDO") is shown in Fig. 3a, with the 95% confidence limit from an auto-regressive lag-1 process with the same lag as the RPC shown for reference. *There are two notable low frequency peaks, at ~11yr and ~22yr; these peaks are also present in the spectrum of the raw time series from (125$^o$W, 20$^o$N) (Fig. 3b).* The North Pacific mode also has a spectral peak at ~22yr, but it is less pronounced.

# FIGURE 1: TWO DOMINANT PATTERNS OF VARIABILITY

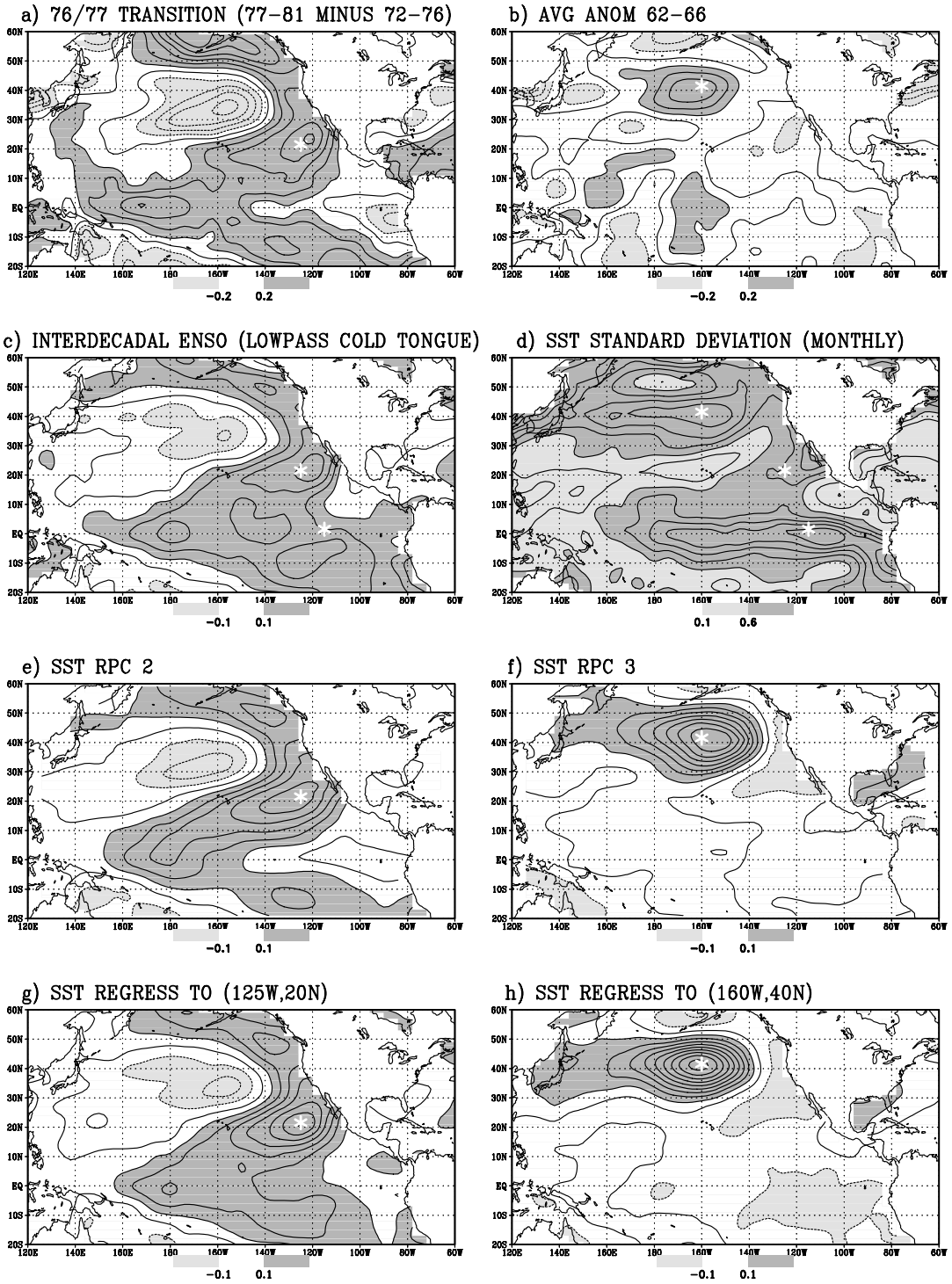


**4. Time evolution of 15-25yr band**

Although the instantaneous spatial pattern for the PDO looks similar at ~11yr (Fig. 2c) and ~22yr (Fig. 2d), the spatial evolution is dramatically different: *the 15-25yr band of the PDO is in quadrature with the 15-25yr band of the North Pacific mode (Fig. 4a)*. The spatial evolution from the PDO to the North Pacific mode is shown in Fig. 4b; the basic aspects of this evolution are observed in the 1976/77 climate transition (in 3yr averages).

# FIGURE 2: PATTERNS IN DIFFERENT FREQ. REGIMES

## RPC 2 – "PDO"

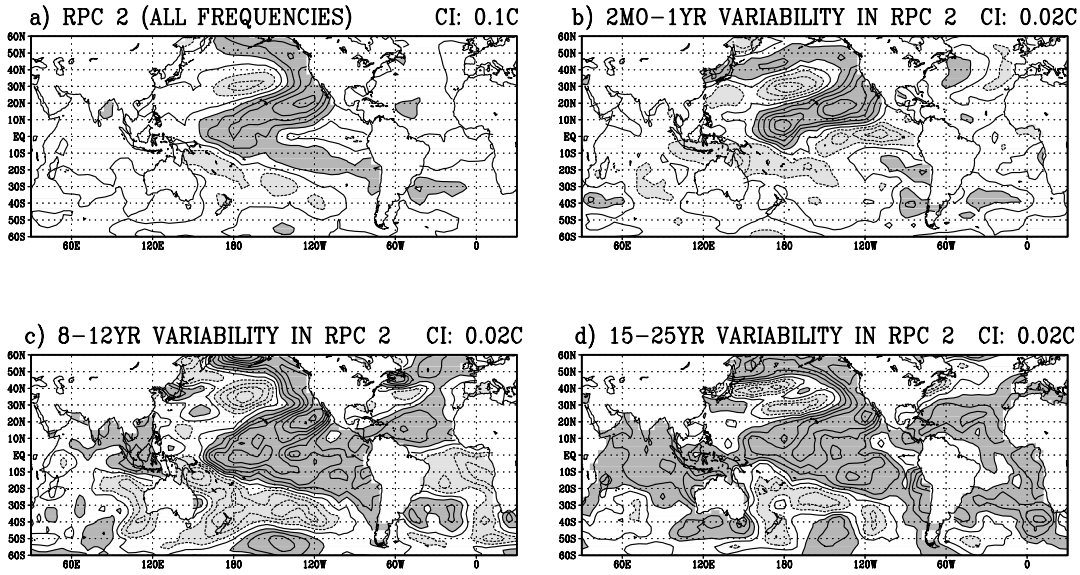


## RPC 3 – "NP"

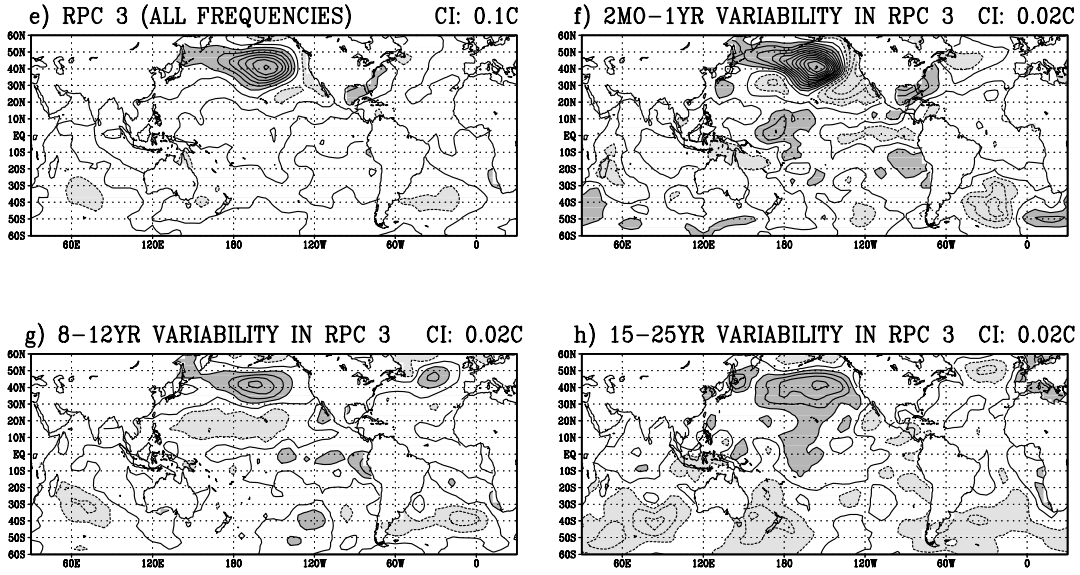


More speculatively, there also appears to be a relationship at the 15- 25yr time scale with polar sea level pressure in a pattern somewhat similar to the Arctic Oscillation. Fig. 4c shows the 15-25yr band of the North Pacific time series and the 15-25yr band of the AO.

# FIGURE 3: POWER SPECTRUM OF PDO

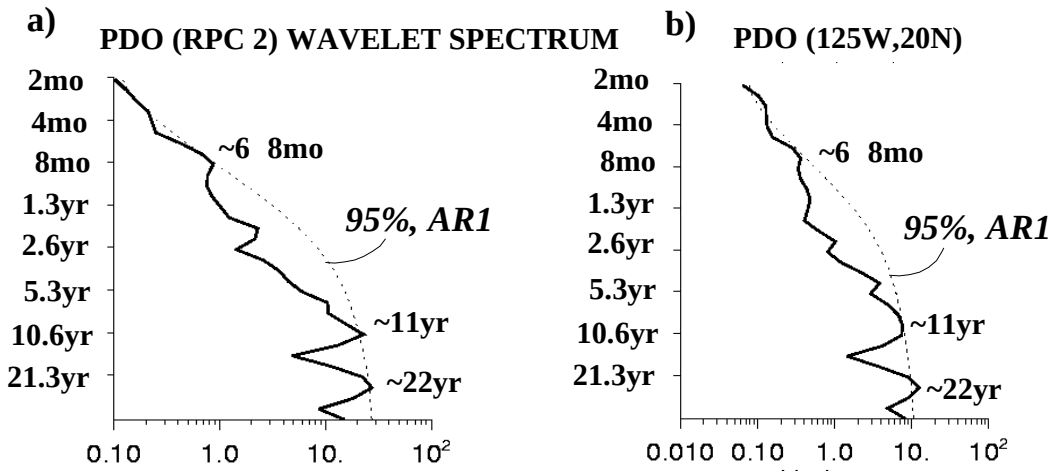


# FIGURE 4: TIME EVOLUTION AT ~22YR

**a) 15-25yr PDO (solid and NP (dashed), 1900-1991**

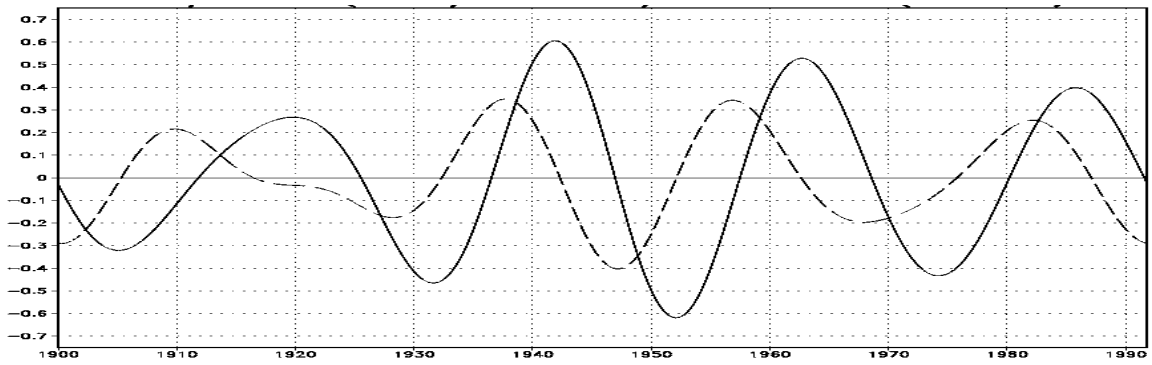


**b) Ω Cycle of 15-25 yr PDO NP Evolution (1945-1993 data)**

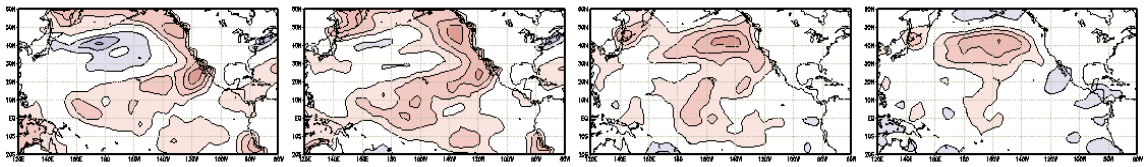

**c)15-25yr Trenberth AO (solid) and NP (dashed)**

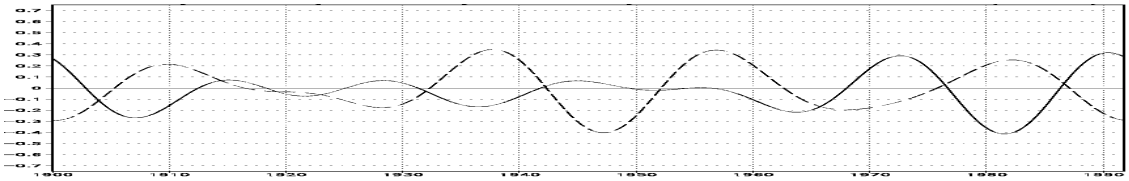

# Diagnostic and prognostic decadal predictability

**George J. Boer**
**Canadian Centre f. Climate Modelling & Analysis, University of Victoria**
**Victoria, Canada**
**George.Boer@ec.gc.ca**

## Introduction

Predictability is an attribute of a physical system which indicates the rate at which two initially close states separate with time. This rate limits attainable forecast skill in the presence of error. The prognostic "perfect model" approach estimates the decadal predictability of the climate system by calculating the rate of separation of a set of coupled model simulations. The diagnostic "potential predictability" approach is rather different. The control simulations of coupled models are analyzed for evidence that the long times-cale variability they exhibit represents a "signal" which is assumed to be predictable given enough information.

## Perfect model predictability

The "perfect model" calculation is based on three independent simulations with the CCCma coupled GCM (Flato et al., 2000, Boer et al., 2000a, b, c). The simulations are initialized with the same three-dimensional oceanic state but with independent 1 January atmospheric states. The analysis is confined to surface air temperature (SAT) as the primary climatological variable. The "rate of separation" of solutions is obtained from the average squared difference

$$\overline{d^2(\tau)} = \overline{(y_i(\tau) - y_j(\tau))^2}$$

between all pairs *(i, j)* of simulations.
The scaled quantity ,

$$f(\tau) = (\overline{d^2}/(2\sigma^2)) = (1 - p(\tau))$$

where $\sigma^2$ is the variance obtained from the control run, gives a suitable measure of the "predictability" *p*. For presentation purposes, the cumulative scaled predictability

$$\tilde{p} = 1 - \tilde{f} = 1 - \left( \frac{1}{\tau} \cdot \int_0^{\tau} f(\tau')d\tau' \right)$$

is used to average over the forecast range. The top panel of the accompanying Figure displays the geographical distribution of cumulative predictability for annual mean SAT at year 10. Values for which $p > 0.4$ are shaded. There is an indication of predictability for the southern ocean and, to a somewhat lesser extent, the northern oceans. Patchy values are seen also for the tropical Atlantic and Pacific.

## Potential predictability

Potential predictability is a measure of the variability of the system which attempts to quantify the fraction of long timescale variability that may be distinguished from the natural variability noise. This "signal", if it exists and is of appreciable magnitude, is deemed to arise from physical processes operating in the system which are, at lease potentially, predictable. The statistical approach generally follows Rowell (1998), and Rowell and Zwiers (1999) and assumes SAT variation is of the form $T_{\alpha\beta} = \mu + s_\alpha + \varepsilon_{\alpha\beta}$ with $\mu$ the climate mean, $s_\alpha$ the slow timescale "signal" component of the variability, and $\varepsilon_{\alpha\beta}$ the remaining unpredictable climate noise. The ratio $\rho = \sigma^2/(\sigma_s^2+\sigma_e^2)$ gives the fraction of the total variance associated with the "potentially predictable" component. The value is tested against the null hypothesis that $\rho = \sigma_s^2 = 0$.

The result is shown in the bottom panel of the Figure. The result does not depend on a single model or simulation but is an ensemble estimate of the potential predictability of the coupled system based on the control simulations of eleven models participating in the Coupled Model Intercomparison Project (CMIP is described briefly in Meehl et al., 1997). The high latitude oceans are the dominant regions exhibiting potential predictability although there is some indication also in the tropical Pacific.

**Discussion**

The decadal predictability of the coupled atmosphere/ocean/ice system is examined using both prognostic "perfect model" and diagnostic "potential predictability" approaches. Both approaches give some evidence of long timescale predictability at high latitudes over oceans and, to a lesser degree, in the tropical Atlantic and Pacific. Decadal predictability over land and sea-ice is generally low. Both predictability approaches have their weak-nesses; the potential predictability approach does not directly denote actual predictability and the prefect model approach may suffer from model imperfections and the smallness of the ensemble of simulations. The results direct attention to the high latitude oceans as the apparent seat of the dominant mechanisms determining decadal predictability.

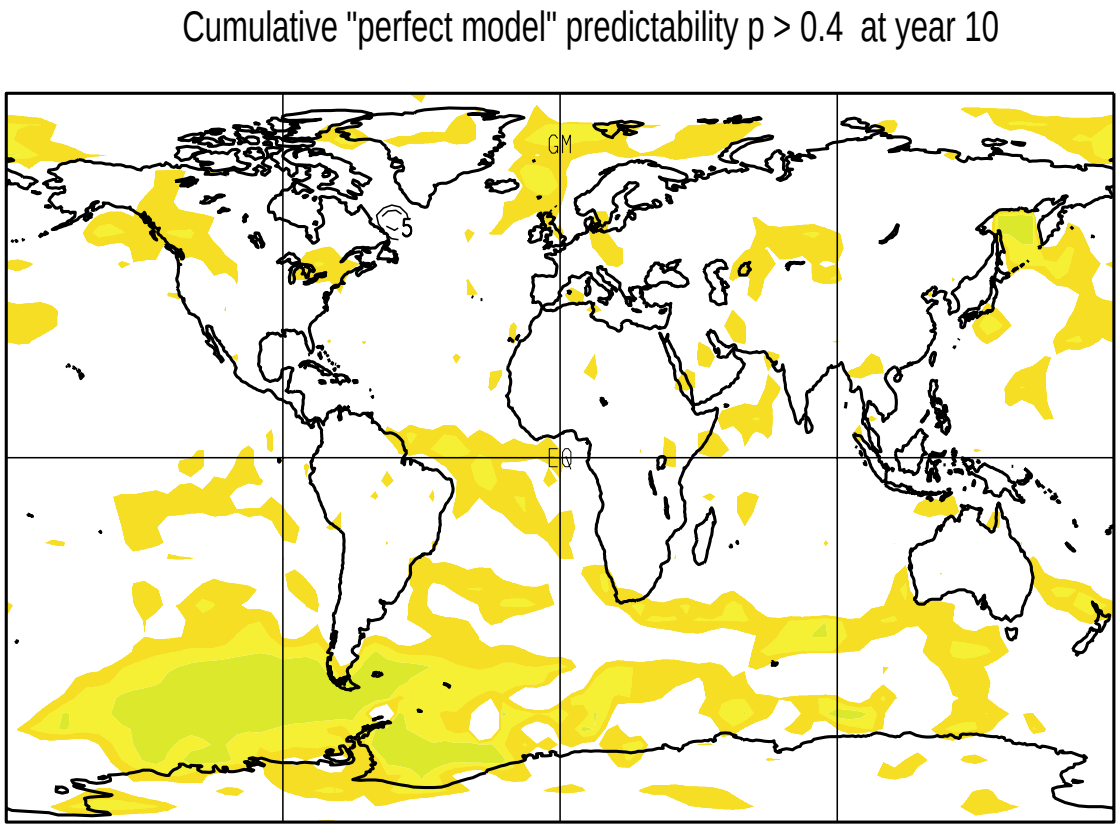

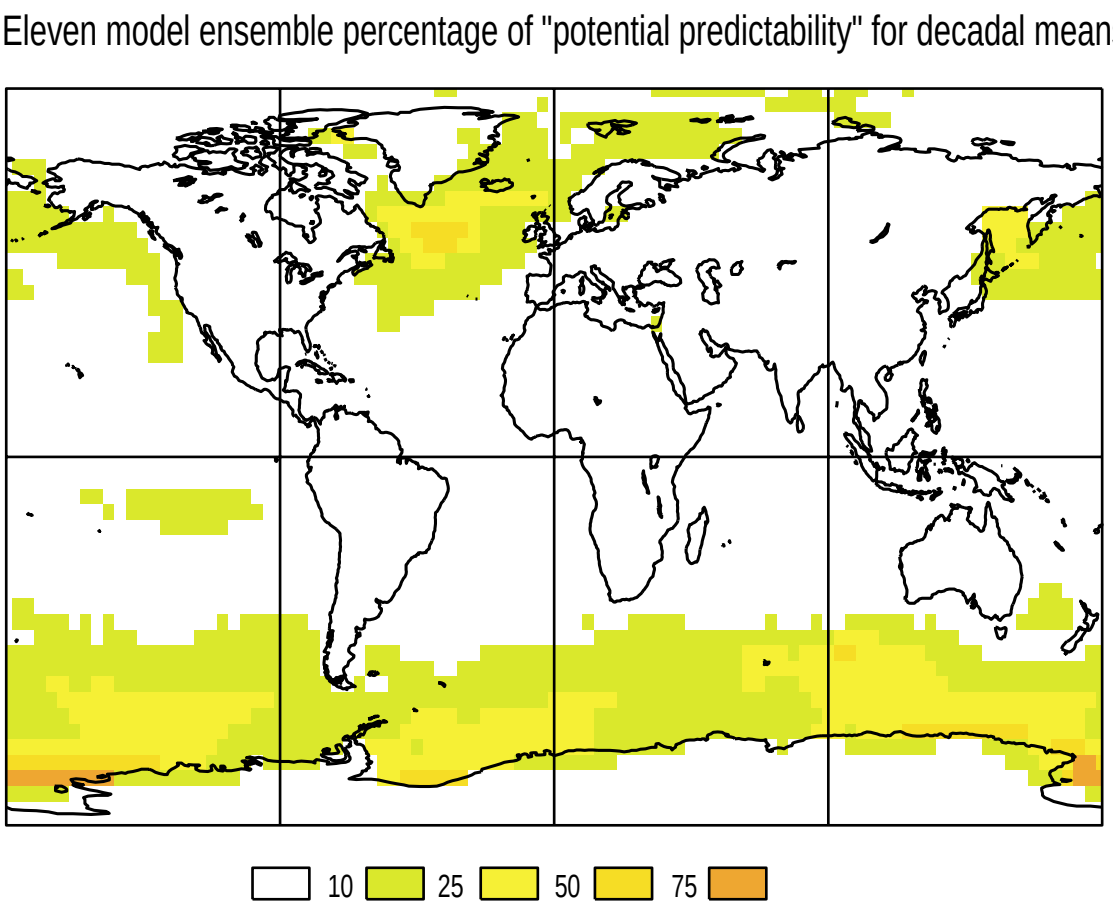


**References**

Boer, G.J., G. Flato, M.C. Reader, and D. Ramsden, 2000a: A transient climate change simulation with greenhouse gas and aerosol forcing: experimental design and comparison with the instrumental record for the 20th century. *Climate Dynamics*, **16**, 405-425.

Boer, G.J., G. Flato, and D. Ramsden, 2000b: A transient climate change simulation with greenhouse gas and aerosol forcing: projected climate for the 21th century. *Climate Dynamics*, **16**, 427-450.

Boer, G.J., 2000c: A study of atmosphere-ocean predictability on long timescales. *Climate Dynamics*, **16**, 469-477.

Flato, G.M., G.J. Boer, W. Lee, N. McFarlane, D. Ramsden, and A.Weaver, 2000: The CCCma global coupled model and its climate. *Climate Dynamics*, **16**, 451-467.

Meehl, G.A., G.J. Boer, C. Covey, M. Latif, and R.J. Stouffer, 1997: Intercomparison makes for a better climate model. *EOS*, **78**, 445-451.

Rowell, D., 1998: Assessing potential seasonal predictability with an ensemble of multidecadal GCM simulations. *J. Climate*, **11**, 109-120.

Rowell, D., and F. Zwiers, 1999: The global distribution of sources of atmospheric decadal variability and mechanisms over the tropical Pacific and southern North America. *Climate Dynamics*, **15**, 751-772.

# Atmospheric Circulation Anomalies and Inter-decadal Climate Variation in China

**Li Chongyin and Mu Mingquan**
**LASG, Institute of Atmospheric Physics, CAS, Beijing, China**
**lcy@lasgsgi4.iap.ac.cn**

## 1. Inter-decadal Climate Variation in China

The climate jump in the 1960's has been indicated in some studies and it was only one climate jump event represented completely by observational data until now (Yamamoti, 1986; Yan, et al., 1990; Wang, 1990). In fact, the climate jump in the 1960's showed clearly the feature of interdecadal variation of the climate. For this climate jump, many elements, such as precipitation, temperature and surface pressure, all had obvious signal. The sudden variations were all in the period from 1962 to 1967, and a precedent large-scale jump signal occurred at 500 mb height over the mid-latitude Atlantic region in the late of the 1950's (Yan, 1992). In order to understand the climate jump in 1960's, two examples in China can be shown as follows: one is shown by using temporal variation of the summer (June-August) precipitation anomaly (%) in Huabei region. It is very clear that there were mainly positive precipitation anomalies before 1964 but mainly negative precipitation anomalies from and after 1964. An obvious climate jump occurred in 1964 in Huabei region. The averaged summer precipitation changed suddenly from the stage more than normal to the stage less than normal. The second is shown in temporal variation of the surface air temperature anomaly in winter (December-February) in Sichuan province. We can find that the winter temperature in Sichuan was changed into the cold period since 1962 because there were mainly negative temperature anomalies after 1962. Even though positive anomalies during the shorter time were in existence, it still means an obvious climate jump occurred in Sichuan in 1962, and the averaged surface air temperature in winter changed suddenly from warm stage to cold stage. The variation feature of winter temperature in Sichuan is similar with that given in the reference by Wang. Obviously, based on above-mentioned analyses and previous research results, it is very evident that a climate jump occurred in the 1960's and the inter-decadal climate variation in China was demarcated in the 1960's.

## 2. Anomalous Patterns Corresponding to Atmospheric Circulation NAO and NPO

In the study of the decadal climate variation in China we have pointed out that the climate of China occurred two different anomalous situations in the 1950s and 1980s, respectively. In the 1950s, North China had more rain in summer, but less rain in the 1980s. In the 1950s, Sichuan Province was warm slightly in summer, but a bit cold in the 1980s. Relative to such climate features, Western Pacific sub-tropical high moved northwestwards and was stronger than its average state in the 1950s, but it located more east and was weaker in the 1980s. Mean 500 hPa circulation situations of the 1950s (average of 10 years from 1953 to 1962) and the 80s (average of 10 years from 1980 to 1989) have been drawn. There are many similarities in the two pictures, especially, the distribution of the general circulation and the location of troughs and ridges in the west hemisphere, because both of them are results of multi-year average.But we can also find the difference between them. For Example, Western Pacific sub-tropical high located over the more western place in the 1950s than in the 1980s, and East Asian trough was weaker and the upper trough near to Balkhash Lake was stronger in the 1950s than in the 1980s. So we can say that climate characteristics are always related to the atmosphere general circulation patterns, even as to the inter-decadal time-scale climate change, we can also find some information from the activity of the general circulation.

## 3. Numerical Simulations with GCM

In this section, the simulated climate characteristics in the eastern China will be discussed, including air temperature and precipitation. Meanwhile, their similarity and difference to the observation will be analysed further. The interdecadal oscillations, including 10~20 and more than 30 years, are striking in the temporal variation of the seasonal mean air temperature departure in the eastern China ($20^{o}$~$40^{o}$N, $110^{o}$~$120^{o}$E) and the time period cross-section of its wavelet coefficient. There is well positive correlation of the air temperature anomaly in the eastern China with East Asian trough variation. Strong East Asian trough (negative height departure) is corresponding to the low air temperature in the eastern China (negative air temperature), vice versa, the weak trough is accompanied by the high temperature in the eastern China. The two variables' association on the inter-decadal time scale is analogous to that on the weather time scale. So, their physical processes are consistent and apparent. In order to be more clearly reflected the characteristics of the climate inter-decadal variation, the variables will be done with the low pass filter so that the variation below the inter-annual time scale (only containing above 7 years oscillation) is ironed out. The features of the inter-decadal variations are considerably apparent not only in the anomaly of East Asian trough and air temperature in the eastern China but also in that of the precipitation in North China. It is specially noticed that the climate abrupt change in the 1960s has been found in the past investigations (Yan et al., 1990; Li and Li, 1999). It further exhibits that this abrupt also exists in the simulated results. At the same time, the abrupt change of air temperature is parallel to the variation of the geopotential height at 500 hPa. All of these are consistent with the observation very well (Wang et al., 1998). Above all, the AGCM can well simulate not only the interdecadal variation of climate and atmospheric circulation but also their associated component, the climate abrupt change during the 1960s.

## 4. Conclusions

The main purpose of the paper is to analyse the inter-decadal change features of the atmosphere general circulation. Although observational data is not enough but the analyses can clearly show that there is the evident inter-decadal variation exists in the evolution of the general circulation, mainly including the 10-20 and more than 30 years quasi-periodical variations. It shows clearly not only in the main atmospheric oscillations, but also in some important weather and climate systems. The intensity changes of Western Pacific subtropical high, East Asian and North American trough are in phase or out-of-phase some time as to the 10-20 years quasi-periodical. To the more than 30 years quasi-periodical, they show mainly in phase, and West Pacific subtropical high change goes ahead of 5-7 years.Parallel to the inter-decadal variation of atmospheric circulation, climate anomalies in the eastern China, including the abrupt change during the 1960s, are quite well grasped by the simulation of the AGCM too. The numerical experiment with GCM is also a useful approach and technique to investigate the inter-decadal variation of atmospheric circulation and global climate.

## References


Chongyin, L., and L. Guilong, 1999: Variation of the NAO and NPO associated with climate jump in the 1960s. *Chinese Sci. Bull*., **44** , 1983-1987.

Shaowu, W., 1990: The variation tendency of temperature in China and the globe during the last one hundred years (in Chinese). *Meteorology*, **16**, 11-15.

Shaowu, W., et al., 1998: Construction of the near 100 years air temperature in China. *Quart. J. Appl. Meteor.*, **9**, 392-401.

Yamamoto, R., T. Iwashima, and N.K. Sanga, 1986: An analysis of climatic jump. *J. Met. Soc. Japan*, Ser. *II*, **64**, 273-281.

Zhongwei, Y., 1992: A primary analysis of the process of the 1960s northern hemispheric summer climatic jump. *Chinese J. Atmos. Sci.*, **16**, 111-119.

Yan, Z., J. Ji, and D. Ye, 1990: Northern hemispheric summer climatic jump in the 1960's, I: Precipitation and temperature. *Science in China* (B), **No.1**, 97-103.

# Labrador sea convection and the path of the North Atlantic current in a coupled model

**Claire Cooper and Chris Gordon**
**Hadley Centre, Met. Office, Bracknell, UK**
**ccooper@meto.gov.uk**

## Introduction

This paper investigates the existence and causal mechanisms of decadal SST anomalies in the NAC region as simulated in the latest Hadley Centre coupled climate model (HadCM3, Gordon et al., 2000). It is the detailed modelling and understanding of these mechanisms which may, in the future, enable some degree of predictability of natural climate variability. Dickson et al. (1996) have shown that co-ordinated changes, forced by the North Atlantic Oscillation (NAO), have been occurring in the region over the last fifty years. Sutton and Allen (1997) analysed observed wintertime North Atlantic SSTs and calculated lagged correlations over the entire basin with a source region in the vicinity of Cape Hatteras. These indicated that anomalies originating near Florida in the subtropics appear to propagate along the path of the NAC, taking approximately nine years to cross the basin. This is much slower than the advective speed of the NAC.

## Model simulation compared to observations

The control integration of HadCM3 has completed over 1000 years and figure 1 shows the NAOI (Hurrell, 1995) from the coupled model for the first 1000 years of the simulation. Choosing a period of the control in which NAO variability is similar to that in the ocean observed record we have made a comparison with LSW production. As in the observations the NAOI and LSW production indicators show a clear anti-correlation relationship during this period. Therefore in the model, as in the observations, there is a positive correlation between the NAO and Labrador Sea convection. As shown in figure 2, the model also simulates propagating SST anomalies similar to those found in the observational data by Sutton and Allen.

## Labrador Sea Convection Experiments

To investigate the possible links between Labrador Sea convection and SST anomalies in the sub-polar gyre a number of sensitivity studies have been performed with the coupled model. Two experiments were designed in order to assess the effects of enhanced or inhibited convection. In order to force such events we utilised additional strong relaxation on salinity applied only to the small region of the Labrador Sea that is associated with deep convection in the model (58.125-60.625$^{o}$N, 58.75-50$^{o}$W). In the first experiment, denoted CONV, enhanced salinity forcing was applied continually to the forcing region of the Labrador Sea in order to promote deep convection. In the second sensitivity experiment (INHIB) a freshwater forcing was applied to have a stabilising effect on the water column and hence inhibit deep convection. The experiments were run for 14 years.

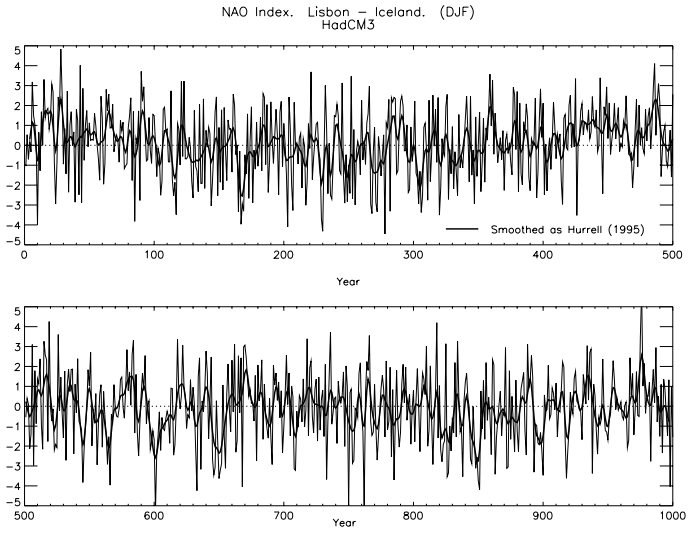


*Figure 1. NAO index for the first 1000 years of the HadCM3 control experiment, calculated using normalised wintertime (DJF) sea level pressure differences between Lisbon (Portugal) and Stykkisholmur (Iceland), defined and smoothed as Hurrell (1995). Heavy line is the smoothed index.*

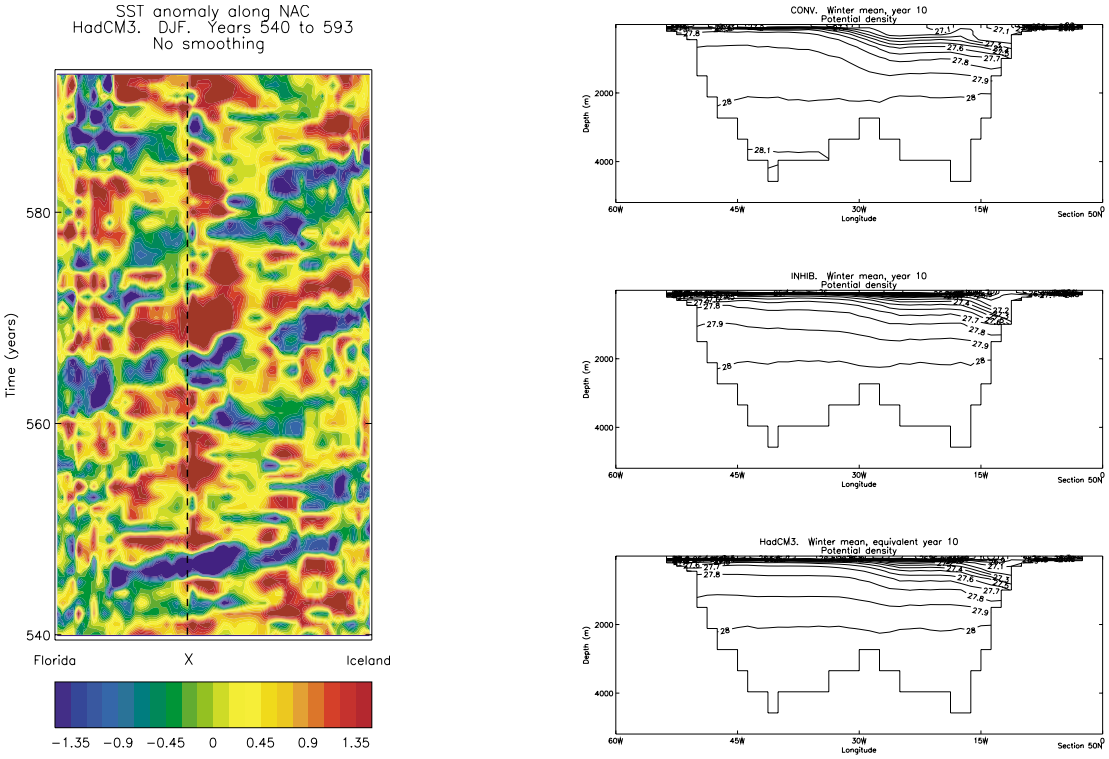


*Figure 2 (left). Model wintertime (DJF) sea surface temperature ($^0$C) anomalies along the mean path of the model North Atlantic current. 'X' marks the region in which the sub-polar and sub-tropical gyres meet (off Newfoundland). No smoothing has been applied.*

*Figure 3 (right). Potential density ($\sigma_0$) cross-section at 50$^0$N. Wintertime mean, year 10 (a) CONV, (b) INHIB and year 10 equivalent (c) HadCM3 control.*

Figure 3 shows annual mean potential density ($\sigma_0$) at year 10 on a cross section at 50$^o$N from the North American coast to the European continent. The increased volume of density class 27.9 to 28.0 in CONV is striking, as is the steepening of the frontal structure at 30$^o$W. There is little change to the structure across the basin in INHIB. This implies that forcing convection has led to a more voluminous water mass (LSW, density 27.9 to 28.0) relative to both the control and the case with inhibited convection. The frontal structure observed at 30$^o$W is associated with the NAC, the steepening of the front being linked with an intensification of the northward component of the current in this location. The development of the 27.9-28.0 water begins on the western side of the basin as a thickening of the layer. The evolution of this feature can be seen in figure 4 a distance-time section of the thickness of the 27.9-28.0 isopycnal layer across 50$^o$N. A thikkening of this layer first appears on the western extreme of the section after approximately four years. This thickening continues and moves eastward until reaching 30$^o$W after a further four years. SST changes at 50$^o$N behave in a similar way to changes in LSW thickness and these changes in SST also propagate eastwards at this latitude. After approximately 3-4 years of convective forcing a large SST anomaly appears to the south of Newfoundland which then propagates north eastwards along the NAC (not shown).

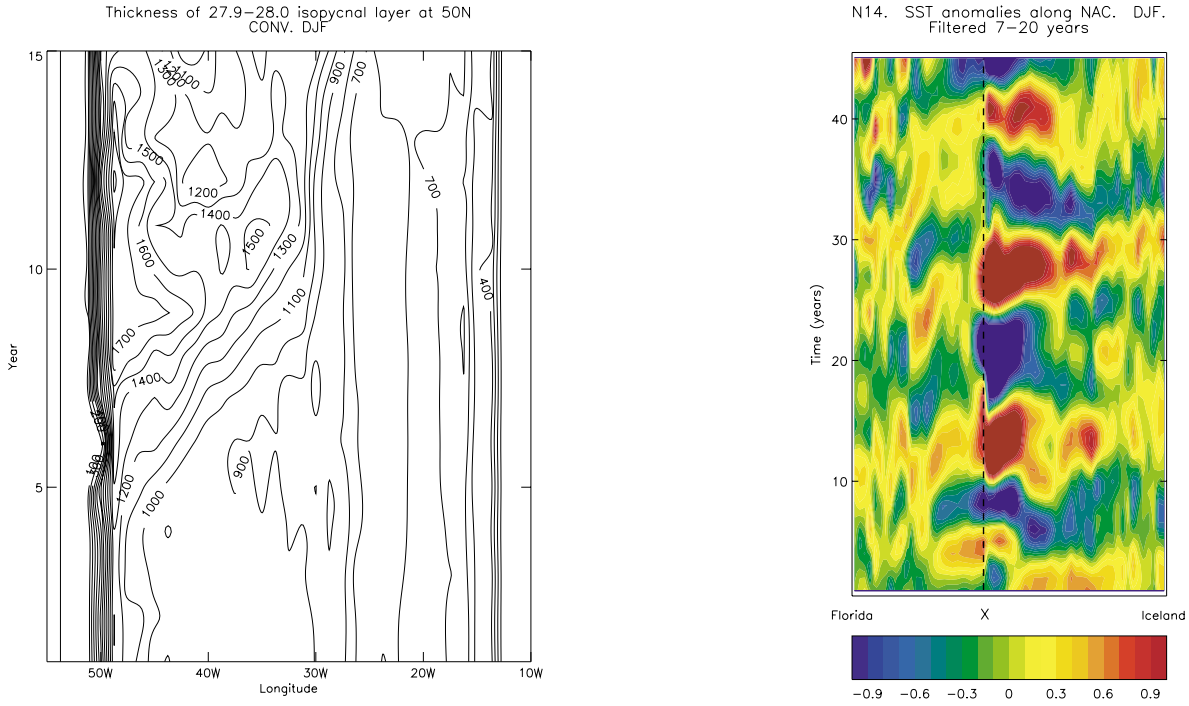


*Figure 4 (left): (a) Thickness of isopycnal layer (27.9<$\sigma_0$<28.0) at 50$^o$N from CONV. Wintertime means (DJF).*

*Figure 5 (right): Cyclic forcing experiment, detrended and filtered (retaining 7-20 years) wintertime SST anomalies ($^0$C) along the mean path of the modelled North Atlantic Current (taken from HadCM3 control). X' marks the region in which the sub-polar and sub-tropical gyres meet (off Newfoundland).*

From the observational record of LSW temperatures there emerges a signal with a period of approximately 14 years, although this is based on a relatively short record which also shows longer timescale variability (Curry et al., 1998). This is indicating an enhancing and then inhibiting of convection in a fourteen-year sequence. In a final sensitivity study we aim to recreate this pattern of forcing in an idealised way. For simplicity we apply sinusoidal fresh water/salt forcing. The range of forcing is such that when it is at a maximum the forcing is the same as in CONV, while at it's minimum the forcing is as in INHIB. In these experiments a cycle time of 14 years was chosen so that the Labrador Sea experiences convection inhibiting conditions for

the first half of thecycle followed by convection enhancing conditions for the later part of the cycle. The experiment was run for 42 years allowing the completion of three cycles. To extract the decadal signal the data have been filtered, removing signals of less than 7 years and greater than 20 years. Figure 5 shows the filtered SST anomalies from this cyclic forcing simulation along the mean pathway of the control NAC. A pulsating 14-year SST anomaly signal is very evident at the point where the NAC turns north. The anomaly then propagates to the east with decreasing amplitude. This experiment gives a clear illustration of how decadal variations of deep convection in the Labrador Sea can lead to corresponding SST variations propagating along the path of the NAC.

**References**


Curry, R., M.S. McCartney and T.M. Joyce, 1998: Oceanic transport of subpolar climate signals to mid depth subtropical waters. *Nature*, **391**, 575-577.

Dickson, R.R., J.R.N. Lazier, J. Meincke, P. Rhines and J. Swift, 1996: Long-term co-ordinated changes in the convective activity of the North Atlantic. *Prog. Oceanogr.*, **38**, 241-295.

Gordon, C., C. Cooper, C.A. Senior, H.T. Banks, J.M. Gregory, T.C. Johns, J.F.B. Mitchell and R.A. Wood, 2000: The simulation of SST, sea ice extents and ocean heat transports in a version of the Hadley Centre coupled model without flux adjustments. *Climate Dynamics*, **16**, 147-168.

Hurrell, J.W., 1995: Decadal trends in the North Atlantic Oscillation: Regional temperatures and precipitation. *Science*, **269**, 676-679.

Sutton, R.T., and M.R. Allen, 1997: Decadal predictability of North Atlantic sea surface temperatures and climate. *Nature*, **388**, 563-567.

# Observations of Atmosphere - Ocean coupling in the North Atlantic

**Arnaud Czaja and John Marshall**
**Department of Earth, Atmospheric, and Planetary Sciences,**
**Massachussets Institute of Technology, Cambridge, MA, USA**
**czaja@ocean.mit.edu**

## 1. Introduction

Deser and Blackmon (1993), on the basis of an Empirical Orthogonal Function (EOF) analysis of surface climate variable in winter (1900-89), have isolated a large - scale SST pattern whose power spectrum shows a broad band peak near the decadal period. The SST pattern shows opposite sign SST anomaly, roughly north and south of the mean position of the separated Gulf Stream, and also extends to the eastern subtropics, such as to form a tripolar SST pattern. The associated surface atmospheric circulation is reminiscent of the North Atlantic Oscillation (hereafter the NAO), and similarly exhibits enhanced power at the decadal period. Although Deser and Blackmon (1993) have suggested that the decadal timescale may be due to changes in the thermohaline oceanic circulation, there is not yet a consensus on the mechanisms governing the low frequency evolution of the SST 'tripole'. Grötzner et al. (1998) have argued that it may reflect an interaction between the NAO and the wind driven ocean circulation, as they found such interactions in a long integration of a coupled Atmosphere - Ocean model. The lack of long observational records of subsurface oceanic data is clearly a limiting factor to evaluate the role of the ocean circulation in the decadal variability seen at the surface. Also, lots of studies lack a theoretical framework to use as a guide in the analysis of the available observations. The interpretation of the results is even made more difficult by the use of complex and elaborate statistical techniques (EOFs, Principal Oscillation Patterns, multivariate frequency domain methods, etc ...).

Here, to explore evidence and possible mechanisms of atmosphere-ocean coupling, we introduce and study a simple SST index $\Delta T$ from a long observational record (1856 - 1998); it measures the strength of the dipole of SST that straddles the Gulf Stream and was chosen because (i) it is a measure of low level baroclinicity to which cyclogenesis at the beginning of the Atlantic storm-track may be sensitive (ii) it may be sensitive to anomalies in ocean heat transport associated with both wind driven gyres and thermohaline circulation. Pronounced decadal signals in $\Delta T$ are found which covary with the strength of sea level pressure (hereafter SLP) anomalies over the Greenland - Iceland Low and subtropical High regions. Using the simple coupled model developed in Marshall et al. (2001), we interpret features of the power spectrum of observed SST and SLP as the signature of coupled interactions between the atmospheric circulation and an anomalous wind driven ocean gyre.

## 2. A cross Gulf Stream SST index

Figure 1 (upper panel) shows the time evolution of the SST index $\Delta T = T_N - T_S$ difference of SST averaged over (60-40$^o$W 40-55$^o$N) and (80-60$^o$W 25-35$^o$N) in late winter February through April), from Kaplan et al. (1997). Typical uctuations of 1 K are found on interannual timescales (blue curve), and are reduced by about a factor two on decadal timescales (green curve, 6 -yr running mean). Using a composite analysis based on yrs when the index is high (denoted by the red stars in Fig. 1, upper panel) and low (blue stars), we investigate the typical evolution of the SST pattern captured by $\Delta T$ once it has been generated (Fig. 1, bottom panel). It is seen that the SST pattern is the tripole (Fig. 1, bottom left panel) and that it shows evidence of a damped oscillatory behaviour. Indeed, if no large scale signal is found three yrs after the

tripole has been generated (Fig. 1, bottom middle panel), the tripole reappears 6 yrs later, but with opposite sign (Fig. 1, bottom right panel).

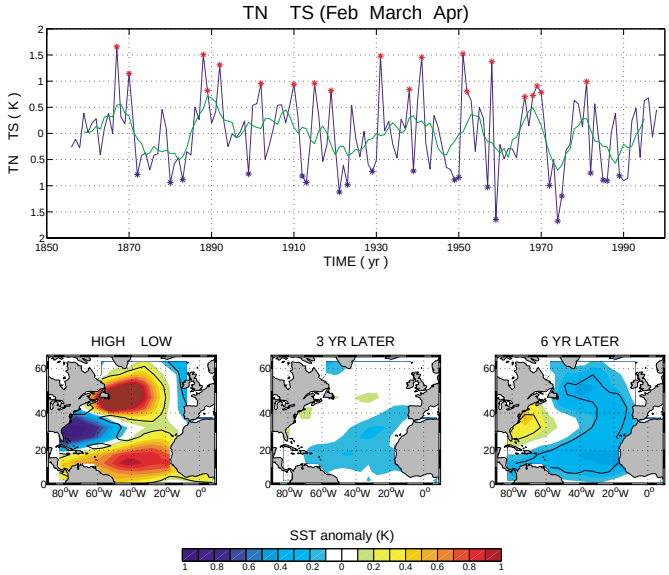


*Figure 1: (Upper panel): timeseries of the SST index $\Delta T = T_N - T_S$. (bottom panel). Composite maps for SST (in K). The black lines indicate the 95% confidence level for the SST composite maps. See text for details.*

Based on a similar composite analysis with the long observational record of SLP by Kaplan etal.(1999), we found that the atmospheric conditions associated simultaneously with $\Delta T$ are reminiscent of the NAO (not shown), although slightly shifted southwestward. They show opposite sign anomalies over the Greenland - Iceland Low (hereafter GIL) and subtropical High (hereafter STH) regions, such that in yrs when SST are warmer north than south of the Gulf stream ($\Delta T > 0$), the surface atmospheric circulation is weakened. We argue in the following that the sign reversal exhibited by the SST tripole after 6 yrs is driven by the delayed adjustment of the wind driven ocean circulation to the NAO surface wind forcing. As shown below, advection can successfully explain the change of sign of SST anomalies near the separated Gulf stream. It is suggested that the sign reversal of subtropical SST is driven locally by turbulent surface heat flux, reflecting the NAO response to changes in $\Delta T$.

### 3. A model for the decadal evolution of ΔT

Using the NCEP - NCAR reanalysis, we have computed the equilibrium response of the ocean circulation to the weakening / strengthening of the surface winds associated with $\Delta T$ anomalies, according to linear at bottom Sverdrup dynamics (Fig. 2). The geostrophic streamfunction consists, following yrs where the winds blow stronger over the ocean (i.e., yrs when $\Delta T < 0$), in an anticyclonic circulation connecting the two boxes used to define $\Delta T$. Following Marshall et al. (2001), we speculate that the path of the separated Gulf stream is anomalously poleward when the gyre circulates anticyclonically, so that the northern box is anomalously warmed and the southern box anomalously cooled. Thus, the wind driven circulation acts to change the sign of an initial $\Delta T$ anomaly. Scaling arguments for the relative magnitude of local surface heat flux (latent+sensible) and advective heat flux due to the anomalous gyre suggest that the two are of same order ($10\ Wm^{-2}$) on decadal time scales (not shown).

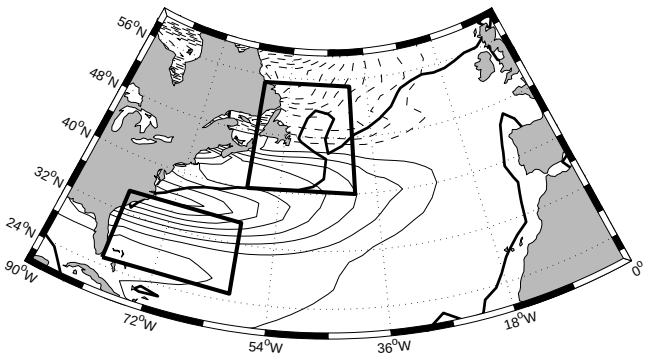

*Figure 2: Anomalous geostrophic transport (contoured every Sv) inferred from linear Sverdrup dynamics. The climatological mean position of the zero wind stress curl line, which separates the subpolar and subtropical gyres, is indicated by the thick black line. The two boxes used to define ΔT are also indicated.*

The previous advective mechanism can be easily be added to the canonical model for SST anomalies (Frankignoul and Hasselmann, 1977), in the form of an oceanic heat flux $Q_o$

$$d\Delta T/dt = a\Delta P - \lambda \Delta T + Q_o$$

where $\Delta P = GIL - STH$ denotes the dipolar SLP anomaly associated with $\Delta T$ (i.e., the NAO signature in SLP), generating surface turbulent heat exchange with the ocean, as measured by the scaling factor a, and where λ is a damping timescale for $\Delta T$ resulting from local air sea interactions (about a yr). We consider the following model for $Q_o$

$$Q_0 = -(b/t_y)\int_{(t-t_y)}^{t} \Delta P dt$$

expressing that, after a delay $t_y$, the anomalous gyre circulates cyclonically in response to positive $\Delta P$ anomalies, and cools $\Delta T$ at a rate set by the parameter $b$ ($b$ is of same order as a, as discussed previously). The delay time $t_y$ is controlled by the baroclinic adjustment of the gyre to surface windstress curl changes, and is set to a nominal value of 10 yrs.

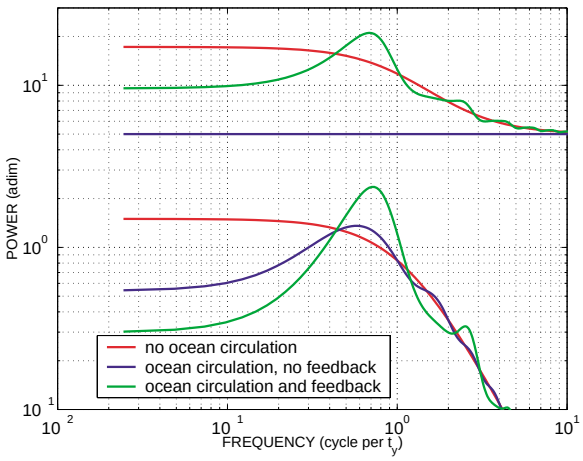


*Figure 3: Model predictions for ΔP (upper plots) and ΔT (lower plots), for b = 0 (red), b≠0 but no feedback of ΔT on ΔP (blue), b≠0 with a small feedback of ΔT on ΔP (green). The frequency is expressed in cyle per $t_y$, i.e., in cycle per 10 yrs. The power is non dimensional.*

One readily sees from (2) that on timescales $> t_y$, $Q_o \cong -b\Delta P$ , so that compared to the hypothetical situation where the ocean currents would not impact SST, the level of the forcing in (1) is reduced from a $\Delta P$ (no ocean currents) to $(a-b)\Delta P$ (ocean circulation included). A signature of the role of ocean circulation is thus to decrease the power of $\Delta T$ on timescales longer than about 10 yrs, thereby peaking the SST spectrum in the decadal band (Fig. 3, lower plots). When a small impact of $\Delta T$ on $\Delta P$ is allowed, the peak is even more pronounced and may also be found in $\Delta P$ (Fig. 3, upper plots).

**4. Comparison with the observations**

Figure 4 shows the observed power spectra for $\Delta T$ (green), GIL (blue) and STH (red). In good agreement with the previous model (Fig. 3, green curve), the power spectrum of $\Delta T$ shows a broad band peak in the decadal band, with no flattening on longer timescales, but instead a continuous decrease of power. The power spectra of GIL and STH are similar up to timescales of about 25 yrs (Fig. 4, blue and red curves respectively). This is consistent with a spectral coherence analysis, which indicates strong coherence and a robust out of phase relationship between GIL and STH up to 25 yrs (not shown), in agreement with the NAO paradigm. On longer timescales, however, the two spectra have different structures and the coherence between them is reduced (not shown). While the STH power spectrum keeps increasing with timescales, that of GIL decreases. The NAO index of Hurrell (1995), the normalized SLP difference between Iceland and Lisbon, has a power spectrum very similar to that of STH (not shown). The decrease of power seen in GIL at timescales > 25 yrs is in agreement with the model predictions when feedback is allowed (Fig. 3, top panel, green curve). We have checked that GIL and $\Delta T$ keep coherent on these long timescales (not shown). Thus, although it is a highly simplified view of the dynamics of GIL, our results are consistent with a control of the strength of the Greenland - Icelandic Low by ocean circulation, through its impact on the surface baroclinicity (as measured by $\Delta T$).

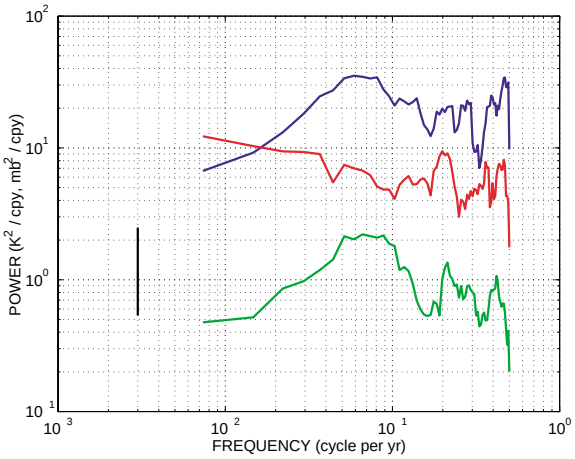


*Figure 4: Observed power spectra of SLP anomalies near Greenland - Iceland (GIL, blue) and near the subtropical High (STH, red). The power spectrum of the cross Gulf Stream SST index ΔT is also plotted (green). The frequency is expressed in cycle per yr and the power in $K^2$/ cpy for ΔT and $mb^2$/cpy for GIL and STH. The vertical bar indicates the 95% confidence level. Note that the colors chosen here do not refer necessarily to those of Fig. 3.*

## 5. Discussion and comparison with previous studies

Our analysis of the observations is close to that of Deser and Blackmon (1993), although we use simpler techniques and a longer dataset. In agreement with the result of their EOF analysis (their 'dipole mode'), we showed evidence for a pronounced decadal timescale in the variability of North Atlantic SST. Both their second SST principal component and the $\Delta T$ index introduced here show a broad band peak in the 10 -20 yr band, as expected from the similarity between our SST index (SST difference across the separated Gulf Stream) and their 2nd EOF pattern. Nevertheless, the power spectra differ at timescales longer than about 25 yrs: whereas $\Delta T$ shows decreasing power with timescales (Fig. 4, green curve), their PC2 shows the opposite (their Fig. 3a). The different data set used (COADS vs Kaplan) may be a possible explanation. However, as the power spectrum of the 1st EOF of North Atlantic SST in winter with the Kaplan et al. (1997) reanalysis shows a similar power spectrum as that of the second EOF in Deser and Blackmon (1993), with very similar pattern (the tripole), this explanation does not seem valid. Instead, the difference in power spectrum is likely to result from the EOF analysis employed by Deser and Blackmon, which emphasizes large - scale pattern and reflects SST variability outside the Gulf Stream region, whereas our analysis only considers the difference of SST across the Gulf Stream. Independently, we showed that a similar spectral feature is found in SLP anomaly near the Greenland - Iceland Low region (Fig. 4, blue), which keep coherent with $\Delta T$ at these long timescales (not shown). The use of a longer dataset in our study (143 yrs instead of 90 yrs) also certainly allows a better, although still limited, investigation of these long timescales.

More fundamentally, we have proposed a plausible mechanism explaining this decrease of power in $\Delta T$ at low frequency. This feature is expected based on linear Sverdrup dynamics, and results primarily, at long timescales, from a partial cancellation of the advective forcing of $\Delta T$ anomalies by anomalous ocean currents (the intergyre gyre of Fig. 2), and the local surface forcing of $\Delta T$ by the atmosphere. We note that the tendency for Atlantic SST anomaly to become of basin extent at interdecadal timescale (Kushnir, 1994) may also be a factor explaining the decrease of power seen in $\Delta T$.

Allowing a small feedback of $\Delta T$ on the NAO, Atmosphere - Ocean coupling may peak the spectra of $\Delta T$ and SLP near the decadal band, in good agreement with the observed $\Delta T$ and GIL spectra. The different structure seen in the latter and that of the NAO or SLP anomaly near the subsidence region (Fig. 4) at low frequency (periods longer than 25 yrs) is intriguing. It is not consistent with our theory which would predict a decrease of power for the whole NAO pattern. This may reflect that, in late winter, other factors than $\Delta T$ / storm - track interactions control the strength of SLP anomaly over the subsidence region. This requires further study.

**References**

Deser C., and M. L. Blackmon, 1993: Surface climate variations over the North Atlantic Ocean during winter: 1900-1989. *J. Climate*, **6**, 1743-1753.

Frankignoul, C., and K. Hasselmann, 1977: Stochastic climate models, part II: application to sea-surface temperature variability and thermocline variability. *Tellus*, **29**, 289-305.

Grötzner, A., M. Latif, and T.P. Barnett, 1998: A decadal climate cycle in the North Atlantic Ocean as simulated by the ECHO coupled GCM. *J. Climate*, **11**, 831-847.

Hurrell, J., 1995: Decadal trends in the North Atlantic Oscillation: regional temperature and precipitation, *Science*, **269**, 676-679.

Kaplan, A., Y. Kushnir, M. Cane, and B. Blumenthal, 1997: Reduced space optimal analysis for historical datasets: 136 years of Atlantic sea surface temperatures. *J. Geophys. Res.*, **102**, 27,835-27,860.

Kaplan, A., Y. Kushnir, and M. Cane, 2000: Reduced space optimal interpolation of historical marine sea level pressure: 1854-1992. *J. Climate*, **13**, 2987-3002.

Kushnir, Y., 1994: Interdecadal variations in North Atlantic sea surface temperature and associated atmospheric conditions. *J. Climate*, **7**, 141-157.

Marshall, J., H. Johnson, and J. Goodman, 2001: A study of the interaction of the North Atlantic Oscillation with the ocean circulation. *J. Climate*, in press.

# North Atlantic Persistence and Decadal Forecasting

**Gidon Eshel**
**Dept. of the Geophysical Sciences, The Univ. of Chicago, Chicago, USA**
**geshel@uchicago.edu**

I examine decadal predictability in the North Atlantic. A region near Cape Code and the Gulf of Maine is identified as featuring the highest North Atlantic persistence (Fig. 1 left), with a unique combination of high- amplitude, persistent sea surface temperature anomalies, associated with substantial upper ocean heat content anomalies (Fig. 1 right). A mechanism is advanced, whereby that region's surface ocean is a `window' to deep upper ocean dynamics, with thermal evolution that tracks heatflux divergence by the slowly adjusting subtropical gyre. This is consistent with the subtropical gyre playing a central role in NA climate variability. The proposed interpretation is supported by broad, high lag correlations between the Bermuda potential vorticity timeseries (representing the subtropical gyre state) and surface anomalies (Fig, 2; the same for SSTA is not shown here). Successive lag correlation patterns reveal surface oscillations that are not apparent in the raw surface data.

Finally, the correlation patterns are used for NAOI forecasting, using a new forecasting method (Fig. 3) that is presented and explained. Forecasts are robust and reproducible, outperforming alternative methods (Fig. 4). At lead times of 25 and 12 years, cross validated skills over 1927-64 (38 yrs) are 0.44 and 0.53, respectively. It is suggested that the combination of skills and lead times may prove societally useful.

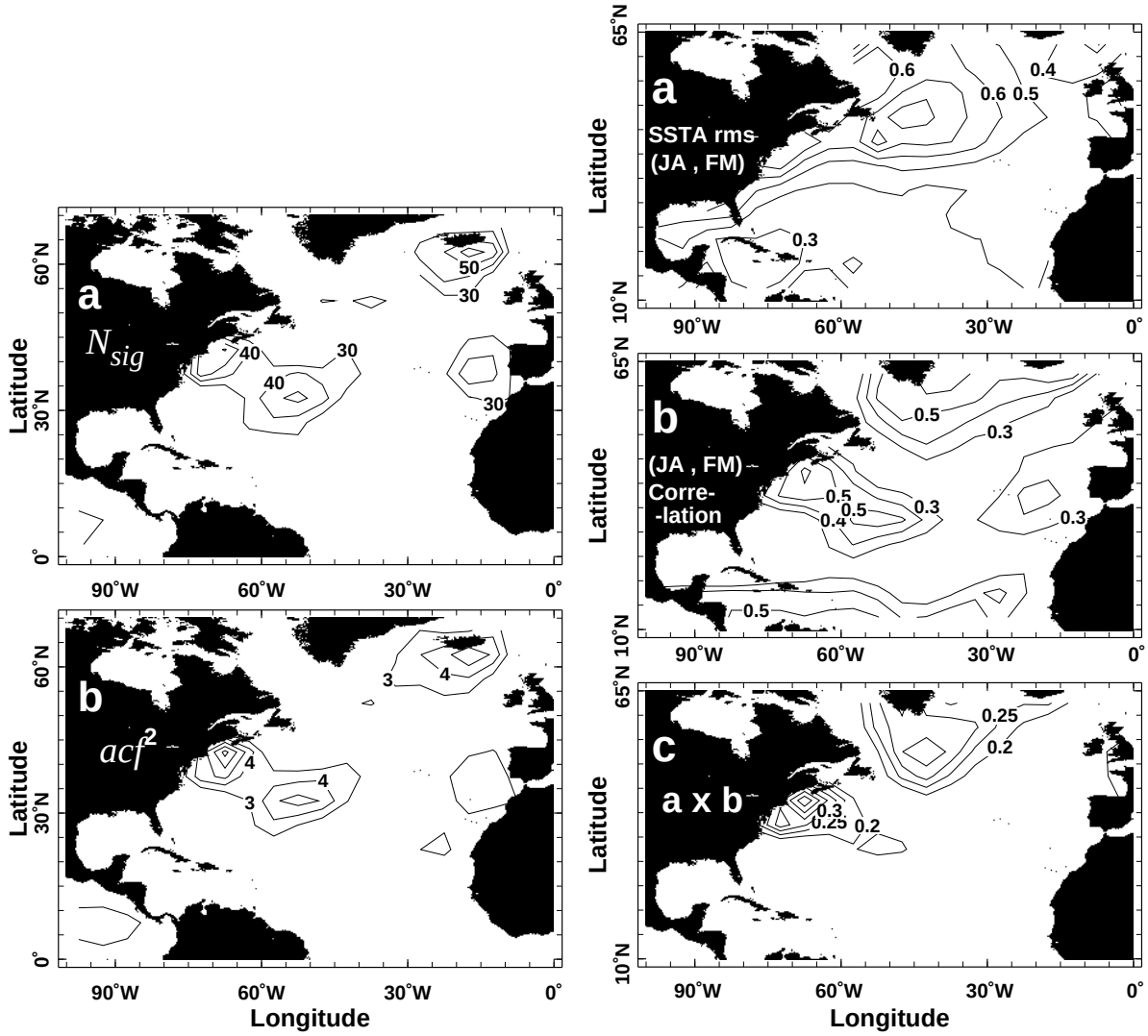


*Figure 1: Left Column: Two measures of `total' persistence. (a) The number of significant lags out of the total number of lags considered. See text for details on the significance test. (b) Sum of squared acf at all lags. Right Column: (a) Root mean square of July-August and February-March SSTA means. (b) The correlations between these 2 means. (c) The product of panels a and b.*

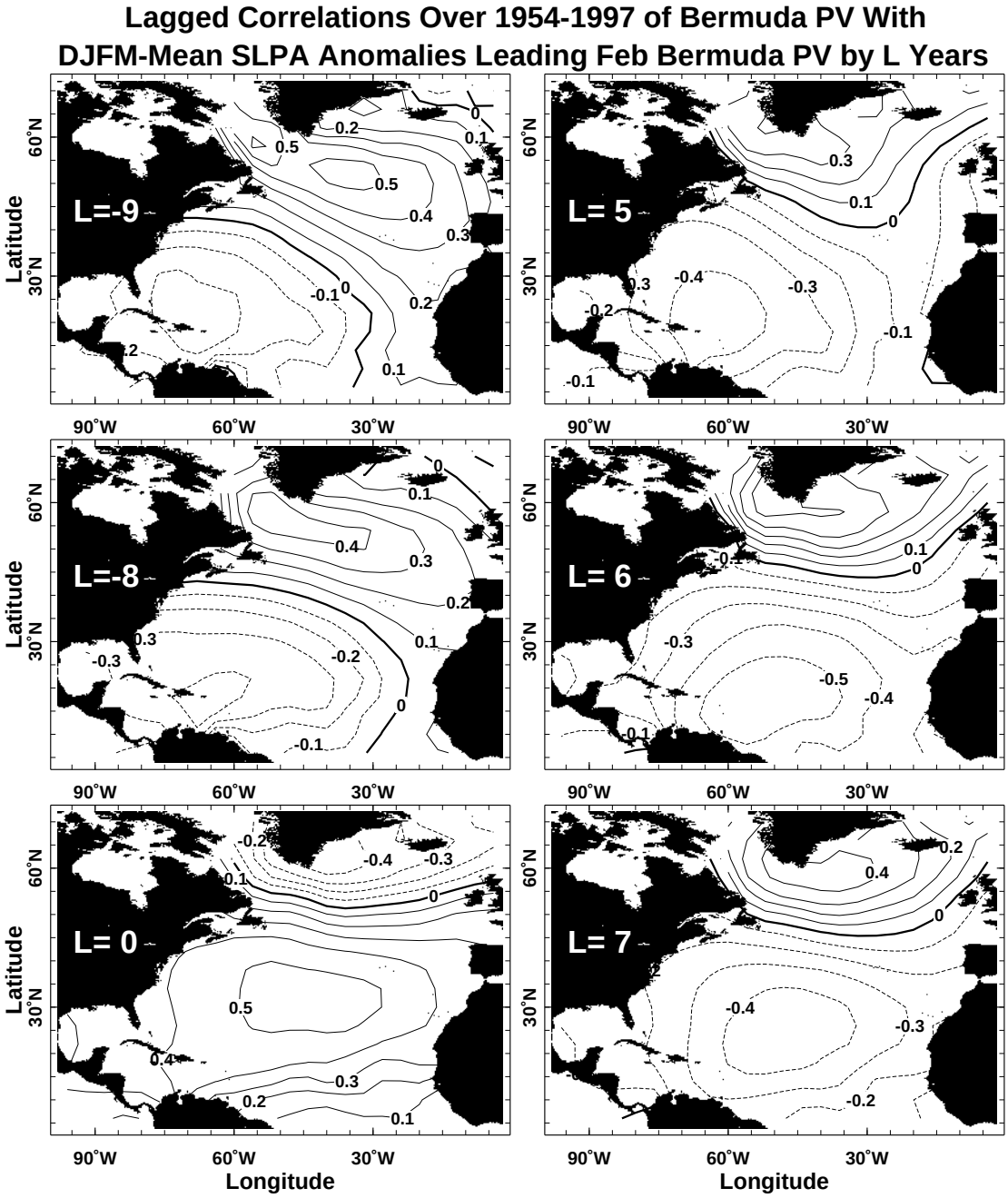


*Fig. 2: Lagged correlation maps between the PV timeseries and those of SLPA at representative lags.*

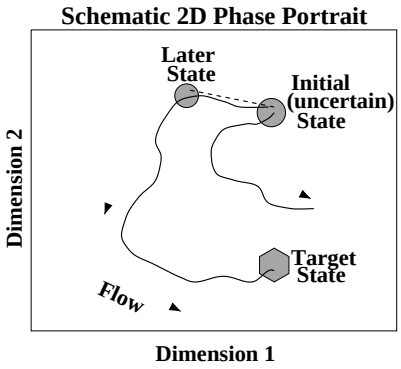


*Fig. 3 (above): A schematic of the forecasting method. See text for deatils.*

*Fig. 4 (right): Cross validation forecasting results for 3 segment combinations against AR(1)-derived, 2000 member population. See text for details.*

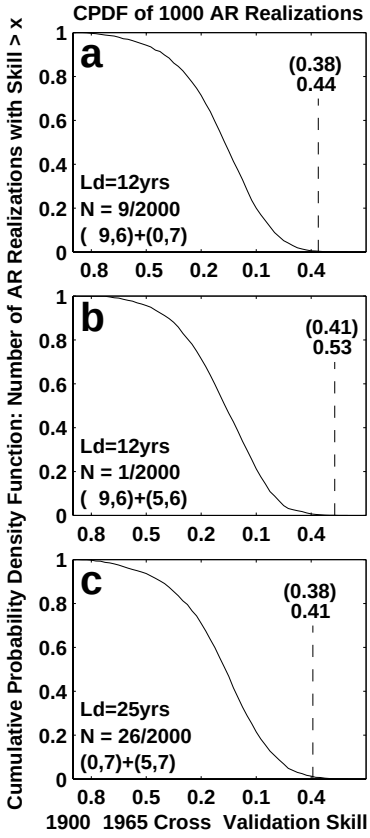

# Observed variations of climate variability over the last 100 years

**Chris Folland and Robert Allan**
**Hadley Centre, The Met Office, Bracknell, UK**
**cfolland@meto.gov.uk**

This selective review concentrates on the longer time scales of variability over the last century or more, mainly on large scales. There is some concentration on the Atlantic. Decadal to multi-decadal climate variability over about the last century must be seen against a background of global warming which itself may influence variability, or affect how variability is observed or interpreted. In addition, many of the data used to study climate variability and change were either not designed for the purpose or have suffered from numerous inhomogeneities. Compounding this problem are time-varying data gaps, some remaining to this day. Indeed the spatial coverage of some data is now declining. Particularly important are radiosonde data needed for studying the spatial structure of decadal phenomena throughout the full depth of the atmosphere, often within the context of reanalyses. Here a decline in coverage has occurred since the 1980s. New methods are, however being developed to estimate data where gaps are large. These techniques, e.g. the method of reduced space optimum interpolation (Kaplan, 2000), must be viewed with caution. Their correct use requires note to be taken of strong non-stationarities in the data (Hurrell and Trenberth, 1999).

At present there is only limited consensus on the topic of decadal to multidecadal variability, so this brief review can only be preliminary. Useful reviews are given by Enfield and Mestas-Nuñez (1999) and Allan (2000). This note gives a more personal slant. The longest time scale of variability over the last century is the anthropogenic warming of the globe. The globe has warmed (to 1999) by $0.6 \pm 0.2^{o}$C (95% confidence limits) since the late nineteenth century in two main phases, 1910-1945 and 1976-the present. The spatial pattern of this warming cannot be regarded as fixed, though it may be estimated usefully on specific time scales using EOF methods. Such patterns may be the result of both external forcing (likely to be the largest component when viewed on the global average) and variability internal to the climate system. The latter is especially likely to be important for regional warming trends. Taken over the century, most parts of the world have warmed, though an exception until recently, at least, has been an area south of Greenland. However, nothing reliable can be said about the trends in the Southern Ocean south of 50 $^{o}$S until the 1980s when there is some evidence of rather muted warming in places. There is also recent evidence of reduced warming of air temperature over the oceans compared to the sea surface in the Indian Ocean and parts of the South Pacific that appeared to commence around 1991. Note that our picture of the magnitude of warming in sea surface temperature (SST) depends on the veracity of large corrections to SST data for their apparent cold biases before 1942.

The second longest time scale of variability is particularly uncertain, but may be a tendency to quasi-interhemispheric variations of temperature, particularly sea surface temperature, as suggested by Folland et al. (1986, 1987) when discussing Sahel drought. Ordinary eigenvector, and both extended and complex eigenvector, analyses show this apparent pattern, which is also evident from a perusal of the decadal average maps in Parker et al. (1994). Figure 1 shows the possible pattern of this fluctuation (from Enfield and Mestas-Nunez, 1999). The time scale is uncertain, but may be 50-80 years from the available data and from analyses of a similar, and seemingly evolving spatiotemporal pattern by Mann et al. (1998) using palaeodata. Fluctuations in the global thermohaline circulation may be implicated (e.g. as suggested in modelling studies by Delworth and Mann, 2000).

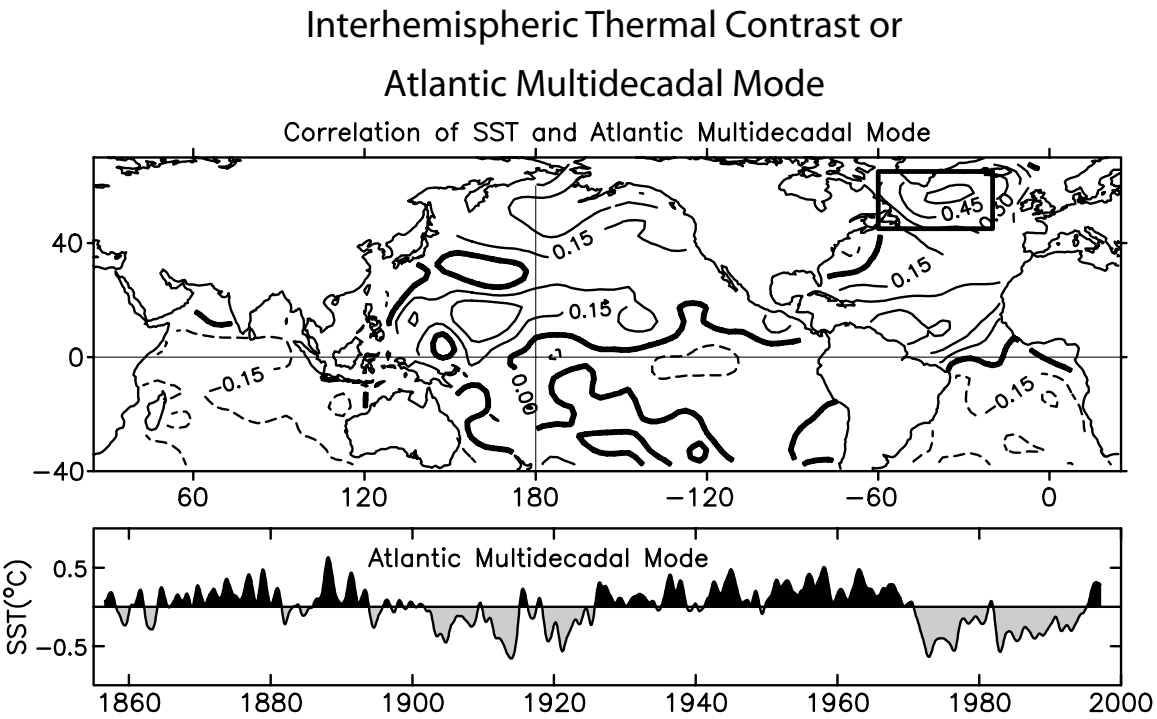


*Fig. 1: a) Distribution of correlations for the years 1857 to 1996 between local monthly SST anomalies versus the third EOF "Atlantic Multidecadal Mode" b) Temporal realization of the Atlantic Multidecadal Mode computed from temporal amplitude time series and the area-average spatial loadings over the rectangular area in the North Atlantic. In Landsea et al. (1999) - from Enfield and Mestas-Nunez (1999).*

An atmospheric pattern that varies on all time scales from days to many decades is the North Atlantic Oscillation (NAO) (Hurrell, 1995) and its close cousin, the Arctic Oscillation (AO) (Thompson and Wallace, 2000, Thompson et al., 2000). The pattern of the AO is one of either relatively high or low pressure across the polar cap and nodes of opposite sign centred near the Azores high and possibly in the mid latitude North Pacific. The NAO exists year round but its pattern varies and it is best developed in winter (but see below). The AO is of larger scale and very often includes the NAO as a component. The main controversy over the AO is whether the weaker mid latitude Pacific component is real or an artefact of analysis. Otherwise it is clear that this is a major component of the mid to high latitude Northern Hemisphere atmospheric circulation, affecting the stratosphere in the winter, particularly around January to March. Both oscillations have undergone pronounced multidecadal variability with a strong tendency since 1970, and particularly 1988, to move to the positive sign of both modes with relatively low pressure over the Arctic.

The NAO is related to a tripole pattern of SST anomalies in the North Atlantic on interannual to quasi-decadal time scales. This pattern has one node in the higher latitudes of the North Atlantic, a node of opposite sign off the east coast of USA stretching across the subtropical Atlantic and a node of the same sign as in the higher latitudes in the tropical North Atlantic. The tripole appears to be driven by the North Atlantic Oscillation on a variety of time scales, and in turn there is evidence that it may force the NAO to some extent (Rodwell et al., 1999).

Thompson and Wallace (2000) show that there is a similar "polar cap" pattern to the AO in the Southern Hemisphere that was in fact first described by Kidson (1988), and called by Thompson and Wallace the Antarctic Oscillation (AAO) and by Kidson the High Latitude Mode. This mode has a similar vertical and horizontal structure to the AAO despite the very different sur-

face conditions represented by Antarctica. The history of this mode is poorly known, but atmospheric data are probably good enough to define its behaviour over the last 30 years. Like the AO, the AAO appears to have multidecadal variability and has also gone into a positive mode since the late 1980s.

There appear to be modulations of the interannual El Niño-Southern Oscillation (ENSO) variations on decadal to multidecadal time scales which are particularly prominent in the Pacific, and to some extent the Indian Ocean. The Pacific Decadal Oscillation is one manifestation, defined over the North Pacific (Mantua et al., 1997), and the Interdecadal Pacific Oscillation is another, defined over all of the Pacific basin. These phenomena may be essentially the same, though this remains to be proved. The former has been defined on decadal and subdecadal time scales whereas the latter was approached from an interdecadal perspective (Power et al., 1999). Key features of these phenomena involve probable subtle changes in the familiar ENSO pattern of SST as we move to decadal and multidecadal time scales. As the time scale gets longer, variance in the North West Pacific and (for the Interdecadal Oscillation) the South West Pacific increases relative to that in the tropical central and east Pacific. The former regions have the opposite sign of SST anomalies to the tropical central and east Pacific when the patterns are well developed. Another change from shorter time scales is that the sign of the SST anomalies is the same in the West Tropical Pacific as in the East Tropical Pacific on multidecadal time scales; on the interannual ENSO time scale the sign is at least weakly opposite. This could change the distribution of diabatic heating with more rainfall in parts of the easternmost part of the west Pacific during the warm Tropical east Pacific phase. If these background SST and diabatic heating variations are real, they should modulate interannual ENSO teleconnections e.g. as suggested for Australia by Power et al. (1999) and for North America (via the PDO – Mantua et al., 1997) by Gershunov and Barnett (1998).

Related to the PDO are variations in North Pacific pressure sometimes called the North Pacific Oscillation. This index measures the mean winter half-year surface pressure over a wide region of the North Pacific. Besides strong interannual variability, there is also clear interdecadal variability.
There is a tendency for quasi-bidecadal variability to occur over a number of regions of the world. The most famous example is bidecadal variability of rainfall in parts of southern Africa. This is so pronounced in the areas affected that the probability of seasonal drought or flood is quite strongly dependent on the current phase of this variation. Folland et al. (1999) noticed that several patterns of SST represented by major near global EOFs were significantly correlated with this phenomenon, particularly their EOF4 which gives weight to the South Indian Ocean. Using cross validation and step-wise multiple correlation methods, substantial hindcast skill was obtained from the three most prominent global SST covariance EOFS in the 1911-95 epoch, but excluding the global warming pattern. Pronounced sub-bidecadal variability has recently been found for New Zealand temperature.

Variations of SST on near decadal time scales appear in the tropical Atlantic. These variations are associated with a dipole of SST anomalies between the tropical South and North Atlantic. An apparent dipole of variability exists on many time scales but only on near decadal time scales does a coherent anticorrelation of SST anomalies exist across the equator (Tourre et al., 1999). North East Brazil rainfall is very sensitive to such anomaly dipoles in the Tropical Atlantic, no matter whether the two nodes vary randomly or coherently. Besides the very strong interannual influences, studies have also detected decadal influences on North East Brazil rainfall, very likely due to this coherent dipole, using SST analyses, and an atmospheric general circulation model forced with observed SST, both for the period 1912-1998.

A feature of higher latitude Southern Hemisphere circulation that has received increasing interest in recent years is the so called Antarctic Circumpolar Wave (ACW). The ACW is an eastward propagating wave with a 3-6 year period, composed of covarying SLP and SST

anomalies that take some 8 years to circle the globe. There is still contention as to whether the ACW is linked to interannual ENSO variability, but there are also intriguing questions about whether the ACW may display decadal-interdecadal fluctuations similar to the 'ENSO-like' modes noted above. At present, data is only sufficient to resolve the ACW effectively since the early 1980s.

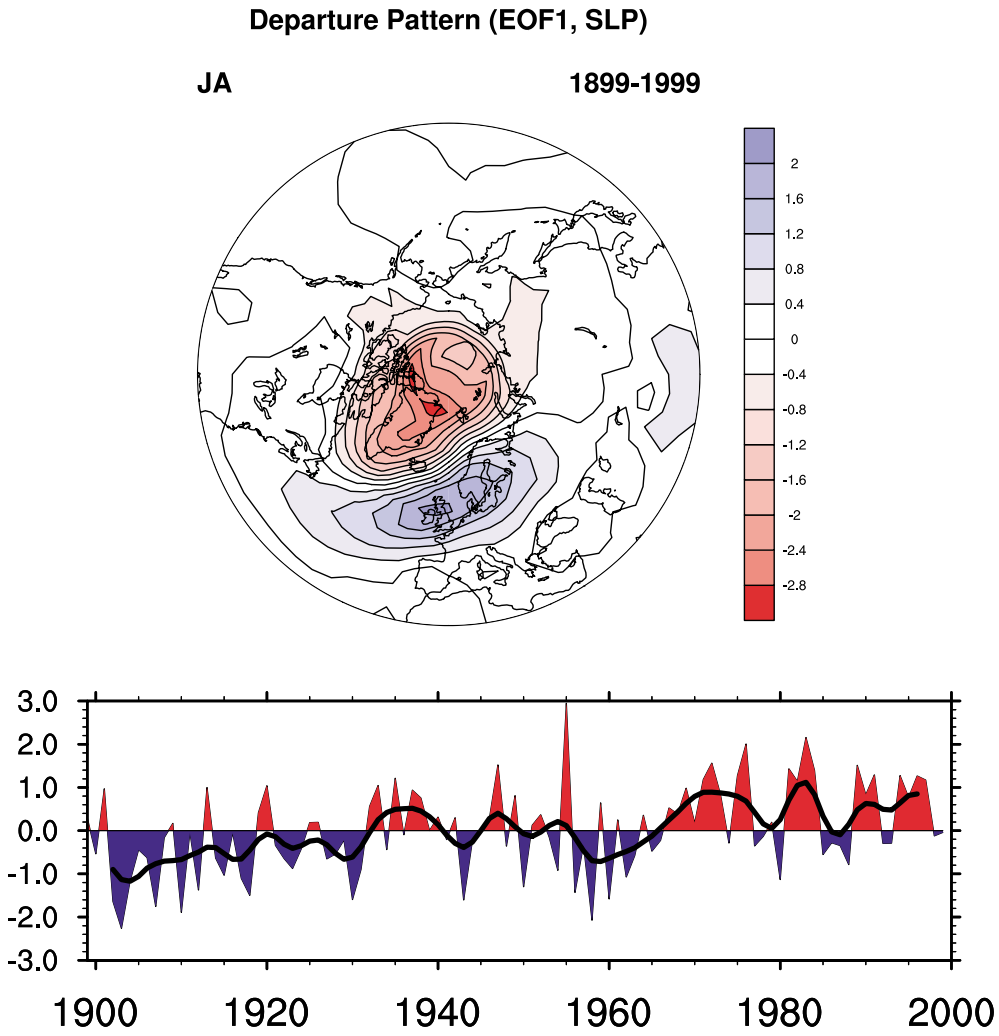


*Fig. 2: First EOF of extra-tropical pressure at MSL in July-August (pattern and time series), courtesy of J. Hurrell*

Finally, we mention a new topic. In the extratropics, much emphasis of research on decadal to multidecadal variability has been on the colder seasons. However UK climatologists have long suspected a strong variation in UK high summer (mainly July and August) rainfall and the associated atmospheric circulation on multidecadal time scales. This variation was linked empirically to Sahelian summer rainfall variations in an unpublished analysis by Folland et al. (1987). Recently Hurrell (personal communication) found that this behaviour of UK summer climate seemed to be strongly related to the first EOF of extratropical pressure at mean sea level in July and August, quite similar to a pattern shown by Thompson and Wallace (2000) in their study of the seasonal cycle of the NAO. Figure 2 from Hurrell (personal communication) shows the pattern and time series of this July and August sea level pressure EOF. A horseshoe-shaped ring of negative correlations is also found in the tropical Atlantic cyclone track that joins the southern half of the midlatitude storm track crossing the UK in other analyses relating Sahel rainfall and July and August sea level pressure over the North Atlantic for the period 1947-1996. Over the UK, correlations are highly significant. A very similar, slightly stronger pattern is seen in the HadAM3 climate model. If confirmed, this phenomenon may involve

tropical-extratropical interactions involving summer Atlantic storm tracks. Cross spectral analysis shows significant coherence between high summer rainfall over England and rainfall in the Sahel on multidecadal time scales, and some coherence on shorter time scales.

**References**


Allan, R.J., 2000: ENSO and climatic variability in the last 150 years, In Diaz, H.F., and V. Markgraf, (eds.), El Niño and the Southern Oscillation: Multiscale Variability, Global and Regional Impacts. Cambridge University Press, Cambridge, UK, in press.

Delworth, T.L and Mann, M.E., 2000: Observed and simulated multidecadal variability in the Northern Hemisphere. *Climate Dynamics*, **16**, 661-676.

Enfield, D.B. and A.M. Mestas-Nuñez, 1999: Multiscale variabilities in global sea surface temperatures and their relationships with tropospheric climate patterns. *J. Climate*, **12**, 2719-2733.

Folland, C.K., D.E. Parker, and T.N. Palmer, 1986: Sahel rainfall and worldwide sea temperatures 1901-85. *Nature*, **320**, 602-607.

Folland, C.K., D.E. Parker, M.N. Ward, and A. Colman, 1987: Sahel rainfall, Northern Hemisphere circulation anomalies and worldwide sea temperature changes. Long Range Forecasting and Climate Technical Note 7a.

Folland, C.K., D.E. Parker, A. Colman, and R. Washington, 1999: Large scale modes of ocean surface temperature since the late nineteenth century. In Navarra , A (ed), Beyond El Niño: Decadal and Interdecadal Climate Variability, pp73-102 . Ed:. Springer-Verlag, Berlin, 374 pp.

Gershunov, A., and T.P. Barnett, 1998: Interdecadal modulation of ENSO teleconnections. *Bull. Amer. Meteor. Soc.*, **79**, 2715-2725.

Hurrell, J.W., and K.E. Trenberth, 1999: Global sea surface temperature analyses: multiple problems and their implications for climate analysis, modeling and reanalysis. *Bull. Amer. Meteor. Soc.*, **80**, 2661-2678.

Kaplan, A., Y. Kushnir, and M.A. Cane, 2000: Reduced space optimal interpolation of historical marine sea level pressure: 1854-1992. *J. Climate*, **13**, 2987-3002.

Kidson, J.W., 1988: Interannual variations in the Southern Hemisphere circulation. *J. Climate*, **1**, 1177-1198.

Mann M.E., R.S. Bradley, and M.K. Hughes, 1998: Global-scale temperature patterns and climate forcing over the past six centuries. *Nature*, **392**, 779-787.

Mantua, N.J., S.R. Hare, Y. Zhang, J.M. Wallace, and R.C. Francis, 1997: A Pacific interdecadal climate oscillation with impacts on salmon production. *Bull. Amer. Meteor. Soc.*, **78**, 1069-1079.

Power, S., T. Casey, C.K. Folland, A. Colman, and V. Mehta, 1999: Inter-decadal modulation of the impact of ENSO on Australia. *Climate Dynamics*, **15**, 319-323.

Rodwell, M., D.P. Rowell, and C.K. Folland, 1999: Oceanic forcing of the wintertime North Atlantic Oscillation and European climate. *Nature*, **398**, 320-323.

Thompson, D.W.J. and J.M. Wallace, 2000: Annual modes in the extratropical circulation Part I: month-to-month variability. *J. Climate*, **13**, 1000-1016.

Thompson, D.W.J., J.M. Wallace, and G.C. Hegerl, 2000: Annual modes in the extratropical circulation Part II: trends. *J. Climate*, **13**, 1018-1036.

Tourre, Y.M., Y. Kushnir, and W.B. White, 1999: Evolution of Interdecadal Variability in Sea Level Pressure, Sea Surface Temperature, and Upper Ocean Temperature over the Pacific Ocean. *J. Phys. Oceanogr.*, **29**, 1528-1541.

# Tropical Pacific/Atlantic Ocean Interactions at Multi-Decadal Time Scales

**Mojib Latif**
**Max-Planck-Institut für Meteorologie, Hamburg, Germany**
**latif@dkrz.de**

Analysis of sea surface temperature (SST) observations (Latif 2001) suggests a pan-oceanic interaction between the tropical Pacific and the Atlantic Ocean at multi-decadal time scales, such that periods of anomalously high SSTs in the eastern tropical Pacific are followed by a basin-wide SST dipole in the Atlantic Ocean with a time delay of a few decades (Figure 1). The SST anomaly structure in the Atlantic Ocean is reminiscent of variations in the North Atlantic thermohaline circulation. The two ocean basins are linked through an "atmospheric bridge" involving anomalous fresh water fluxes. Based on the observational findings, the Atlantic thermohaline circulation may strengthen during the next decades in response to the strong decades- long increase in eastern tropical Pacific SST, which will have strong impacts on the climates of North America and Europe through changes in the North Atlantic has been shown in a recent paper (Latif et al., 2000) that changes in the tropical Pacific stabilise the North Atlantic thermohaline circulation (THC) in a greenhouse warming simulation, with the atmosphere serving as a coupling device between the two oceans. The proposed mechanism works as follows: The long-term changes in the eastern tropical Pacific SST induce changes in the fresh water flux over the tropical Atlantic, which will lead to anomalous sea surface salinities (SSSs) in the tropical Atlantic Ocean. The SSS anomalies are advected poleward by the mean ocean circulation, eventually affecting the density in the sinking region of the Northern Hemisphere, thereby affecting the convection and the strength of the thermohaline circulation.

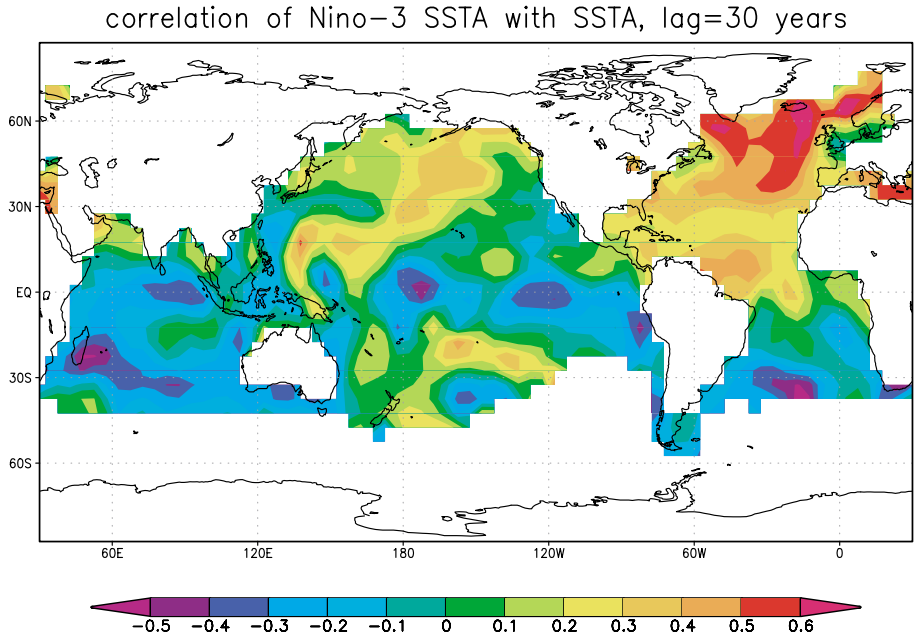


*Fig. 1: Spatial distribution of correlation coefficients between the Niño-3 SST anomaly time series and the global SST anomalies at lag 30 years. The anomaly structure is reminiscent of variations in the THC, indicating that variations in the THC follow variations in tropical Pacific SST with a time lag of 30 years. The data were low-pass filtered with a 11-year running mean prior to the correlation analyses.*

**References**

Latif, M., E. Roeckner, U. Mikolajewicz, and R. Voss, 2000: Tropical stabilisation of the thermohaline circulation in a greenhouse warming simulation. *J. Climate*, **13**, 1809-1813.

Latif, M., 2001: Tropical Pacific/Atlantic Ocean Interactions at Multi-Decadal Time Scales. *Geophys. Res. Lett.*, **28** , 539-542.

# Low frequency climate variability simulated in the North Atlantic by a coupled ocean-atmosphere model

**Carine Laurent and Herve Le Treut**
**Laboratoire de Meteorologie Dynamique, Institut Paris, France**
**claurent@lmd.jussieu.fr**

**Abstract**

The low-frequency climate variability simulated in the North Atlantic by a coupled ocean-atmosphere model is diagnosed and compared to available observations. A variety of statistical methods is used to study the quasi-decadal (QD) oscillations. They tend to show that local direct interactions between the atmosphere and the ocean may help maintaining them.

## 1. Observed low-frequency variability

The observed power spectrum of climate records shows significant variability at different time scales. Some well defined periods, as those of the diurnal or annual cycle, are governed by astronomy. At the other extreme of the frequency record, variability at the scale of thousand years has been documented by paleoclimatic indicators. Following Milankovitch's theory (1941), periodic variations of the orbital parameters can serve to trigger the glacial/inter-glacial cycles over the last 3 millions years. Between those extremes, we may define for our purpose a low frequency variability (LFV), at the scale of inter-annual to inter-decadal variability. We are interested in these time scales because they are those of our life time, although they are not dominant in the power-spectrum.

The spatial pattern associated with this LFV is well characterized. In the North Atlantic, the atmospheric variability at any time scale is dominated by a large-scale fluctuation, between the Azores Anticyclone and the Iceland Low: this is the North Atlantic Oscillation (NAO). A positive phase of this oscillation corresponds to both a strengthening of the high and low pressures, intensifying western winds (figure 1, left). This is clearer in winter. To represent this feature, Hurrell (1995) defined a NAO index as the difference of sea-level pressure (SLP) anomalies between Azores and Iceland, respectively normalized by their standard deviation. From 1864 to 1995, this index shows a strong high-frequency variability, modulated by "low-frequency" fluctuations. A positive trend since 1960, which implies an increase of the positive phase of NAO, is also apparent in the record. The sea surface temperature (SST) anomalies associated to this zonal SLP pattern (figure 1, right) are warmer in the west side of the basin, south of New-Foundland and near Europe, and colder in the subpolar gyre and trade-winds zone. This association of atmospheric (SLP) and oceanic (SST) modes is prevailing at both inter-annual and intraseasonal time scales.

NAO potential importance comes from its clear correlation with other climatic fields over Europe, like precipitation. In a positive phase of the NAO, there is a deficit of precipitation above the Mediterranean Sea and in the South of Europe, with an opposite excess in the North of Europe.

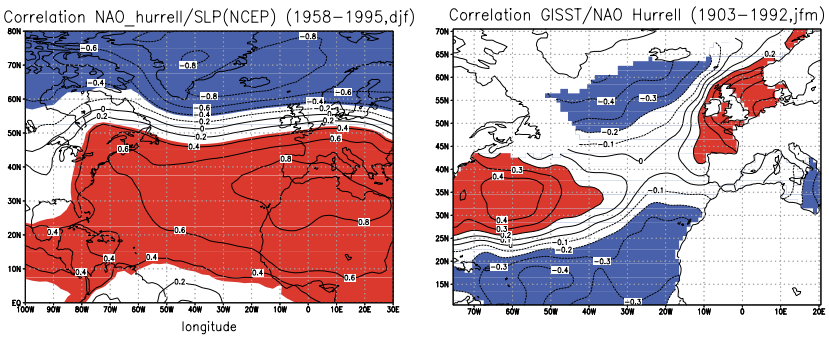


*Figure 1: Left: Correlation map between NAO index (defined by Hurrell) and SLP (NCEP data) from 1958 to 1995, in winter means. Right: Correlation map between SST (GISST data) and NAO index from 1903 to 1992, in winter means.*

The study of this LFV shows some evidence of weak peaks which organize or dominate the variability. In the atmosphere, Hurrell's NAO index frequency spectrum shows some decadal time scales, between 6 and 8 years (from winter means). On the contrary, the first two modes of variability for SST anomalies in winter are characterized by longer periods of about 10 and 13 years. A first mode is more zonal and appears as NAO's signature on the ocean surface. A second mode exhibits marked anomalies off New-Foundland. The apparent difference of time scales between the atmosphere and the ocean shows the inherent complexity of the mechanisms affecting climate variability. Further diagnostics are needed and an additional useful tool is the M-SSA analysis. It tends to reveal a 13-year oscillation.

To investigate the main physical mechanisms playing a role in LFV, we try to find evidences of atmosphere-ocean connections. We use for that purpose a coupled ocean-atmosphere model, in which we first study the role of the atmospheric heat fluxes and the SST. The mathematical manifestation of climate variability may take different forms, and in consequence we also use different statistical methods to study it. If the fluctuations are near-linear oscillations they will probably be captured by an Empirical Orthogonal Function (EOF) analysis followed by harmonic analysis. Non-linear oscillations will be best detected by an auto-regressive analysis (a M-SSA analysis). Then to study the mechanisms of rapid transitions between modes (Palmer, 1993; 1999), we use a weather regimes analysis - or an adaptation of it to the seasonal time scale.

**2. General appreciation of the ISPL model**

The low-frequency climate variability over the North Atlantic middle latitudes is studied in two-century long simulations of the IPSL coupled ocean-atmosphere General Circulation Model (Institut Pierre Simon Laplace). The model used is constituted of the LMD AGCM for atmosphere (version LMD5.3), the OPAICE OGCM for ocean (version OPA7). The coupler used has been developed at CERFACS (OASIS2.1). The simulation considered here lasts 225 years and is very stable.

The first modes of both the geopotential height at 500 hPa (z500) and the SST exhibit QD time scales. The power spectrum of the first principal components (PC) shows significant peaks at 6 years for the atmosphere and around 9-10 years for the ocean. As for the observations, the atmosphere evolves at shorter periods than the ocean. The simulated spatial structures are also comparable with the observed ones. An M-SSA analysis confirms the robustness of the QD oscillation: both for the SST and the sea-surface salinity (SSS), we find a 8-year oscillation. This oscillation is not confined at the surface but exists over a 500 m depth.

### 3. Analysis of the relation: atmospheric forcing (flux) / sea surface temperature in the coupled model

To study the phase relation between SST anomalies and oceanic heat flux anomalies at inter-seasonal to inter-annual time scales, we plot the lagged correlation function between the SST PC1 and the net oceanic heat flux in zonal mean, at 40$^o$N, latitude of the maximum of the simulated QD variability (figure 2). The maximum of the correlation appears for a lag of 1 year when atmosphere leads (correlation of 45%). To interpret the sign change of the function near lag 0, we use the concepts illustrated by Frankignoul et al. (1998) through their simple model, which considers the role of an atmospheric forcing associated with a negative atmospheric feed-back. They show that in such a case the flux/SST covariance is anti-symmetric (between positive and negative lags) and decreases towards zero when the lag increases. In the coupled model, there is a sign change of the correlation function near zero lag, but the function doesn't decrease towards zero and oscillates around zero with a periodicity of 8 years, which is the QD period found before. The atmospheric forcing is organized as a dipole SLP structure, corresponding to a positive phase of NAO (not shown), with a gain of energy for ocean south of New-Foundland and a deficit in the subpolar gyre.

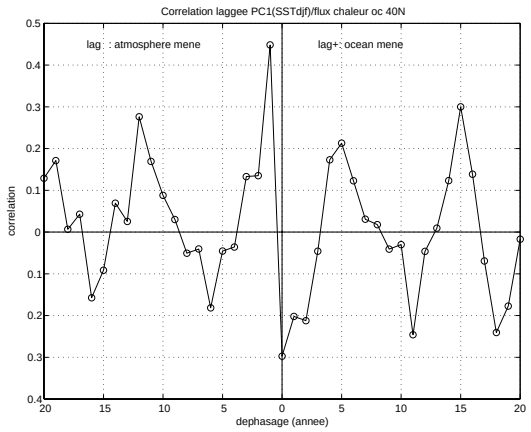


*Figure 2: Lagged (in years) correlation function between the SST PC1 and net oceanic heat flux in zonal mean at 40$^o$N. Ocean leads for negative lags. Atmosphere leads for positive lags.*

In these analyses, we define the atmospheric forcing at a seasonal time scale (mean over DJF). Its role is difficult to analyse, though, because the heat fluxes also and predominantly vary at shorter daily and intraseasonal modes. For this reason, we also use a weather-regime analysis and the associated notion of "climate regime" to better characterize this atmospheric forcing. Weather regimes are defined as the states of the atmosphere with the highest probability of occurrence. We use a partitioning algorithm developed by Michelangeli et al. (1995) to obtain compact clusters. The optimal number of clusters is given by the number for which the distance between a calculated index of classifiability and a 90% confidence level is positive and maximum. For NCEP analysis, on z500, we find with daily winter values, 4 weather regimes, as found by Michelangeli et al. (1995) and defined by Vautard (1990) as the blocking regime, the Greenland Anticyclone, the zonal regime and the Atlantic ridge. The results of the coupled model are best described by a slightly larger number of regimes (7), whose structures are however in good correspondence with the observed ones. We also apply this idea of finding recurrent structures to the seasonal winter means (to get a closer correspondence with the seasonal heat fluxes, as noted above). We find a similar number of climate regimes (6). For these climatic regimes, the amplitude is smaller and we recognize the zonal regime and the Greenland Anticyclone. To check the robustness of the structures obtained through EOF and M-SSA analysis, we may know calculate SST anomaly composites associated, for example, with the zonal regime. We do find the same structure that was characterized as the NAO's signature on the ocean surface. When the atmosphere leads with a lag of 1 year, the SST amplitude is stronger, but the structure disappears after lag 1.

These "climate regimes" are therefore a pertinent tool to characterize the evolution of climate. To determine the complexity of the climate behaviour we wish to know the weather regimes which participate to a winter "climate regime", and therefore to the associated mean winter atmospheric forcing. We plot for each of the climate regimes the number of days correspond-

ing to any of the 7 weather regimes (figure 3). We see that a climatic regime is an aggregation of the different weather regimes, with a different weighting. This complex aggregation is the main driver of climate fluctuations at QD scales.

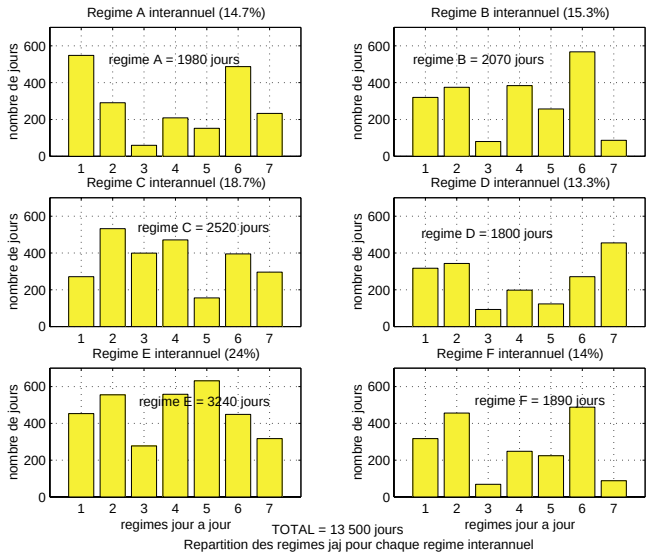


*Figure 3: Repartition of the 7 weather regimes in the 6 "winter climate regimes" (z500)*

## Conclusions

In our model, the atmosphere forces the ocean (which is a well-known result) but the ocean-atmosphere interactions are also apparently important. This is shown in particular by the flux/SST lagged correlation which shows a quasi-decadal periodicity which would be impossible to explain through a passive answer of the ocean to the atmosphere. There is in particular a strong local relation between flux and SST south of New-Foundland. The "winter climate regimes" notion (on z500) permits to study intermittent fluctuations of the atmospheric forcing. The way it associates SST composites with the atmospheric forcing is in agreement with other statistical methods (EOF, M-SSA, correlation), with the same lag of 1 year. But the correspondence between the weather regimes based on daily values, and the actual structures that force the slow variability of climate remains a statistical one, which is not fully understood.

We also underline the necessity of using a large number of statistical tools as long as the true nature of these oscillations has not been elucidated.

## References


Frankignoul, C., A. Czaja, and B. L'Heveder, 1998: Air-sea feedback in the North Atlantic and surface boundary conditions for ocean models. *J. Climate*, **11**, 2310–2324.

Hurrell, J.W., 1995: Decadal trends in the North Atlantic Oscillation: regional temperatures and precipitation. *Science*, **269**, 676–679.

Michelangeli, P. A., R. Vautard, and B. Legras, 1995: Weather regimes: recurrence and quasi stationarity. *J. Atmos. Sci.*, **52**, 1237–1256.

Palmer, T. N., 1993: A nonlinear dynamical perspective on climate change. *Weather*, **48**, 313–348.

PalmerT. N., 1999: A nonlinear dynamical perspective on climate prediction. *J. Climate*, **12**, 575–591.

Vautard, R., 1990: Multiple weather regimes over the north Atlantic: analysis of precursors and successors. *Mon. Weather. Rev.*, **118**, 2056–2081.

# Proxy-based reconstructions of decadal climate variability

**Michael E. Mann**
**Department of Environmental Sciences, University of Virginia, Charlottesville, Virginia, USA**
**mann@virginia.edu**

## Introduction

With the latest available "proxy" climate evidence, the spatial patterns of large-scale climate change during the past millennium have now begun to be characterized (Briffa 2000; Mann et al., 1998; 1999; 2000ab; Jones et al., 1998). Recent climate reconstructions of Mann and colleagues have used networks of diverse high-resolution proxy climate indicators ("multiproxy" networks) to reconstruct large-scale surface temperature patterns (Mann et al. 1999; 2000ab), indices of the ENSO phenomenon (Mann et al., 2000ab), North Atlantic Oscillation (Mann, 2000a; Cullen et al., 2000), and estimate natural (Delworth and Mann, 2000) and externally-forced (Waple et al., 2000) patterns of climate variability during this period. Here we focus on insights from these reconstructions into decadal climate variability in past centuries.

## Background

The details of the approach to paleoclimate reconstruction are discussed elsewhere (see Mann et al., 1998; 1999; 2000ab). The method involves a multivariate calibration of the leading eigenvectors of the 20th century surface temperature record against a global network of diverse proxy indicators to exploit the large-scale structure and complementary seasonal and climatic information in a diverse network of climate proxy indicators in reconstructing past global surface temperature patterns. Significant skill in these reconstructions has been indicated in independent cross-validation exercises (see Mann et al., 1998; 1999; 2000ab) and appropriate self-consistent uncertainties have been estimated back in time. The annual-mean reconstructions of Mann et al. (1998) have recently recently been extended to include distinct warm and cold-season reconstructions (Mann et al., 2000b). The underlying principle in this work is that natural (and human) proxy archives of information can be used to capture the variations in the main patterns of seasonal or annual temperature in the modern instrumental record, and that these patterns can be used to reconstruct the surface temperature field back in time, as well as yield global, hemispheric, or regional mean quantities of interest. Our methodology only assumes that each proxy record exhibits a linear relationship with one or more of the principal components (PCs) of the instrumental record, and not that the proxy itself necessarily be a temperature record. Only carefully-screened records with annual resolution and dating were used. For the period after A.D. 1820, when all 112 records were available, it was possible to skillfully reconstruct 11 PCs, or temperature patterns, calibrating (and cross-validating) between 30-40% of the total instrumental surface temperature variance, and 70-80% of the instrumental variance in Northern Hemisphere (NH) mean tempeature. As the dataset becomes sparser at earlier times, the number of patterns that can be skillfully reconstructed decreases. Back to AD 1000 roughly 40% of the variance in NH is resolved in calibration and verification. The primary feature of the NH reconstruction, which has sometimes been referred to as the "Hockey Stick", is a gradual decline from A.D. 1000 to the mid-19 th century, significant variation about this trend at interannual and decadal time scales, and then a sudden reversal.

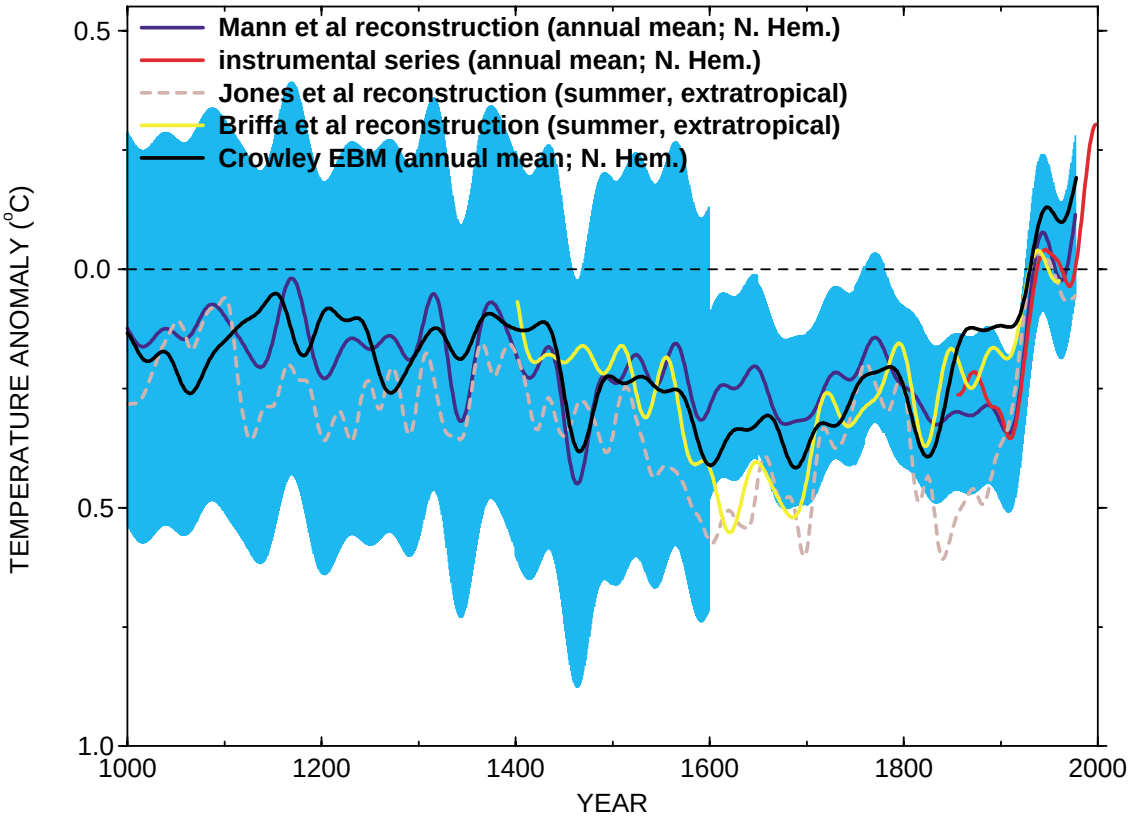


*Fig.1: Comparison of empirical and EBM-estimated millennial changes in Northern Hemisphere annual mean temperatures during the past millennium.*

**Patterns of Decadal Variability**

The primary sources of interannual variability in global surface temperature patterns during past centuries are the ENSO phenomenon (Mann et al., 2000ab) and, in the Northern Hemisphere cold-season, the North Atlantic Oscillation or "NAO" (Cullen et al., 2000; Mann, 2000a). Decadal ENSO-like variability, as well as decadal and multidecadal modulation of interannual ENSO variability, is also a prominent feature in the reconstructed climate of the past few centuries (Mann et al., 2000a). At multidecadal and century timescales, other patterns appear more important. This is particularly true in the North Atlantic sector, where multidecadal and century-scale changes in the North Atlantic Oscillation and related patterns, appear important in describing the regionally prominent "Medieval Warm Period" and "Little Ice Age" of the North Atlantic and neighboring regions (see e.g. Keigwin and Pickart, 1999). There is also evidence, however, that basin-scale changes in North Atlantic sea surface temperatures distinct from the NAO may also play a role in these changes. Black et al. (1999) emphasize prominent tropical Atlantic variability in past centuries at decadal timescales, while Delworth and Mann (2000) highlight (see also Kerr, 2000) the importance of an intrinsic mode of North Atlantic climate variability on multidecadal climate changes in the North Atlantic sector (Mann et al., 1995). The relationship between these interannual, decadal, and multidecadal temperature patterns, and changes in regional drought, and atmospheric circulation patterns is an area of active current research. One possible mechanism is that low-frequency variations have modulated the behavior of ENSO. Significant multidecadal modulation of interannual ENSO teleconnection patterns is evident in past centuries (e.g. Cole and Cook, 1998; Mann et al., 2000a). It is evident, furthermore, that regions such as equatorial east Africa which are influenced by ENSO in modern history, have undergone significant changes in drought/wetness during the past 1000 years (Verschuren et al., 2000). Multidecadal changes in atmospheric circulation, and drought

in North America (Woodhouse and Overpeck, 1998) may be associated with the impacts of a significant pattern multidecadal climate variability originating in the North Atlantic sector discussed above (Delworth and Mann, 2000).

**Forced Variability**

Recent studies invoking statistical comparisons of reconstructions of surface temperature with time series estimates of natural (solar and volcanic) radiative forcing during past centuries (e.g., Lean et al., 1995; Overpeck et al., 1997; Mann et al., 1998; Damon and Peristykh, 1999; Crowley and Kim, 1996; Waple et al., 2000) suggest that both solar and volcanic influences have a detectable influence on decadal and longer-term temperature variations in past centuries. Similar conclusions have been reached in studies that have used these forcing time series to drive energy balance models (EBMs), producing surface temperature estimates that can be compared to empirical temperature reconstructions (Crowley and Kim, 1999; Free and Robock, 1999; Crowley, 2000). Using such an EBM simulation, Crowley (2000) has shown that between 40% and 60% of the decadal and longer-term pre-anthropogenic variability in the Northern Hemisphsere temperature reconstructions of both Mann et al. (1999) and Crowley and Lowery (2000) can be explained in terms of the response to a natural forcing (Figure 1). The 20th century warming, however, requires the additional contribution of anthropogenic (greenhouse gas plus sulphate aerosol) forcing. Crowley's model prediction underpredicts the observed cooling of the the late 19th century, which may arise from albedo changes associated with anthropogenic land-cover changes which are not incorporated in his analysis (see Mann, 2000b). Equally importantly, Crowley shows that the spectrum of the residuals (i.e. the remaining component after this forced variability is accounted for) agrees almost precisely with that of unforced variability from control runs of coupled models, reinforcing the notion that coupled ocean-atmosphere climate models used for "fingerprint detection" of anthropogenic climate change (e.g., IPCC, 1996) provide reasonable estimates of the amplitude of unforced variability at decadal-to-century teimscales. The latter finding reinforces model-based claims of detection and attribution of observed climate change.

**References**


Black, D.E., L.C. Peterson, J.T. Overpeck, A. Kaplan, M.N. Evans, and M. Kashgarian, 1999: Eight Centuries of North Atlantic Ocean Atmosphere Variability. *Science*, **286**, 1709-1713.

Briffa K.R., 2000: Annual climate variability in the Holocene: interpreting the message of ancient trees. *Quaternary Science Reviews*, **19**, 87-105.

Cole, J.E., and E.R. Cook, 1998: The changing relationship between ENSO variability and moisture balance in the continental United States. *Geophys. Res. Lett.*, **25**, 4529-4532.

Crowley, T.J., 2000: Causes of Climate Change Over the Past 1000 Year. *Science*, **289**, 270-277.

Crowley, T.J., and K.Y. Kim, 1996: Comparison of proxy records of climate change and solar forcing. *Geophys. Res. Lett.*, **23**, 359-362.

Crowley, T.J., and K.Y. Kim, 1999: Modeling the temperature response to forced climate change over the last six centuries. *Geophys. Res. Lett.*, **26**, 1901-1904.

Crowley, T.J., and T. Lowery, 2000: How Warm Was the Medieval Warm Period?. *Ambio*, **29**, 51-54.

Cullen, H., R. D'Arrigo, E. Cook, M.E. Mann, 2000: Multiproxy-based reconstructions of the North Atlantic Oscillation over the past three centuries. *Paleoceanography*, in press.

Damon, P.E., and A.N. Peristykh, 1999: Solar Cycle Length and 20th Century Northern Hemisphere Warming: Revisited. *Geophys. Res. Lett.*, **26**, 2469-2472.

Delworth, T.D., M.E. Mann, 2000: Observed and Simulated Multidecadal Variability in the North Atlantic. *Climate Dynamics*, in press.

Free, M., and A. Robock, 1999: Global Warming in the Context of the Little Ice Age. *J. Geophys. Res.*, **104**, 19,057-19,070.

Intergovernmental Panel on Climate Change (IPCC), 1996: Climate Change 1995: The Science of Climate Change, J. T. Houghton et al., Eds., Cambridge Univ. Press, Cambridge.

Jones, P.D., K.R. Briffa, T.P. Barnett, and S.F.B. Tett, 1998: High-resolution palaeoclimatic records for the last millennium: interpretation, integration and comparison with General Circulation Model control run temperatures. *Holocene*, **8**, 477-483.

Keigwin, L.D., and R.S. Pickart, 1999: Slope Water Current over the Laurentian Fan on Interannual to Millennial Time Scales. *Science*, **286**, 520-523.

Kerr, R.A., 2000: A North Atlantic Climate Pacemaker For the Centuries. *Science*, **288**, 1984-1986.

Lean, J., J. Beer, R.S. and Bradley, 1995: Reconstruction of solar irradiance since 1610: Implications for climatic change. *Geophys. Res. Lett.*, **22**, 3195-3198.

Mann, M.E., 2000a: Large-scale climate variability and connections with the middle east during the past few centuries. *Climatic Change*, accepted.

Mann, M.E. , 2000b: Lessons For a New Millennium. *Science*, **289**, 253-254.

Mann, M.E., R.S. Bradley, and M.K. Hughes, 1998: Global-Scale Temperature Patterns and Climate Forcing Over the Past Six Centuries. *Nature*, **392**, 779-787.

Mann, M.E., R.S. Bradley, and M.K. Hughes, 1999: "Northern Hemisphere Temperatures During the Past Millennium: Inferences, Uncertainties, and Limitations." Geophys. Res. Lett., **26**, 759-762.

Mann, M.E., R.S. Bradley, and M.K. Hughes, 2000a: Long-term variability in the El Niño Southern Oscillation and associated teleconnections. In: Niño and the Southern Oscillation: Multiscale Variability and its Impacts on Natural Ecosystems and Society, Eds.: Diaz, H.F. & Markgraf, V. , Cambridge University Press, Cambridge, UK, 321-372, in press.

Mann, M.E. et al., 2000b: Annual Temperature Patterns in Past Centuries: An interactive presentation. *Earth Interactions*, in press.

Overpeck, J., et al., 1997: Arctic environmental change of the last four centuries. *Science,* **278**, 1251-1256.

Verschuren, D., K.R. Laird, and B.F. Cumming, 2000: Rainfall and drought in equatorial east Africa during the past 1,100 years. *Nature*, **403**, 410-414.

Woodhouse, C. A., and J.T. Overpeck, 1998: 2000 years of drought variability in the central United States. *Bull. Amer. Meteor. Soc.*, **79**, 2693-2714.

Waple, A., M.E. Mann, and R.S. Bradley, 2000: Long-term Patterns of Solar Irradiance Forcing in Model Experiments and Proxy-based Surface Temperature Reconstructions. *Climate Dynamics*, accepted.

# Interdecadal Modulation of Australian Climate

**Gerald A. Meehl and Julie M. Arblaster**
**National Center for Atmospheric Research, Boulder, CO, USA**
**meehl@ncar.ucar.edu**

## Introduction

Decadal variability of tropical Pacific SSTs has been shown to be associated with Australian rainfall anomalies in observations (Power et al., 1999). They noted a decadal modulation of interannual teleconnections between El Niño events and Australian rainfall. When tropical Pacific SSTs are warm on the decadal timescale, the interannual correlation between El Niño and La Niña events and Australian rainfall decreases, with the converse being true during periods of anomalously cold tropical Pacific decadal SSTs.

The purpose of this study is to use a global coupled model to study the possible mechanisms that may be producing these decadal climate fluctuations. We analyse the NCAR/DOE Parallel Climate Model (PCM), with a T42 18L atmosphere, a 2/3 degree (down to 1/2 degree in the equatorial tropics) 32L ocean, dynamic and thermodynamic sea ice and the LSM land surface scheme. A general description and simulation results from the PCM are given in Washington et al. (2000). This model has been shown to simulate El Niño amplitude close to observed (Meehl et al. 2000), with the observed negative correlation between interannual Niño3 SSTs and Australian rainfall ($10^{o}$S-$40^{o}$S, $110^{o}$E-$155^{o}$E) of -0.48. A more detailed description of these results appears in Arblaster et al. (2000).

## Results

Power et al. (1999) show that EOF3 of low-pass filtered seasonal SST has an El Niño-like pattern with a decadal timescale but with a more broad off-equatorial maximum in the tropical Pacific, and with like-sign anomalies stretching right across the Pacific. They use the principal component time series of this EOF as an index of the Interdecadal Pacific Oscillation (IPO). They show that in periods of positive IPO (when tropical Pacific SSTs are warm), there is reduced interannual teleconnectivity between El Niño and Australian climate variables, and vice versa for periods of negative IPO.

We derive an IPO index for the PCM by first low-pass filtering surface temperature from the 300 year control run with a 13 year cut-off. The first EOF of the filtered data has many features in common with the IPO pattern of Power et al. (1999). Performing a similar calculation of correlations in 13 year running blocks between SOI and Australian rainfall in the model shows some periods when the observed decadal modulation of interannual teleconnections occurs in the model, but some periods when the relationship does not hold. Since these linkages are intermittent in the model, either the model is not consistently capturing the observed teleconnections, or the limited period of observations (about 100 years) samples only a strong period of decadal teleconnectivity.

We use the model as a tool here to study mechanisms by choosing 3 periods of positive IPO and 3 periods of negative IPO when there is decadal modulation of interannual teleconnections between ENSO and Australian rainfall as in the observations. We then formulate composites of positive and negative IPO to address three possible mechanisms that could be producing the decadal modulation of interannual variability. For periods of positive IPO, 1) A decrease of El Niño amplitude could reduce interannual teleconnections to Australian rainfall, 2) An eastward shift of the rising branch of the Walker Circulation away from Australia during periods of positive IPO could reduce the interannual teleconnections from the tropical Pacific,

and 3) Western Pacific SST anomalies associated with Pacific decadal variability could have a regional influence on Australian rainfall and disrupt the larger scale teleconnections from the central and eastern Pacific.

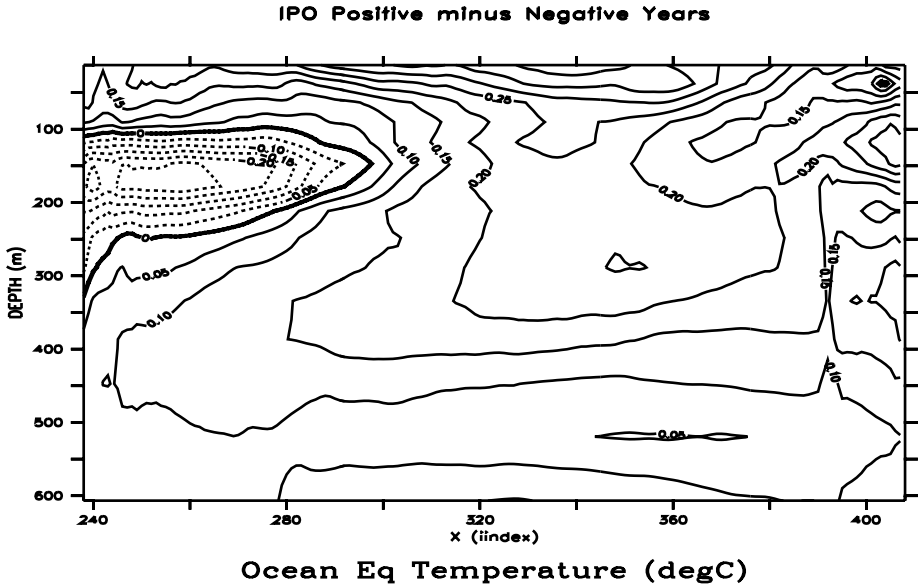


*Fig. 1: Difference, positive minus negative IPO, of upper ocean temperatures along the equator in the Pacific.*

Concerning the first mechanism, the interannual standard deviation for all years of annual Niño3 SST is 0.65°C. For periods of positive IPO, this drops to 0.48°C, and for negative IPO it rises slightly to 0.70°C. This suggests that reduced El Niño/La Niña amplitude during positive IPO could provide less forcing of the large-scale east-west circulation and reduce the interannual correlations between Niño3 and Australian rainfall. The reason El Niño amplitude is reduced during positive IPO is shown in Fig. 1 which is the difference, positive minus negative IPO, of upper ocean temperatures along the equator in the Pacific. A relaxation of the thermocline slope is indicated by negative differences at the depth of the thermocline in the western Pacific near 200m, with positive differences in the central and eastern Pacific. It has been shown that in this model if the thermocline deepens or becomes less intense in the central and eastern Pacific, El Niño variability decreases (Meehl et al., 2000). This is the case here on the decadal timescale.

Fig. 2 illustrates the second mechanism as the difference of 200 hPa velocity potential for positive minus negative IPO periods. The eastward shift of the Walker Circulation in positive IPO periods is indicated by negative differences to the north and east of Australia, and positive differences over Australia. This would essentially contribute to isolating Australia from the centres of action of the east-west circulation in the Pacific and reduce interannual teleconnectivity between Niño3 SSTs and Australian rainfall.

To investigate the third mechanism, we have run AMIP simulations with SSTs in the tropical western Pacific enhanced by 0.5°C, and compared the interannual correlation between Niño3 SSTs and north-east Australian rainfall in that run to an AMIP control run. The correlations decrease from -0.57 in the control run to -0.47 in the warm SST run and -0.44 in the cold SST run. A second set of integrations with anomalously cold and warm SSTs in the western Pacific shows a comparable decrease for both experiments. Since both warm and cold SSTs decrease the inter-annual correlations somewhat, there are two possible interpretations. Since all correlations are still significant at the 10% level, one possibility is that the western Pacific SST variations on the decadal timescale do not significantly affect the interannual teleconnections.

Another possibility is that since in both warm and cold experiments the interannual correlations decrease, any decadal deviation from near the mean state, either positive or negative, changes the base state precipitation regime over northern Australia and disrupts somewhat the interannual teleconnections. Thus neither decadal base state in the western Pacific is preferential in actually increasing interannual teleconnectivity. In either case, the western Pacific decadal SST variations appear to be less of a factor in disrupting the interannual teleconnectivity than the other two mechanisms.

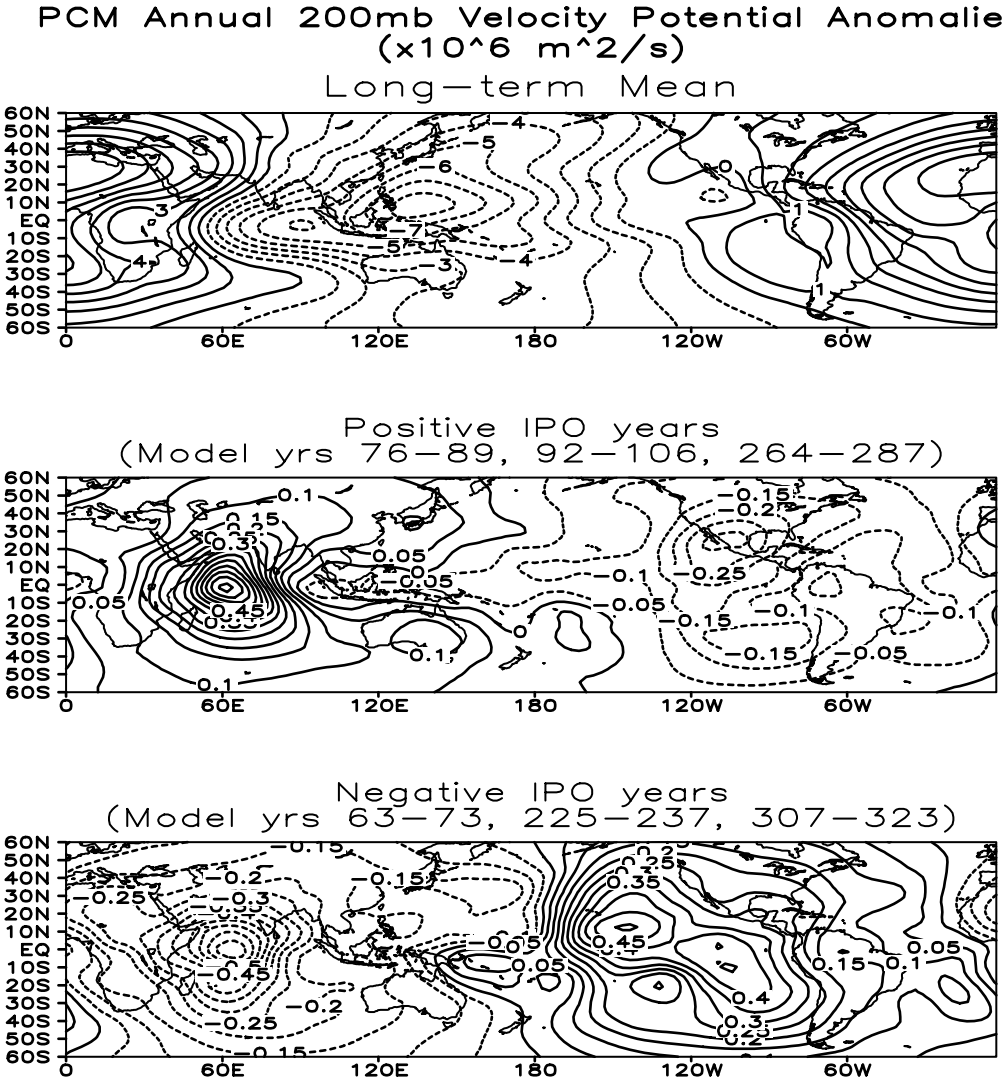


*Fig. 2:* ***a)*** *Annual mean 200hPa velocity potential for a long-term mean. Negative contours indicate rising motion, positive contours indicate sinking motion. Units are* $10^6$ $m^2$ $s^{-1}$*. Anomalies from the long term mean are shown for* ***b)*** *positive interdecadal periods and* ***c*** *negative interdecadal periods of 200 hPa velocity potential for positive minus negative IPO periods.*

**Conclusions**

A global coupled model, the NCAR/DOE PCM, shows some evidence of interannual and decadal links between tropical Pacific SSTs and Australian rainfall. The decadal links are intermittent in the model, suggesting that either the model is not consistently capturing he observed teleconnections, or the limited period of observations (about 100 years) samples only a strong period of decadal teleconnectivity. For decadal periods of positive SSTs in the tropical Pacific in the model when the observed relationship holds:

1. El Niño variability is less, contributing to weaker interannual teleconnections with Australian rainfall.
2. The ascending branch of the Walker Circulation shifts eastward away from Australia and contributes to reduced interannual teleconnections to Australian rainfall.
3. GCM sensitivity experiments show that western Pacific SST anomalies on the decadal timescale can have a regional influence on Australian rainfall, though these SST anomalies appear to be less of a factor in disrupting the interannual teleconnectivity between ENSO and Australian rainfall than the other two mechanisms.

We further examined periods in the model when the interannual and decadal links did not work. These are evidenced by a weaker connection of the IPO to the western Pacific with less influence on the shifts in Walker Circulation and almost no impact on El Niño amplitude. Thus, in the model, for the decadal modulation of interannual variability to work, there must be a sufficiently high amplitude excursion of the IPO with a relatively strong change in base state to allow the disruption of the interannual teleconnections.

**References**


Arblaster, J.M., G.A. Meehl, and A.M. Moore, 2000: Interdecadal modulation of Australian rainfall, *Climate Dynamics*, submitted.

Meehl, G.A., P. Gent, J.M. Arblaster, B.L. Otto-Bliesner, E. Brady, and A.P. Craig, 2000: Factors that affect amplitude of El Niño in global coupled climate models. *Climate Dynamics*, in press.

Power, S., T. Casey, C. Folland, A. Colman, and V. Mehta, 1999: Interdecadal modulation of the impact of ENSO on Australia, *Climate Dynamics*, **15**, 319-324.

Washington, W.M., and co-authors, 2000: Parallel Climate Model (PCM) control and 1%/ year $CO_2$ simulations with a $2/3^o$ ocean model and a 27 km dynamical sea ice model, *Climate Dynamics*, in press.

# Experimental predictions of North Atlantic climate on the decadal time scale

**James Murphy, *Doug* Smith and Steven Murray**
**Hadley Centre, Meteorological Office, United Kingdom**
**jmurphy@meto.gov.uk**

We aim to increase the skill of climate predictions up to about 10 years ahead by initialising a coupled ocean-atmosphere GCM with atmospheric and oceanic observations. This will allow us to predict the evolution of low frequency anomalies arising from natural variability as well as secular trends arising from the response to anthropogenic or natural changes in radiative forcing. Our project focuses mainly on the North Atlantic and Europe, however we use a global coupled model which is initialised by assimilating global data. This allows the possibility of obtaining useful predictions for any part of the globe where the physics of coupled ocean-atmosphere variability leads to potential predictability on seasonal time scales or beyond. Here we report early experiments with the HadCM3 coupled model (Gordon et al., 2000) in which we initialise the ocean with observations and attempt to hindcast the early 1970s. These hindcasts do not include the effects of anthropogenic changes in radiative forcing.

**HadCM3 as a decadal prediction tool**

The model reproduces quite well the observed variability of global mean surface temperature and also possesses a vigorous and generally realistic ENSO cycle (Collins et al., 2000). Its relatively high resolution of 1.25x1.25 degrees in the ocean allows a realistic simulation of heat transports in upper ocean current systems such as the Gulf Stream/ North Atlantic Current (NAC). This enables it to reproduce the observed characteristics of SST anomalies which propagate along the NAC on the decadal time scale. The links between these anomalies and variations in Labrador Sea convection and the North Atlantic Oscillation (NAO) are also simulated in a qualitatively realistic manner (Cooper and Gordon, 2000). On the other hand, observed relationships with North Atlantic SSTs leading the atmospheric circulation are not well captured (Rodwell and Folland, 2000) while the correlation between wintertime atmospheric variability over the North Pacific and North Atlantic oceans is too strong (Collins et al., 2000). Thus HadCM3 possesses a number of characteristics which are essential in a credible seasonal to decadal forecasting tool, however it also possesses significant limitations which will reduce the potential for skilful forecasts in the North Atlantic until they are addressed in future (see Smith et al., 2000, this volume).

**Early attempts to initialise the ocean**

We first tried using the assimilation scheme employed in short range operational ocean forecasting at the Meteorological Office (Bell et al., 2000). Starting from a random state selected from the control integration of HadCM3, temperature and salinity observations made in the upper 1000m during the 1960s (Levitus and Boyer, 1994, Levitus et al., 1995) were assimilated using the iterative analysis correction method of Lorenc et al. (1991). Observations were assimilated as anomalies relative to the model climatology in order to minimise the risk of climate drift once assimilation was switched off. Observations were nudged into the model over a 10 day period assuming that the spatial correlation between observations at different locations follows a second order autoregressive function with an e-folding scale of 300km (increased to 600km near the equator). Sea surface temperatures were strongly relaxed towards monthly global analyses taken from the GISST 3.0 dataset (Rayner et al., 1998). In a typical month temperature observations were available everywhere at the surface but only at 5-15% of model grid boxes sub-surface. Surface or In most parts of the world ocean the model assimilated the observations effectively, however unacceptable biases developed in the north Atlantic in win-

ter, characterised by positive errors in SST, erroneous deepening of the mixed layer and negative temperature errors at the base of the mixed layer. The feedback responsible for these errors is illustrated in Fig. 1: In response to positive SST errors the assimilation scheme generated negative temperature increments which drove convection, thus deepening the mixed layer. This restored the original SST error and created negative errors at the base of the mixed layer, since the sub-surface water is warmer than the surface water at high latitudes in winter. The assimilation scheme then generated further negative increments at the surface and positive increments below, thus driving further deepening of the mixed layer.

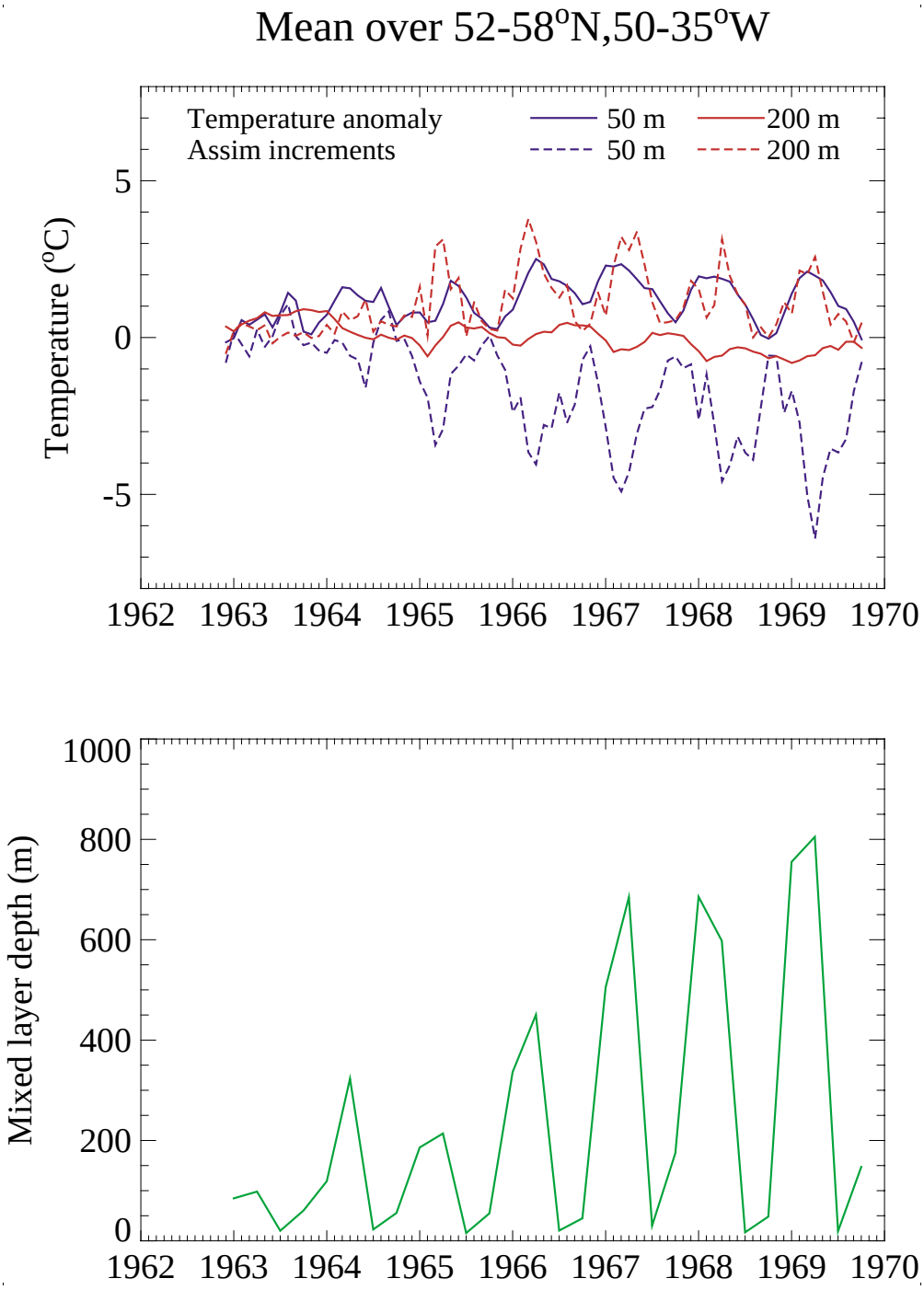


*Figure 1: Monthly temperature anomalies, assimilation increments and mixed layer depths averaged over part of the northern North Atlantic during an experiment using the original assimilation scheme*

The development of the mixed layer feedback implies that the available observations were not being allowed to constrain the model strongly enough during assimilation. Several limitations of the assimilation scheme were identified as likely contributors to this problem:

1. No attempt was made to infer salinity from temperature observations;
2. In most parts of the ocean the correlation scale is much larger than 300km, thus individual observations should influence a much wider area;
3. No account is taken of vertical correlations between observations- for example the SST should be assimilated throughout the mixed layer rather than just at the surface itself.

A simple attempt was made to address (1) by using synthetic salinities chosen to balance the effect on density of temperature increments, however this was only partially successful. It was therefore decided to address all the above shortcomings using a new approach.

**New assimilation scheme**

In the new scheme the influence of available observations is extended by using horizontal and vertical correlations simulated by HadCM3 to infer temperature and salinity values at locations remote to the actual observation sites. In addition local correlations between temperature and salinity are used to infer salinity from temperature. These correlations are used to produce gridded monthly analyses from the raw observations using optimal interpolation (OI). Only statistically significant correlations (greater than 0.5 or less than –0.5) are used in the OI equations. The use of model rather than observed correlations leads to analyses which are consistent with the simulated natural variability of HadCM3 as well as with the available observations.

In OI the analysis at any grid point is computed as a weighted sum of the observations, the weights being chosen to minimise the expected error of the analysis. This involves inverting a KxK square matrix, where K is the total number of observations. In order to reduce the computational burden the analysis was performed in two steps: horizontal followed by vertical. The horizontal step analyses all observations on a given level. This greatly reduces the time needed to analyse sub-surface levels where there are typically less than 1,000 observations in a given month, cf. ~10,000 for SST. The vertical step then spreads information vertically by combining the horizontally analysed data in each model column. Finally the monthly analyses are smoothed in time: this is done by combining each analysis with that from the preceding and following months using OI based on persistence correlations obtained from HadCM3.

It was found that the GISST analyses of SST were often inconsistent with contemporaneous near-surface observations from the Levitus and Boyer dataset, so it was decided to use monthly SST observations from the Comprehensive Ocean-Atmosphere Dataset (COADS) (Slutz et al., 1985), which showed much better consistency with the sub-surface data. Typical results from the analysis procedure are shown in Fig. 2a, b. The horizontal interpolation produces a smoothly varying and complete analysis of SST from the COADS observations. Even at sub-surface levels the horizontal interpolation produces an analysis with relatively few gaps, despite the sparse distribution of raw observations. This reflects the large horizontal correlation scales associated with the patterns of variability simulated by the model. The vertical interpolation substantially increases the weights associated with the sub-surface analysis (the weight is the expected error if climatology is used as the analysis divided by the expected error in the actual analysis), due to the downward propagation of information from the surface. The analysed sub-surface anomalies increase in magnitude, however the large scale pattern remains quite similar to that obtained from the horizontal analysis alone. This suggests that the HadCM3 spatial correlation patterns used to make the horizontal analysis are broadly realistic. The analysis procedure also produces distributions of salinity with relatively few gaps (not shown), obtained by combining salinity values inferred from local temperature with real salinity observations using OI.

The analyses are assimilated into the model by combining them with the model fields, which are assumed to possess an expected error equal to the standard deviation of the model climatology.

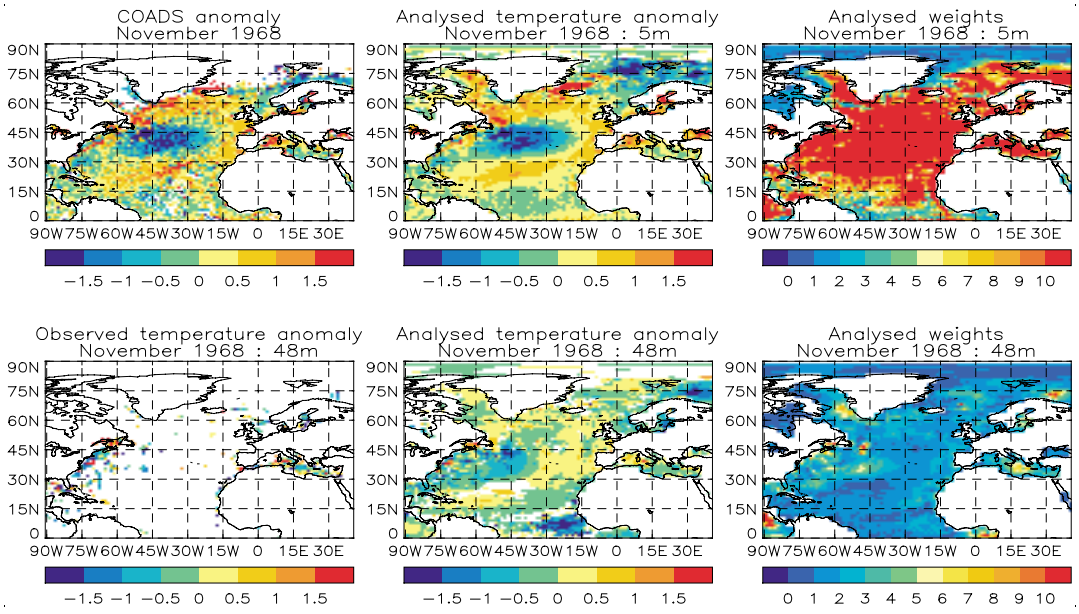


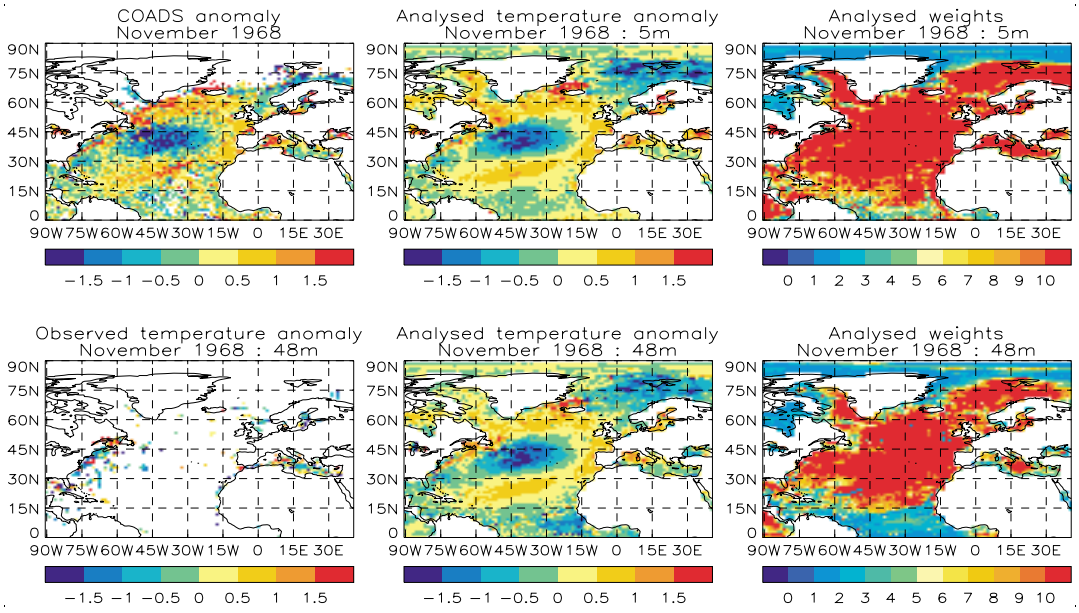


*Figure 2a (upper panels): First-stage analyses of ocean temperature at 5m and 48m for November 1968, and associated weights, derived from a horizontal optimal interpolation (OI) of observations using model correlation statistics*
*Figure 2b (lower panels): Second-stage analyses for November 1968 after combining the horizontal analyses in the vertical OI step*

**Experimental hindcasts**

An experiment was carried out in which observations were assimilated from 1 June 1968 to 30 November 1968 using the new assimilation scheme, following which assimilation was switched off to allow HadCM3 to hindcast the period December 1968 to December 1973. An ensemble hindcast of four members was produced with each member initialised from consecutive days at the end of the assimilation period. A corresponding experiment was carried out using the old assimilation scheme to initialise the hindcast.

During assimilation the model accepts the specified SST anomalies better using the new scheme than the old scheme (Fig. 3). The contrast between the new and old schemes is even more pronounced for sub-surface temperatures. In particular, the new scheme suppresses the mixed layer feedback. The ultimate test for an assimilation scheme, however, is whether it leads to improvements in forecast skill (measured here by the correlation between hindcast and observed anomalies). The new scheme does lead to improved skill in the ocean, both at the surface (Fig. 3) and sub-surface (not shown). This is confirmed by a second hindcast experiment initialised from 1 December 1973. Nevertheless the hindcast skill is significantly below an estimated theoretical upper limit obtained by calculating the average correlation between pairs of ensemble members. This indicates considerable scope for improving skill in future, either by improving the initialisation, the model, or both. Note that the estimated upper limit of skill is itself dependent on the simulated representation of low frequency variability, and could change as the model is improved.

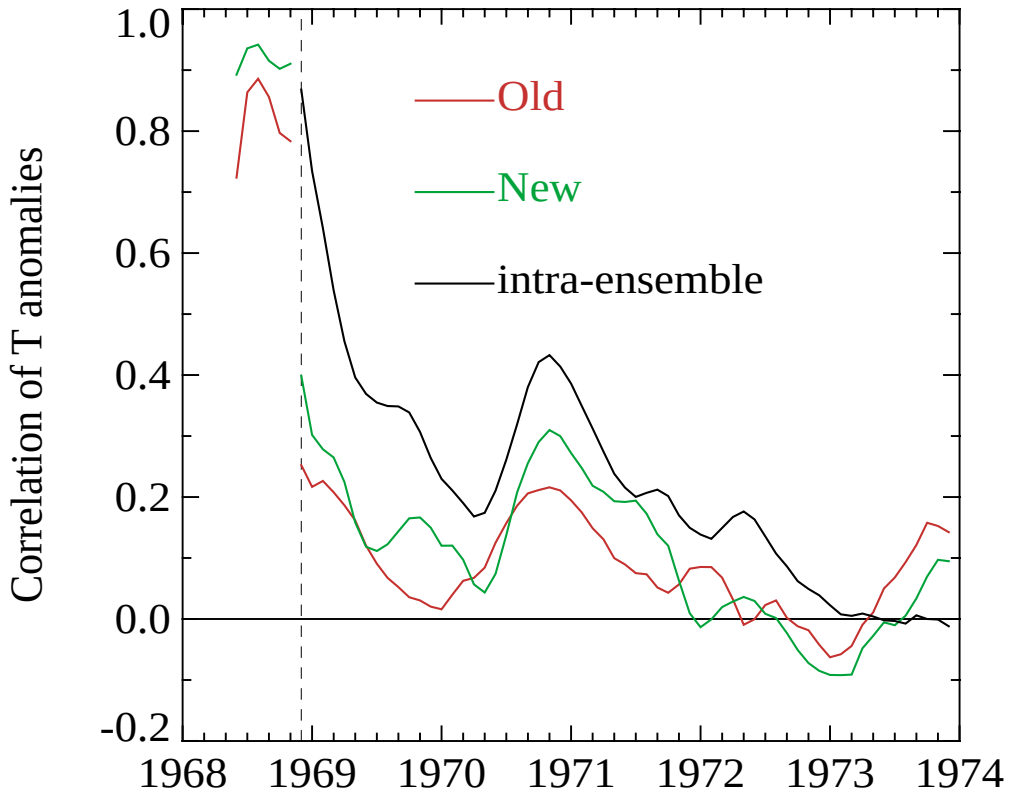


*Figure 3: The red and green curves to the right of the dashed line show the correlation between simulated and observed SST anomalies (5 month running means) during hindcasts initialised from December 1968 following six month assimilations performed using the old and new assimilation schemes. Each hindcast is the mean of a four member ensemble. The black curve is the average correlation between pairs of ensemble members in the hindcast initialised using the new scheme. The curves to the left of the dashed line show the correlations between model SST anomalies and the anomalies being assimilated.*

Figure 3 shows an interesting return of skill during months 18-30 of the hindcast. This is due to a skilful prediction of a La Niña event which occurred in 1970-71 (Fig. 4). The fact that all ensemble members predicted this event at a lead time of 2 years is encouraging, however a large sample of hindcast experiments is needed to determine whether this was fortuitous, or a real indication of predictability beyond the seasonal time scale.

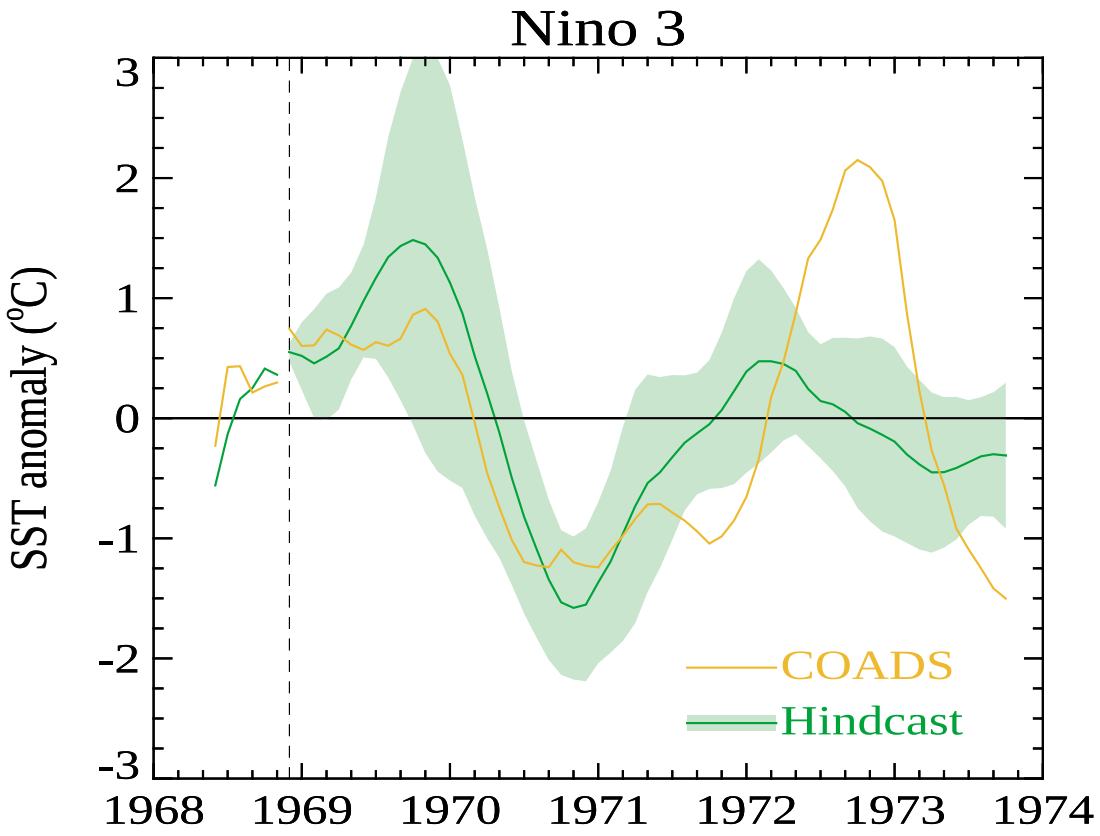


*Figure 4.: Time series of the observed SST anomaly for the Niño3 region (90-150°W, 5°S-5°N) compared with hindcast anomalies from the four member ensemble initialised using the new assimilation scheme. The green curve shows the ensemble mean and the green shading shows the ensemble spread defined by the mean plus and minus one standard deviation.*

**Future developments in initialisation**

We plan a number of improvements to the initialisation of forecasts:

- Assimilation of atmospheric reanalyses into the coupled model

  This will allow us to initialise the wind-driven ocean circulation via atmosphere-ocean coupling during assimilation, and should also improve the initialisation of temperature and salinity via improved specification of surface heat and water fluxes. It will also allow us to start forecasts from the observed atmospheric initial state. The (ERA) reanalyses will be assimilated as anomalies in order to minimise the risk of climate drift in the atmosphere once assimilation is switched off.
- Assimilation of sea surface height anomalies from satellite altimetry

  We will assess the scope for improving ocean initialisation by assimilating global sea surface height observations derived from satellite altimetry during the 1990s. Sea surface height observations will be used to improve analyses of temperature and salinity using correlations obtained from the HadCM3 ocean, consistent with the approach used to generate analyses from temperature and salinity observations.

- Improved specification of model background error during ocean assimilation

  At present the weights for combining the analyses with the model fields are calculated by assuming that the model fields possess a fixed error. In fact the error should vary in space and time, dependent on the data previously assimilated and the error growth characteristics of the model. The assimilation scheme is being refined to update the model error interactively in order to optimise the calculation of the weights during assimilation.

**References**


Bell M.J., R.M. Forbes and A. Hines, 2000: Assessment of the FOAM global data assimilation system for real-time operational ocean forecasting. *J. Mar. Sys.*, **25**, 1-22

Collins M., S.F.B. Tett, and C. Cooper, 2001: The internal climate variability of a version of the Hadley Centre coupled model without flux adjustments. *Climate Dynamics,* **17**, 61-81.

Cooper C., and C. Gordon, 2000: North Atlantic oceanic decadal variability in the Hadley Centre coupled model. *J. Climate*, submitted.

Gordon C., C. Cooper, C.A. Senior, H. Banks, J.M. Gregory, T.C. Johns, J.F.B. Mitchell, and R.A. Wood, 2000: The simulation of SST, sea ice extents and ocean heat transports in a version of the Hadley Centre coupled model without flux adjustments. *Climate Dynamics*, **16**, 147-168.

Lorenc A.C., R.S. Bell, and B. McPherson, 1991: The Meteorological Office analysis correction data assimilation scheme. *Q. J. R. Meteor. Soc*. **117**, 59-89.

Levitus S., and T.P. Boyer, 1994: World Ocean Atlas 1994 Volume 4: Temperature. NOAA/ NESDIS E/OC21, US Dept of Commerce, Washington DC, 117pp.

Levitus S., R. Burgett, and T.P. Boyer, 1995: World Ocean Atlas 1994, Volume 3: Salinity. NOAA/NESDIS E/OC21, US Department of Commerce, Washington, DC,99pp

Rayner N.A., E.B. Horton, D.E. Parker, C.K. Folland, 1998: Versions 2.3b and 3.0 of the global sea-ice and sea surface temperature (GISST) data set. Hadley Centre Internal Note No. 85.

Rodwell M.J., and C.K. Folland, 2000: Atlantic air-sea interaction and seasonal predictability. Q. J.R. Meteor. Soc., to be submitted .

Slutz R.J., S.J. Lubker, J.D. Hiscox, S.D. Woodruff, R.L. Jenne, D.H. Joseph, P.M. Steurer, and J.D. Elms, 1985: Comprehensive Ocean-Atmosphere Data Set; Release 1. NOAA Environmental Research Laboratories, Climate Research Program, Boulder, CO, 268 pp.

Smith D.M., J.M. Murphy, and S. Murray, 2000: Predictability experiments using HadCM3 with a perfectly initialised ocean. See this volume

# Inter-decadal modulation of ENSO's impact on Australia

**Scott Power**
**National Climate Centre, Australia**
**Rob Colman (BMRC) and William Wang (NCC)**
**s.power@bom.gov.au**

**Introduction**

The success of an ENSO-based statistical rainfall prediction scheme and the influence of ENSO on Australia has been shown to vary in association with a coherent, inter-decadal oscillation in surface temperature over the Pacific Ocean. When this Inter-decadal Pacific Oscillation (IPO) raises temperatures in the tropical Pacific Ocean, the relationship between year-to-year Australian climate variations and ENSO weakens substantially (Fig. 1), as does the vigour of ENSO itself (Power et al., 1999).

IPOI=INTER-DECADAL PACIFIC OSCILLATION INDEX
(t-series of UKMO SST EOF)

| Correlation Coefficient between the SOI & | IPOI < -0.5 | IPOI > +0.5 |
|---|---|---|
| Rainfall | 0.7 | 0.0 |
| Murray River flow | 0.4 | 0.1 |
| Temperature | -0.8 | 0.1 |
| Crop yield | 0.7 | 0.1 |

Power, Casey, Colman, Folland & Mehta,1999
Climate Dynamics

NT\COREL\R3157-4

*Figure 1: Shows the correlation coefficients between the SOI and various quantities sensitive to climate variability over Australia. Two sets of correlation coefficients are calculated – one for those decades in which the IPO index is positive (> +0.5) and the other set covering those decades when the IPO index is negative (< -0.5).*

This waxing and waning is also reflected in the skill scores of the prediction scheme, with skill dropping off when the relationships are weak and picking up when they are strong (Figure 2).

The impact of ENSO on Australia is currently being investigated using a 200 year long integration of the BMRC CGCM (Power et al., 1998). This model includes a R21 L17 version of the flux adjusted BMRC AGCM (Colman, 1999; see also Colman and McAvaney, 1995 for more details on where this model originated), a thermodynamic sea-ice model (Colman et al., 1992; Semtner, 1976) and a global version of MOM (Power et al., 1995; Pacanowski et al., 1991; 1993) with 25 vertical levels, a zonal spacing of 2 degrees with a telescopic meridional spacing down to

0.5 degrees near the equator. The model was specifically designed with ENSO and long-term climate change and climate variability in mind. In fact an earlier version of this model was incorporated into a system which is now being used to perform ongoing experimental seasonal predictions (Wang et al., 2000).

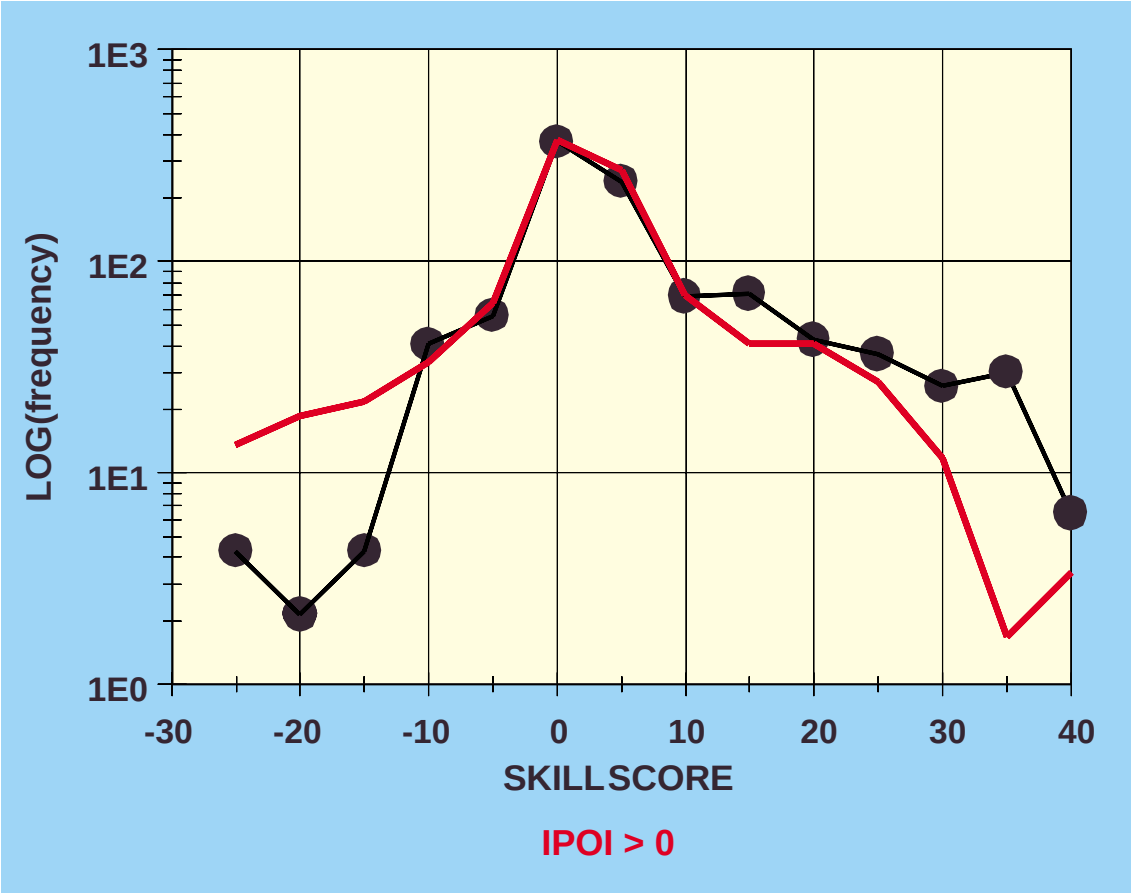


*Figure 2: Frequency distribution of skill scores taken from hindcasts back to 1900 using a statistical prediction scheme for Australian seasonal rainfall anomalies based on the SOI. Positive scores correspond to skillful forecasts. The black line with dots show the scores when the IPO index is negative. The red line shows the scores when the IPO index is positive. Note that the latter has more negative (un-skilful) scores and fewer positive scores. Thus the IPO appears to have modulated our ability to predict seasonal rainfall anomalies over Australia.*

**Results**

The modelled impact of ENSO in this coupled model varies on inter-decadal time-scales. For example, correlation coefficients between NIÑO3 and All-Australia rainfall in running 13 year blocks vary from less than –0.9 to over 0.2 during the 200 year control integration conducted. The key questions being addressed here are: do these inter-decadal changes in the "strength" of the relationship between ENS O and Australia arise randomly or is there something in the system like the IPO which favours decadal periods during which strong or weak teleconnections are favoured? To address these questions we are conducting a number of perturbation experiments each 13 years long. As expected, the predictability of seasonal anomalies in NIÑO4 appears lost in the preliminary experiments after about 2 years or less. Here, however, we are more interested in the predictability and robustness of statistical relationships between ENSO and Australian climate variability on decadal time-scales. Some of the perturbation experiments begin where the teleconnections are strong and others where they are weak. Additional perturbation experiments begin when the IPO is estimated to be in a negative phase and others when the IPO is estimated to be in a positive phase.

## Conclusions

Interesting and potentially important variability in the strength of ENSO-Australia teleconnections have occurred on inter-decadal time-scales over the past century and similar variability occurs in a 200 year long free-wheeling integration of our coupled GCM. Perturbation experiments are being used to help assess the degree to which this variability is predictable by testing the null hypothesis that the variability is a purely random phenomenon. An alternative possibility is that the system is modulated by the IPO and this pre-conditions the climate system to produce either strong or weak ENSO-Australia teleconnections.

## References


Colman, R., J. Fraser, and L. Rotstayn, 2001: Climate Feedbacks in A General Circulation Model Incorporating Prognostic Clouds. Climate Dynamics, in press.

Colman, R., and B. McAvaney, 1995: Sensitivity of the Climate Response of an Atmospheric General Circulation Model To Changes in Convective Parametrization and Horizontal Resolution. *J. Geophys. Res*., **100**, 3155-3172.

Colman, R., B. McAvaney, J. Fraser, and R. Dahni, 1992: Mixed layer ocean and thermodynamic sea-ice models in the BMRC GCM. *BMRC Res. Rep*. No. 30.

Pacanowski, R., K. Dixon, and A. Rosati, 1991: The GFDL MOM users guide, v. 1.0. GFDL Ocean Group, Tech. Rep. No.2, 376 pp.

Power, S., T. Casey, C. Folland, A. Colman, and V. Mehta, 1999: Interedecadal modulation of the impact of ENSO on Australia. *Climate Dynamics*, **15**, 319-234.

Power, S., R. Kleeman, F. Tseitkin, and N. Smith, 1995: A global versiuon of the GFDL modular ocean model for ENSO studies. *BMRC Tech. Rep*., 18 pp.

Power, S., F. Tseitkin, R. Colman, and A. Sulaiman, 1998: A CGCM for seasonal prediction and climate change research. *BMRC Res. Rep*., No. 66, 52 pp.

Semtner, A., 1976: A model for the thermodynamic growth of sea icein numerical investigations of climate. *J. Phys. Oceanogr*., **6**, 379-389.

Wang, G., R. Kleeman, N. Smith, and F. Tseitkin, 2000: Seasonal predictions with a coupled global ocean-atmosphere model. *BMRC Research Report*, Bur. Met., Melbourne, Australia, 34pp

# Anatomy of North Pacific Decadal Variability

**Niklas Schneider, Arthur J. Miller and David W. Pierce**
**Scripps Institution of Oceanography, La Jolla, CA, USA**
**nschneider@sio.ucsd.edu**

Climate variations on decadal time scales have a profound influence on human activities. The possibility of predicting them requires investigating the underlying physics. This entails establishing (a) the relationships and physical linkages between the different variables and (b) the dynamics that set the decadal time scale. In analogy to a simple oscillator, (a) deals with the multi-variate polarization relation or 'anatomy' of decadal variability, while (b) concerns its dynamics.

The purpose of this study is to revisit the coupled model decadal variability investigated by Pierce et al. (2001) and Barnett et al. (1999) in the 128-year ECHO-2 coupled model run. This model is an updated and improved version of the coupled model studied by Latif and Barnett (1994), and hence should contain the 20-year decadal mode whose fundamental physical mechanism has remained uncertain. We seek here to understand the relationships among decadal anomalies of various physical fields in the central Pacific and the Kuroshio-Oyashio Extension (KOE) region, the oceanic heat budgets in the central Pacific and KOE region, possible regional responses of the atmosphere to temperature anomalies caused by ocean dynamics, and the consistency of the evolution of the run with mid-latitude coupled ocean- atmosphere dynamics. In addition, we compare the findings with the available observations. Complete details of our results are given by Schneider et al. (2001).

Our study focuses on model streamfunction variability in the North Pacific which exhibits a strong decadal component especially in the KOE and is clearly due to ocean dynamics (Pierce et al., 2000) but can not be explained by spatial resonance (Saravanan and McWilliams, 1998; Pierce et al., 2000). A complex empirical orthogonal function analysis of streamfunction evolution captures the bulk of its decadal variability and provides via the associated patterns clear linkages with SST, atmospheric pressure, Ekman pumping and precipition. These are shown for a typical magnitude of decadal variability and correspond to half a cycle of the leading CEOF of ocean streamfunction(Fig. 1, 2). Coupled model decadal variability in the North Pacific evolves in accordance with the schematic of Miller and Schneider (2000). Changes of wintertime atmospheric pressure in the North Pacific, primarily due to intrinsic, low-frequency and global atmospheric variability, alter the surface heat budget in the central North Pacific by changing Ekman advection and vertical mixing. This causes the development of the 'canonical' SST anomaly pattern in the central and eastern North Pacific (Fig. 1) where anomalies of opposing signs occur in those two areas (Zhang et al., 1997). The model central Pacific SST anomalies are then subducted southwestward towards the equator while diffusion extinguishes them.

Anomalies of Ekman pumping associated with changes of the North Pacific sea level pressure excite changes of the oceanic stream function. Its anomalies (Fig. 2) are a superposition of a larger-amplitude stationary forced response and a smaller-amplitude westward propagating component associated with long Rossby waves. On average, the KOE region is affected up to five years after anomalies in the central Pacific reach their maximum. In the KOE region, the changes of the geostrophic circulation persist year-round. During summer, subsurface temperature anomalies are insulated from the atmosphere by the seasonal thermocline and attain largest values, while the anomalies at the sea surface are small. During winter, deep mixed-layers bring the subsurface anomalies to the surface and lead to KOE SST anomalies with the same sign as the preceding SST anomalies in the central Pacific (Fig. 1). The associated anomalous heating of the surface layer is vented to the atmosphere by changes of the turbulent

surface heat fluxes (mainly latent). These anomalous surface conditions lead to anomalous precipitation in the western boundary region, such that warm SSTs and increased transfer of sensible and latent heat from the ocean to the atmosphere coincide with increased precipitation. Thus the atmosphere responds locally to oceanically induced KOE surface flux anomalies.

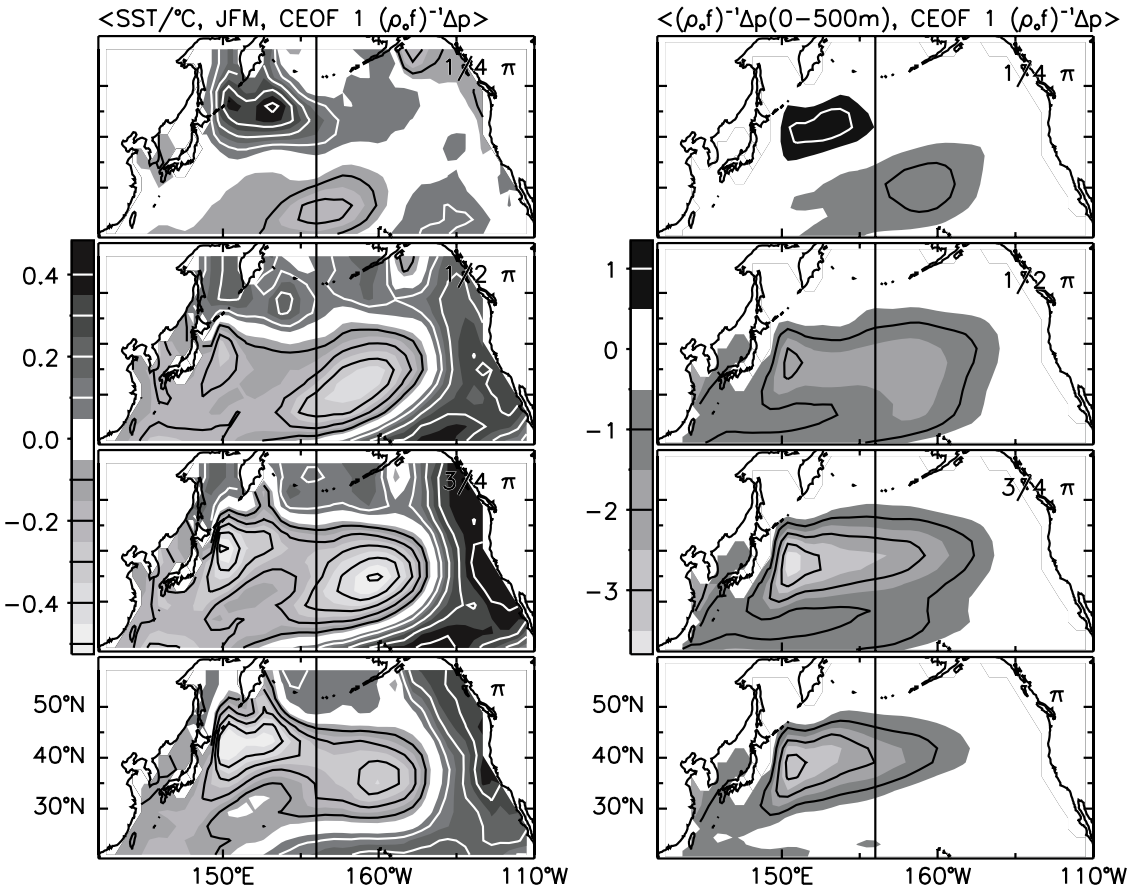


*Figure 1 (left): Decadal anomalies of winter sea surface temperature (January through March). The anomalies are scaled to a typical magnitude and are in units of degree K. Panels are approximately 3 years apart and corresponds to half a cycle of decadal variability*
*Figure 2 (right): Decadal anomalies of oceanic stream function, vertically integrated between the surface and a depth of 500m. Units are $10^3 m^2 s^{-1}$. The sequence of panels correspond to Fig. 1.*

The response of the wind stress suggests a positive feedback, with anomalies of wind-stress curl over the western North Pacific reinforcing the existing KOE anomalies. This result is based on experiments with an equivalent barotropic ocean model that captures the dynamics of linear, forced, mid-latitude Rossby waves and is successful in reproducting the results of the coupled model (Fig. 3, left panel).

Experiments with this simple model suggest that the decadal time scale of the KOE variability results from the integration along Rossby wave trajectories of stochastic forcing due to internal atmospheric dynamics (Fig. 3, centre). The positive feedback of pressure in the KOE region with North Pacific wind stress curl enhances the low frequency variability of the ocean stream function due to a reddening of the spectra of wind stress curl (Fig. 3, right).

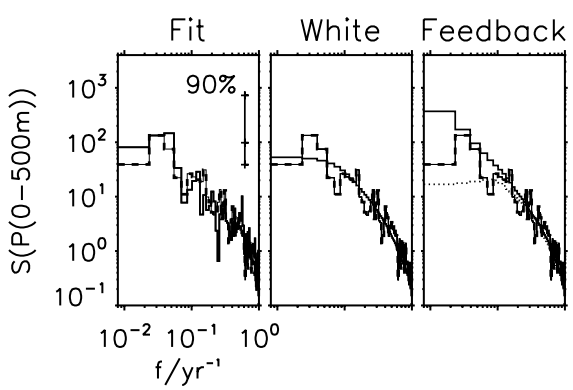


*Figure 3: Spectral power of ocean pressure at 151$^o$E, averaged from 34$^o$N to39$^o$N and integrated vertically over the top 500 m of the water column. The left panel shows spectra for results of ECHO-2 (solid line) and from the best fit solution to an equivalent barotropic Rossby wave forced by ECHO-2's wind stress curl (dashes connected by thin line). This spectra is repeated as a reference on the centre and right panels. The centre panel shows as a solid line the spectrum expected for wind stress curl that has a white frequency spectrum while conserving the spatial coherences and variances of ECHO-2. The right panel displays as a solid line the solution with positive feedback estimated from results of ECHO-2. The dotted line shows results for the same feedback, but with reversed sign.*

It does not, however, select a time scale. The inconsistency of a negative feedback with model results (Fig. 3, right) and the absence of a closed feedback loop are inconsistent with the assumptions often invoked in simple coupled models of North Pacific decadal variability. Instead, the results are consistent with the stochastically forced ocean model of Frankignoul et al. (1997) with a local atmospheric response to SST that may act as a positive feedback.

Comparisons with observations confirm the coupled model results. In both observations and model, decadal anomalies of atmospheric forcing and SST are largest during winter. The SST anomalies occur in two centres of action (c.f.: Deser and Blackmon, 1996; Nakamura et al., 1997): first in the central North Pacific, and then, with like sign and a lag of up-to-five years, in the KOE region.

There, the latent heat flux damps the SST anomalies consistent with an oceanic, rather than an atmospheric, generation (Cayan, 1992; Battisti et al., 1995; Xie et al., 2000). This points to the role of gyre adjustment in linking anomalies in the central Pacific to those in the KOE region with a lag of up-to-five years (Deser et al., 1999; Miller et al., 1998) and implies that observed anomalies in the KOE region can be predicted from the preceding wind stress forcing over the central North Pacific (Schneider and Miller, in preparation, 2001). Prediction of SST anomalies in the KOE region several years in advance could aid the study of sardine fisheries and zooplankton populations which are sensitive to oceanic temperature.

Likewise, if KOE temperature anomalies drive an atmospheric response in nature that is similar to the coupled model, precipitation over the northwestern North Pacific (and perhaps concomitant climate anomalies elsewhere in the Northern Hemisphere) could also be predicted at several-year lead time. Thus, even in the absence of a closed feedback loop, the time horizon of such predictions is several years, and could be of significant value to society.

**Acknowledgments**

We gratefully acknowledge financial support from NSF (OCE-9711265), DOE (DE-FG03-98ER62605) and NOAA through ECPC (NA77RJ0453) and CORC (NA47GP0188), and computer time from NCAR (SCD and CSL) and NERSC.

**References**


Barnett, T. P., D. W. Pierce, M. Latif, D. Dommenget, and R. Saravanan, 1999: Interdecadal interactions between the tropics and midlatitudes in the Pacific basin. *Geophys. Res. Lett*., **26**, 615-618.

Cayan, D. R., 1992: Variability of latent and sensible heat fluxes estimated using bulk formulae. *Atmos.-Ocean*, **30**, 1-42.

Deser, C., and M. L. Blackmon, 1995: On the relationship between tropical and North Pacific sea surface temperature variations. *J. Climate*, **8**, 1677-1680.

Deser, C., M. A. Alexander, and M. S. Timlin, 1999: Evidence for a wind-driven intensification of the Kuroshio Current Extension from the 1970s to the 1980s. *J. Climate*, **12**, 1697-1706.

Frankignoul, C., P. Müller, and E. Zorita, 1997: A simple model of the decadal response of the ocean to stochastic wind forcing. *J. Phys. Oceanogr*., **27**, 1533-1546.

Latif, M., and T. P. Barnett, 1994: Causes of decadal climate variability over the North Pacific and North America. *Science*, **266**, 634-637.

Miller, A. J., D. R. Cayan, and W. B. White, 1998: A westward intensified decadal change in the North Pacific thermocline and gyre-scale circulation. *J. Climate*, **11**, 3112-3127.

Miller, A. J., and N. Schneider, 2000: Interdecadal climate regime dynamics in the North Pacific Ocean: Theories, observations and ecosystem impacts. *Prog. Oceanogr*., **27**, 257-260.

Nakamura, H., G. Lin, and T. Yamagata, 1997: Decadal climate variability in the North Pacific during recent decades. *Bull. Am. Meteor. Soc.*, **78**, 2215-2225.

Pierce, D. W., T. Barnett, N. Schneider, R. Saravanan, D. Dommenget, and M. Latif, 2001: The role of ocean dynamics in producing decadal climate variability in the North Pacific. *Climate Dynamics*, submitted.

Saravanan, R., and J. C. McWilliams, 1998: Advective ocean-atmosphere interaction: An analytical stochastic model with implications for decadal variability. *J. Climate*, **11**, 165-188.

Schneider, N., A. J. Miller, and D. W. Pierce, 2001: Anatomy of North Pacific Decadal Variability. *J. Climate*, sub judice.

Xie, S. P., T. Kunitani, A. Kubokawa, M. Nonaka, and S. Hosoda, 2000: Interdecadal thermocline variability in the North Pacific for 1958-1997: A GCM simulation. *J. Phys. Oceanogr.*, **30**, 2798-2813.

Zhang, Y., J. M. Wallace, and D. S. Battisti, 1997: ENSO-like interdecadal variability: 1900-93. *J. Climate*, **10**, 1004-20.

# Looking for the role of the ocean in tropical Atlantic decadal climate variability

**Richard Seager, Yochanan Kushnir, Naomi Naik, John Chiang and Jennifer Miller**

**Lamont-Doherty Earth Observatory of Columbia University, Palisades, NY, USA**

**rseager@ldeo.columbia.edu**

## 1.Introduction

Interannual variability of tropical Atlantic SST and the location of the Atlantic ITCZ display a strong mutual relationship, particularly during the boreal spring season.In this relationship ITCZ location is linked to the basin-wide cross equatorial SST gradient, (Hastenrath and Greischar, 1993; Nobre and Shukla, 1996; Ruiz- Barradas et al., 1999; Sutton et al., 2000). When the SST gradient anomaly is positive, the ITCZ stays north of its normal position, particularly during boreal spring. The opposite is true when the anomalous SST gradient is reversed. This pattern of variability exhibits decadal time scales that have puzzled scientist (e.g., Mehta and Delworth, 1995; Carton, 1997; Rajagopalan et al., 1998). Understanding the mechanisms governing this variability is of importance to the semi-arid regions of northeast Brazil and west Africa because rainfall there is governed by the location of the ITCZ (Hastenrath and Heller, 1977).

During the last decade or so oceanographers began to suggest that it is the tropical Atlantic ocean that sets the pace for the decadal time-scale of the ITCZ/SST gradient fluctuations. They have argued that it is the interaction between atmospherically forced SST anomalies and the slow, meridional, upper-ocean circulation that gives rise to the quasi-periodic oscillation of SST north and south of the equator and, in turn, the location of the ITCZ (Chang et al., 1997; Xie, 1999). While the proposed mechanisms differed in details they both call upon a positive heat flux – SST feedback in the trade wind regions offset by advection of the upper ocean temperature anomaly.

In an effort to understand the mechanisms governing SST variability in the tropical Atlantic basin we recently conducted a study in which a hierarchy of ocean models was forced by observed surface winds between 1958-1997 (Seager et al., 2001). Each of the ocean models was coupled to a two-dimensional advective atmospheric mixed layer model (AML) that given the wind field, interacts with the predicted SST to produce consistent surface heat fluxes.(for more details about the AML see Seager et al., 1995). These ocean model experiments show that SST variability in the region can be well simulated in an ocean model in which the 3-dimensional flow field is held fixed at its climatological value (see Fig. 1). Based on these considerations we construct a simple model to describe the evolution of zonally averaged SST anomalies in the tropical Atlantic Basin from a linear balance between atmospheric heat flux forcing and mean ocean advection. We will hereafter refer to this model as SAM (for simple Atlantic Model).

The link between the ITCZ location and the gradient of SST across the equator has been interpreted as the atmospheric response to the latter (e.g., Saravanan and Chang, 2000; Sutton et al., 2000). This motivated us to devise a statistical model that predicts ITCZ-associated meridional winds across the equator based on the SST anomaly. With this statistical model we create a simple coupled system (hereafter CSAM) in which SST anomalies in the trade-wind regions north and south of the equator are forced by random, "white-noise" wind fluctuations, generating a coupled atmospheric wind response close to the equator. This paper describes early results from the integration of SAM and CSAM aimed at studying the mechanisms of decadal variability in the region.

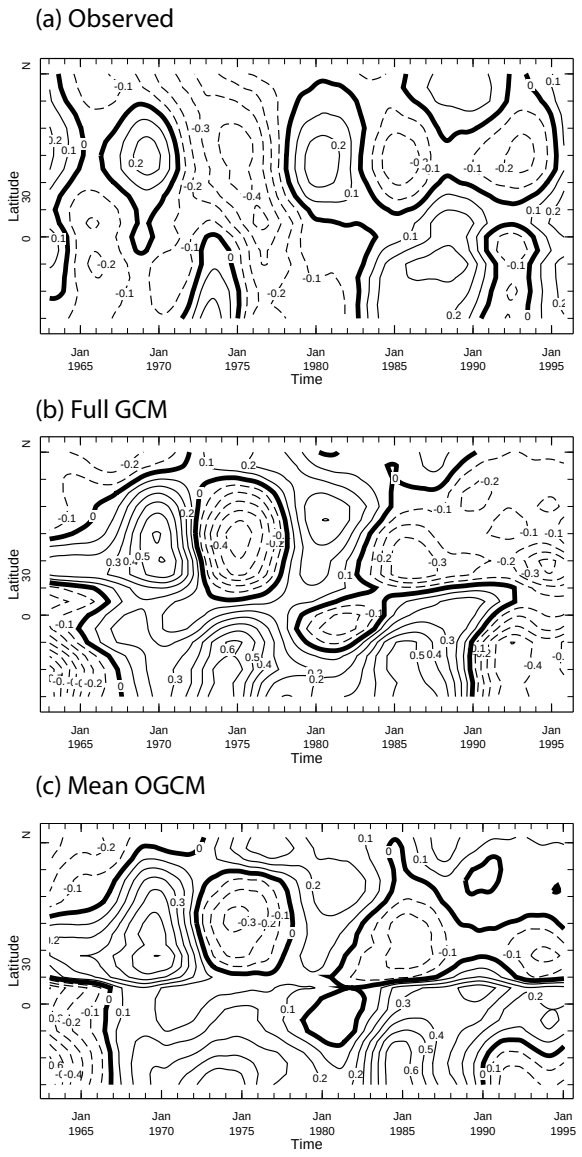


*FIigure 1: Results from two ocean model simulations of tropical Atlantic decadal SST variability 1958-1997 compared with observations.The model simulations are described in Seager et al.(in press.) and briefly in the text above. SST is low-pass filtered with two applications of a 36-months running means and zonally averaged across the basin.Shown are: (a) observed values (from NCEP/NCAR "reanalysis" data); (b) a full ocean GCM simulation; (c) a simulation with an ocean GCM in which the 3-dimensional flow field is kept at its climatological value.*

## 2. Model formulation

Because SST variability in the tropical Atlantic Basin is largely Zonally Symmetric, and because the leading mechanism of SST variability, as found in our three dimensional modelling study (Seager et al., in press and see above Fig. 1) is a balance between latent heat flux forcing and damping by the mean meridional flow in the ocean, we write down the equations governing zonally averaged SST as:

(1)

$$\frac{\partial T'}{\partial t} + \overline{v}_o \frac{\partial T'}{\partial y} + \frac{\overline{w}_o T'}{H} = -\frac{Q_{LH}'}{\rho c_p H}$$

where
T′ = SST anomaly,
$\overline{v}_o$ = mean ocean meridional current
$\overline{w}_o$ = mean ocean upwelling
$Q'_{LH}$ = latent heat flux anomaly, and
$H$ = mixed layer depth

All variables are zonally averaged.

The latent heat flux is derived from a linearized version of the Seager et al. (1995) advective atmospheric mixed layer model so that: (2)

$$Q'_{LH} = \rho_a L h \left( v_a \frac{\partial q_a'}{\partial y} + v_a \frac{\partial \overline{q}_a}{\partial y} \right) + \rho_a L C_E \mu (|\boldsymbol{u}'| \bar{q}_a + |\bar{\boldsymbol{u}}| q_a')$$

Where:
$\rho_a$ = density of air,
$h$ = depth of the atmospheric mixed layer,
$L$ = latent heat of evaporation,
$C_E$ = the exchange coefficient,
$v_a$, $v'_a$ = mean and anomalous atmospheric meridional wind
$\bar{q}_a$, $q'_a$ = mean and anomalous atmospheric humidity,
$|\bar{\boldsymbol{u}}|$, $|\boldsymbol{u}'|$ = mean and anomalous wind speed.

The model makes the simplification that the relative humidity in the air above the sea surface is constant, given by:
(3)

$$\delta = \frac{q_a}{q_s} = (1+\mu)^{-1} \approx 0.8$$

where $q_s$ is the saturation specific humidity at the sea surface. This allows us to express the anomalous air humidity in terms of the SST anomaly:
(4)

$$q_a' = \delta\left(\frac{\partial \overline{q_s}}{\partial T}\right)T'$$

When (4) is substituted for $q_a$ in (2) and (2) is substituted in (1) we can solve the latter for $T'$ given $|u'|$ and $v'_a$. We derive this solution numerically on a 2° latitudinal grid from 29°S to 29°N, using a time step of one month. Monthly mean values of $|u'|$ and $v'_a$ are taken from observations as are the climatological values of the atmospheric variables (the corresponding anomalies and long-term means of the NCEP/NCAR "reanalysis" fields). The oceanic variables are taken from the full GCM integration described in Seager et al. (in press).

### 3. Forcing with observed winds

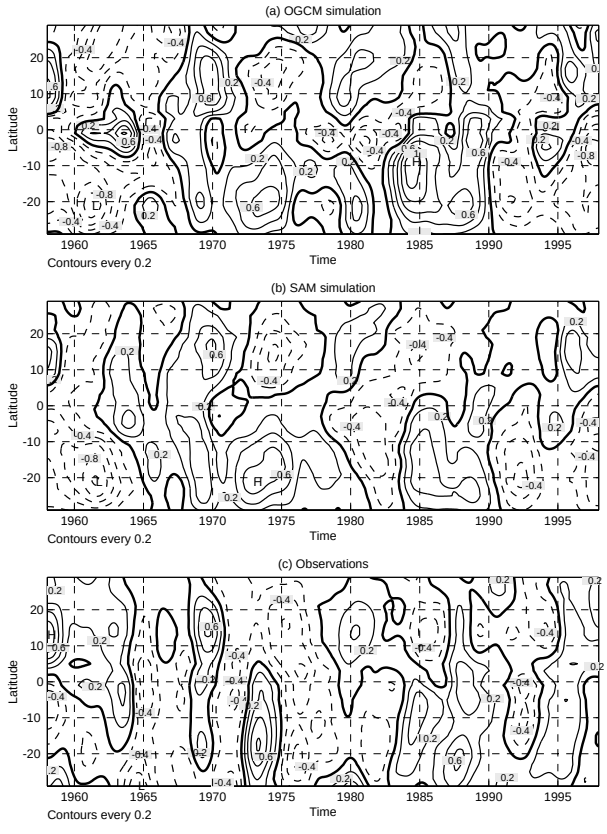


The results from the model run forced with observed (NCEP/NCAR "reanalysis") monthly winds for the interval 1958-1997 are shown in Fig. 2. Clearly SAM is successful in reproducing the full-and mean-ocean GCM results obtained with two-dimensional wind forcing when it comes to the low-frequency (decadal) part of the SST field. The SAM simulation displays somewhat smaller SST anomalies but their evolution is similar to those of the full GCM. This indicates that SAM can provide insight into the mechanisms responsible for decadal SST variability in the tropical Atlantic Basin. We thus feel justified in proceeding to build a statistical model of the interaction between the tropical Atlantic wind systems and the SST so we can study the coupled ocean-atmosphere aspect of the problem.

*Figure 2: A comparison between the SST simulation of (a) a full ocean GCM forced with the 2-dimensional wind field and (b) the SAM forced with the zonally averaged windspeed and meridional wind. Observations are shown for comparison in (c). All SST fields were low-pass filtered to emphasize fluctuations with periods longer than 3-years and zonally averaged in (a) and (c). Contour interval is 0.2°C negative contours are dashed.*

## 4. The statistical atmosphere model

Using observed monthly mean winds and SST, zonally averaged across the tropical Atlantic Basin, we derive a statistical representation of the joint evolution of ocean and atmosphere in the region. The statistical analysis rests on the calculation of the wind and SST EOFs, selecting a subset of the leading patterns, and looking for the relationship between them in a procedure akin to canonical correlation analysis (CCA, see Barnett and Preisendorfer, 1987).

### 4.1 Trade wind EOFs

First we calculated EOFs of the zonally averaged windspeed on a 2°-latitude grid from 29°S to 29°N.The two leading patterns (Fig. 3 below) correspond to uncorrelated (on monthly time scales) fluctuations in the strength of the trade winds north and south of the equator. Together both EOFs explain ~57%of the total variance. These fluctuations correlate with fluctuations in local SST but the relationship here is clearly that of the former forcing the latter, and is thus reproducible by the ocean model component (SAM). Thus in the statistical model, the first two windspeed EOFs are viewed as external forcing agents, which we shall assume follow an entirely stochastic time evolution and lacking a preferred time scale. Note that the two EOFs are not well separated, as their variances are quite similar. They are however, well separated from the higher order EOFs.Thus they can be used for the purpose of reducing the dimension of the domain- wide windspeed variability. Care must be taken however, not to interpret these patterns as indicative of physical "modes" of variability.

### 4.2 SST-meridional wind relationship

When the leading EOFs of monthly averaged meridional wind are correlated with the leading EOFs of SST in a CCA analysis, a clear coherent pattern emerges in which variations in the cross equatorial flow are linked to the variability in the north-south SST gradient (Fig. 4). When anomalous SST in the Northern Hemisphere is warmer than in the Southern Hemisphere, the wind is directed northward across the equator with a maximum at about 5°N. The north-south SST gradient seems to be dominated by variability north of the equator. This picture is entirely consistent with the two dimensional analysis of Nobre and Shukla (1996). In the analysis we used two SST EOFs and three meridional wind EOFs. The resulting pattern explains 16% of the total SST variance and 28% of the meridional wind variance. Locally, in the Northern Hemisphere SST maximum and in the equatorial wind maximum the variance explained reaches ~50% and ~90% of the SST and wind variance, respectively.

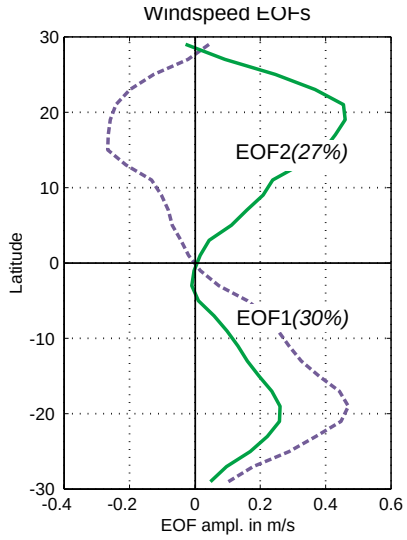


*Figure 3: The leading EOFs of tropical Atlantic monthly windspeed variability. The numbers in parentheses are the percent of total variance explained by each pattern.*

Note that the SST meridional wind relationship is such that in the vicinity of the equator a positive feedback occurs between the two fields. This is because the zonally-averaged windspeed is affected as well (see Fig. 4). When the cross-equatorial meridional wind perturbation is positive, windspeed weakens north of the equator, over the warm SST anomaly, and intensifies south of the equator, over the cold SST anomaly.

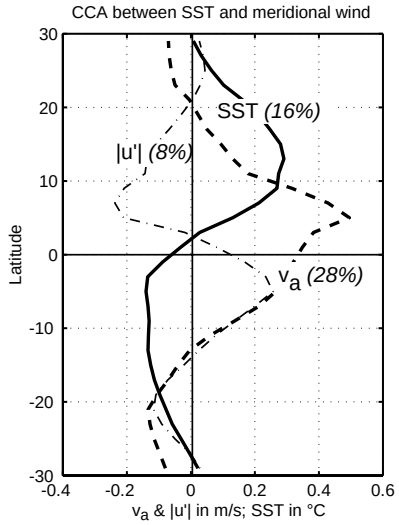


*Figure 4: The leading pattern of the canonical correlation analysis between SST and meridional wind ($v_a$). Also shown is the projection of the zonally- averaged windspeed field ( | u ' | )on the CCA "mode "of meridional wind.The numbers in parentheses are the percent of total variance explained by each pattern.*

### 4.3 SST simulation with EOF winds

To test the ability of the statistical model to simulate the observed SST variability we forced the SAM using windspeed anomalies reconstructed from the first two leading EOFs of that field. The meridional wind changes in the trade wind belts was also included by fitting the observed variability to the windspeed one, using simple linear regression. We then feed the model generated SST anomalies to the statistical CCA model to generate a meridional wind respond with a realistic sign and meridional pattern (specifically, we projected the SST field on its CCA pattern and used the derived amplitude to appropriately scale the CCA pattern of meridional wind). We also add to the windspeed anomaly field a component corresponding to the change in the "predicted" meridional wind (see Fig. 4). The results of this simulation are shown in Fig. 5 below.

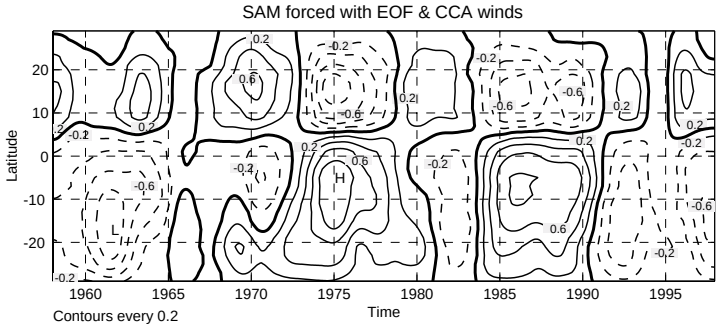


*Figure 5: As in Fig.2(b)but with SAM forced with EOF reconstruction of the windspeed and the CCA model for the cross-equatorial meridional wind response.*

## 5. Coupled model

We couple the SAM to the statistical model of the tropical wind system in the following way:

a. A random time amplitude with no preferred time scale (Gaussian white noise) is imposed on the first two EOFs of the zonally-averaged windspeed which peak in the middle of the trade wind regions.
b. Together with that random amplitude we also perturb in a consistent manner the zonally-averaged meridional wind using a linear regression based on observations.
c. The model calculated zonally-averaged SST field is then projected on the EOFs of the observed SST EOFs, and the results are used to calculate the zonally-averaged, cross-equatorial meridional wind response according to the CCA analysis.
d. The zonally averaged windspeed is modified in a manner consistent with the meridional wind perturbation using a linear fit based on observations.

With this formulation, the model is continuously forced by "noise" in the trade wind region. The slowly responding ocean mixed layer presumably imposes its time scale of a few months on the SST evolving anomalies. However, the feedback in the equatorial region, where the meridional wind response in significant, may impose an even longer time scale. We turn to the model to see if this is so.

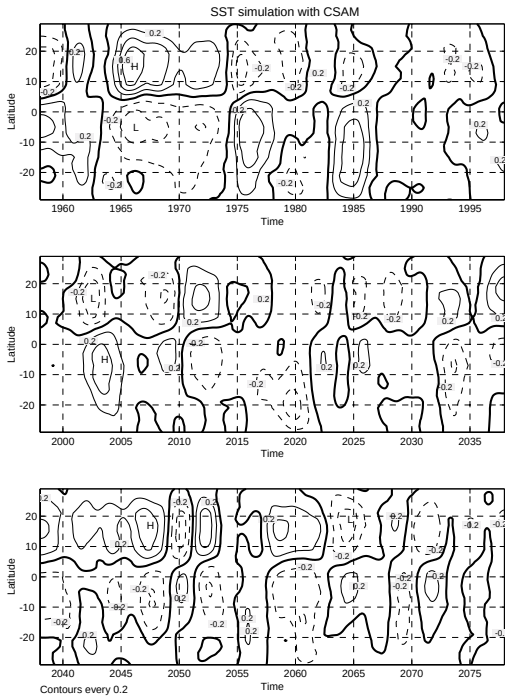


*Figure 6: A 120-year evolution of the SST field simulated by CSAM -the statistically coupled simple model of the zonally averaged tropical Atlantic ocean- atmosphere interaction. The model was forced with "white-noise" windspeed variability with a spatial structure depicted by the two EOFs of Fig. 3. Contours as in Fig. 2 above. Data were filtered with lowpass cutoff of 3-years. Time was arbitrarily set to start in January 1958.*

Fig. 6 shows an extended (120-year) simulation of SST in a coupled model run. The data were lowpass filtered to emphasize fluctuations with a time scale longer than 3-years. Clearly the model generates "decadal" SST variability even when its forcing has no preferred time scale. The spectrum of this simulation is shown in Fig. 7. The striking feature about these decadal anomalies is that they tend to form a dipole, such when SST is colder than normal north of the equator it is warm to the south. This tendency of the model to produce dipole-like features can be seen in the runs forced with the EOF expansion of the observed winds (Fig. 5 above). Apparently, the statistical atmospheric model is giving rise to this consistent equatorial asymmetry through the strong coupling between SST and the meridional wind along the equator. The issue of whether SST variability in the tropical Atlantic is "dipole-like" has been extensively discussed in the literature (e.g., Houghton and Tourre,1992; Rajagopalan et al., 1998; Enfield et al.,1999; Tanimoto and Xie, 1999). The observed SST field (Fig. 3c above) does not support such anti-symmetric behaviour.

## 6. Conclusions

A simple, two-dimensional, coupled linear model of the tropical Atlantic Basin was constructed to study the mechanisms of decadal variability in this region. We find that when the model is forced with observed wind anomalies, it is able to simulated aspects of the observed SST variability and is even more successful is reproducing the SST variability in a full three-dimensional ocean GCM forced with observed winds.

The coupling between the meridional SST gradient and the meridional surface wind component in the equatorial region appears to produce very long time-scale variability in the entire domain. This is despite the fact that the model is forced with "white-noise" windspeed variations off the equator, in the core of the trade- wind belts. The resulting low-frequency SST fluctuations north and south of the equator are strongly negatively correlated, unlike the impression given by the observations. This could be because of the built in atmosphere-ocean coupling is too strong or because the variability in nature is affected by other process, not well represented in this model. We plan to use the model for further study of the role of ocean advection and ITCZ-SST coupling in regional climate variability.

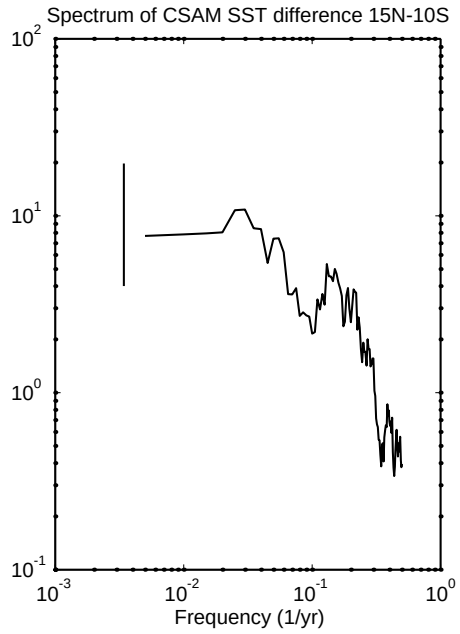


*Figure 7: Power spectral density of an SST index calculated from CSAM forced with "white-noise" windspeed variability (see Fig. 6). The index is the SST anomaly difference between 15°N and 10°S.The vertical bar to the left of the curve is the 95% confidence interval for all frequencies.*

## 7. References


Barnett, T.P., and R.W. Preisendorfer, 1987: Origin and levels of monthly and seasonal forecast skill for United States surface air temperatures determined by canonical correlation analysis. *Mon. Wea. Rev.*, **115**, 1825-1850.

Carton, J.A., 1997: See-saw sea. *Nature*, **385**, 487-&.

Chang, P., L. Ji, and H. Li, 1997: A decadal climate variation in the tropical Atlantic Ocean from thermodynamic air-sea interactions. *Nature*, **385**, 516-518.

Chang, P., R. Saravanan, L. Ji, and G.C. Hegerl, 2000: The effect of local sea surface temperatures on the atmospheric circulation over the tropical Atlantic sector. *J. Climate*, **13**, 2195 –2216.

Enfield, D.B., A.M. Mestas-Nunez, D.A. Mayer, and L. Cid-Serrano, 1999: How ubiquitous is the dipole relationship in tropical Atlantic sea surface temperatures? *J. Geophys. Res.*, **104**, 7841-7848.

Hastenrath, S., and L. Heller, 1977: Dynamics of Climatic Hazards in Northeast Brazil. *Quart. J. Roy. Meteor. Soc.*, **103**, 77-92.

Hastenrath, S., and L. Greischar,1993: Circulation Mechanisms Related to Northeast Brazil Rainfall Anomalies. *J. Geophys. Res.*, **98**, 5093-5102.

Houghton, R.W., and Y.M. Tourre, 1992: Characteristic low-frequency sea surface temperature fluctuations in the tropical Atlantic. *J. Climate*, **5**, 765-771.

Mehta, V.M., and T. Delworth, 1995: Decadal Variability of the Tropical Atlantic-Ocean Surface-Temperature in Shipboard Measurements and in a Global Ocean- Atmosphere Model. *J. Climate*, **8**, 172-190.

Nobre, P., and J. Shukla, 1996: Variations of sea surface temperature, wind stress, and rainfall over the tropical Atlantic and South America. *J. Climate*, **9**, 2464-2479.

Rajagopalan, B., Y. Kushnir, and Y.M. Tourre, 1998: Observed decadal midlatitude and tropical Atlantic climate variability. *Geophys. Res. Lett.*, **25**, 3967-3970.

Ruiz-Barradas, A., J.A. Carton, and S. Nigam, 1999: Structure of interannual-to-decadal climate variability in the tropical Atlantic sector. *J. Climate*, **12**, 1-43.

Seager, R., M.B. Blumenthal, and Y. Kushnir, 1995: An Advective Atmospheric Mixed-Layer Model for Ocean Modeling Purposes-Global Simulation of Surface Heat Fluxes. *J. Climate*, **8**, 1951-1964.

Seager, R., Y. Kushnir, P. Chang, N. Naik, J. Miller, and W. Hazeleger, 2001: Looking for the role of the ocean in tropical Atlantic decadal climate variability. *J. Climate*, in press.

Sutton, R.T., S. P. Jewson, and D.P. Rowell, 2000: The elements of climate variability in the tropical Atlantic region. *J. Climate*, **13**, 3261- 3284.

Tanimoto, Y., and S. P. Xie, 1999: Ocean- atmosphere variability over the Pan-Atlantic basin. *J. Met. Soc. Japan*, **77**, 31-46.

Xie, S.-P., 1999: A dynamic ocean-atmosphere model of the tropical Atlantic decadal variability. *J. Climate*, **12**, 64-70.

# An extreme climatic event in the GFDL AOGCM

**Ronald J. Stouffer and Alex Hall**
**NOAA/GFDL, Princeton, NJ, USA**
**rjs@gfdl.gov**

A low resolution coupled ocean-atmosphere model is integrated for 15,000 years. During the integration two extreme cooling events occur: one in the high latitudes of each hemisphere. Both events are quite extreme in that they fall well outside of what would be expected in an integration of this length and are caused by the capping of oceanic convection by a fresh water anomaly. In order to successfully integrate the coupled model for long time periods, the resolution is relatively low, approximately 4 degrees. During the integration, there are no interannual changes in the radiative forcing of the model.

We concentrate our analysis on the extreme cooling event in the Greenland Sea region which lasts for about 20 to 30 years. During the event, the sea surface temperature (SST) and sea surface salinity (SSS) fall about 10 standard deviations below their mean values. This event is qualitatively similar to the quasi-periodic great salinity anomalies already documented in this model (Delworth et al., 1997). It also resembles some of the abrupt cooling events seen in the Holocene record (Bond et al., 1997) although it is shorter in duration.

The dramatic cooling is caused by an unusual southward current anomaly that transports cold, fresh water out of the Arctic, along the coast of Greenland to the N. Atlantic. Several feedbacks amplify the cold anomaly as it moves south. The fresh SSS anomaly shuts down convection all along the Greenland coast concentrating the wintertime cooling of the ocean near the surface, further depressing the SST. The cooling also reduces evaporation, thereby increasing the freshening, inhibiting convection further, and inducing further cooling. A large increase in sea ice and therefore albedo also accompanies the event which acts to cool the region. Finally about half way through the event, the surface freshening slows down the thermohaline circulation, significantly depriving the entire N. Atlantic region of warm, salty water from the south.

**References**

Bond, et al. 1997: A pervasive millenial-scale cycle in North Atlatic Holocene and glacial climate. *Science*, **278**, 1257-1266.

Delworth, T., S. Manabe, and R.J. Stouffer, 1997: Multidecadal climate variability in the Greenland Sea and surrounding regions: a coupled model simulation. *Geophys. Res. Lett.*, **24**, 257-260.

# Predictability experiments using HadCM3 with a perfectly initialised ocean

**Doug Smith, James Murphy and Steven Murray**
**Hadley Centre for Climate Prediction and Research, The Met Office, Bracknell, UK**
**dsmith@meto.gov.uk**

## 1. Introduction

Successful simulations of the North Atlantic Oscillation (NAO) using atmosphere models forced by observed sea surface temperature (SST) distributions (Rodwell et al., 1999; Mehta et al., 2000; Latif et al., 2001 suggest that the low frequency variability of the NAO is potentially predictable provided the evolution of SST can be predicted. However, hindcasts of the 1970s using HadCM3 initialised by assimilating ocean observations (Smith and Murphy, 1999; Smith et al., 2000) showed very little predictability of the NAO. This lack of skill probably arises from a combination of imperfect initialisation of the ocean model and imperfections in both the atmosphere and ocean models and the coupling between them.

Given the sparsity of ocean observations and the difficulty of assimilating them into a dynamic model (Murphy and Smith, 1999) it is likely that imperfect initialisation is a major factor in the lack of hindcast skill. This limitation has been removed in this study by attempting to predict the evolution of the NAO which occurred in the control run of the HadCM3 coupled model, using a perfectly initialised ocean. This is achieved by joining an ocean state selected from a positive (negative) NAO period of the control integration with an atmosphere state taken from a negative (positive) NAO period and comparing the subsequent evolution with the original control integration. An ensemble of such experiments were performed in order to obtain statistically robust results.

## 2. Experiment Design

The NAO index from part of the HadCM3 control integration is shown in Figure 1 together with four selected periods of high NAO index (shown in red and orange) and four selected periods of low NAO index (shown in blue and green). A total of four experiments were performed, two aimed at predicting the evolution of the high NAO index periods shown in red in Figure 1 and two aimed at predicting the evolution of the low NAO index periods shown in blue. Each experiment consisted of four ensemble members generated by combining one ocean state with four different atmospheres from the opposite phase of the NAO. Thus, the ocean states from the beginning of each of the periods shown in red were combined with the atmosphere states from the beginning of each of the periods shown in blue and green in the two experiments aimed at predicting the evolution of the high NAO periods. Similarly, the ocean states from the beginning of each of the periods shown in blue were combined with the atmosphere states from the beginning of each of the periods shown in red and orange in the two experiments aimed at predicting the evolution of the low NAO periods. The integrations were started in June so that any imbalances arising from the use of different atmosphere and ocean dumps would have settled down before the first predicted winter NAO.

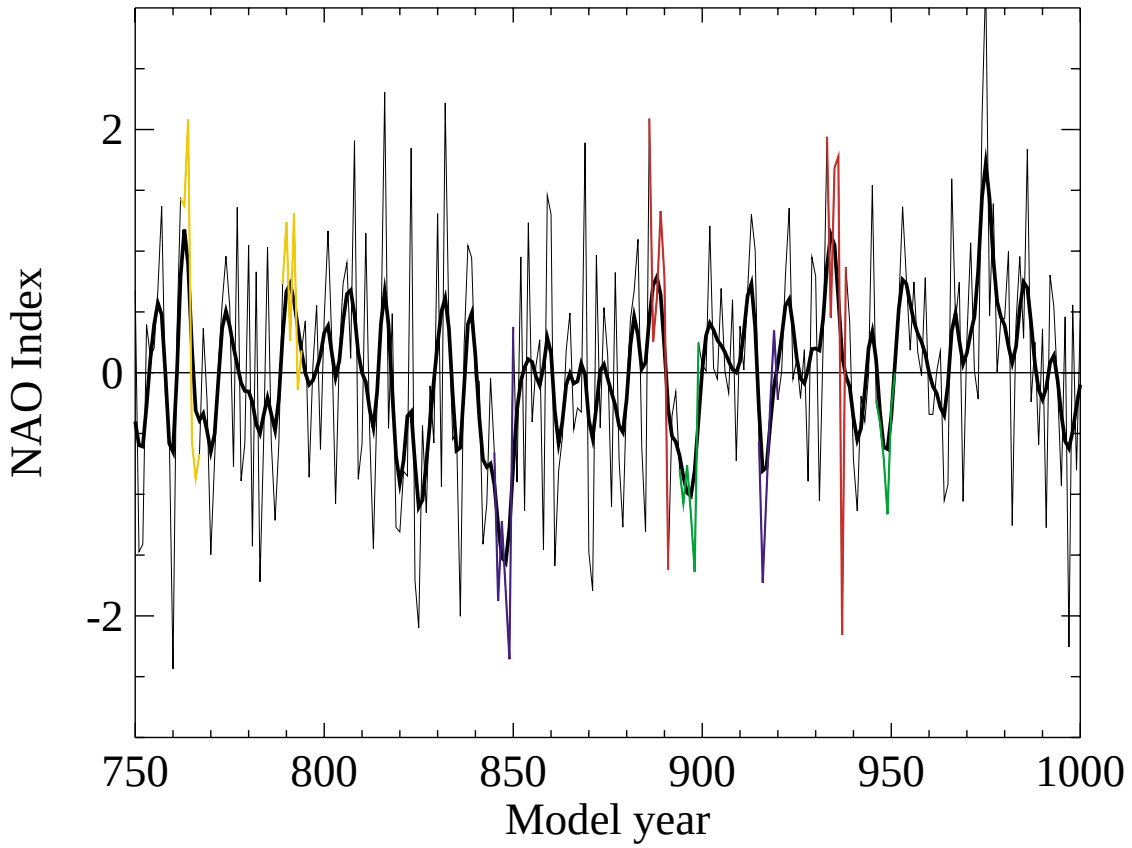


*Figure 1: NAO index from part of HadCM3 control run. The thick black line shows the NAO smoothed by applying a 1-2-1 binomial filter three times. The coloured curves show the periods of high and low NAO selected for use in this study as described in the text.*

## 3. Results

The winter NAO was not predictable in any of the experiments and was generally not within the ensemble spread (Figure 2). Similar results were obtained for all other seasons (not shown). The possibility that the NAO is not forced by SST cannot be discounted from these experiments. However, lead-lag analysis of SVD patterns (Rodwell and Folland, 2000) suggests that any possible forcing of the atmosphere by North Atlantic SST is much weaker in HadCM3 than in reality. Future work is therefore required in order to develop a coupled model in which links between North Atlantic SST and the NAO are as strong as in observations.

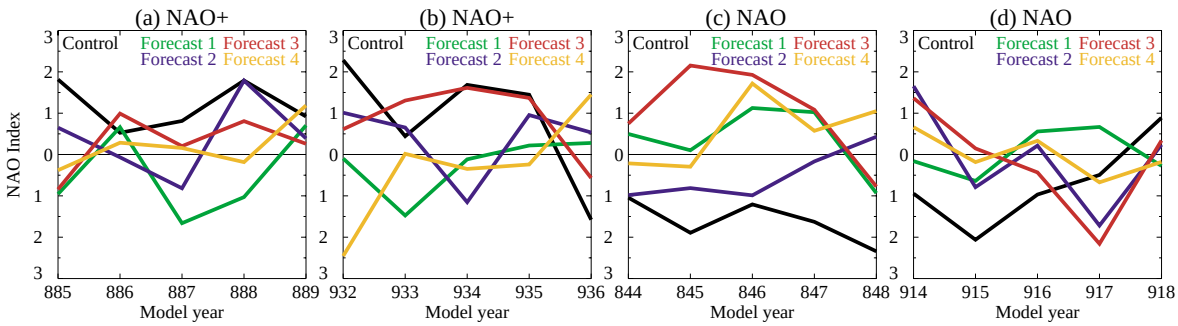


*Figure 2: NAO index (DJF) predicted by each ensemble compared with the original control integration.*

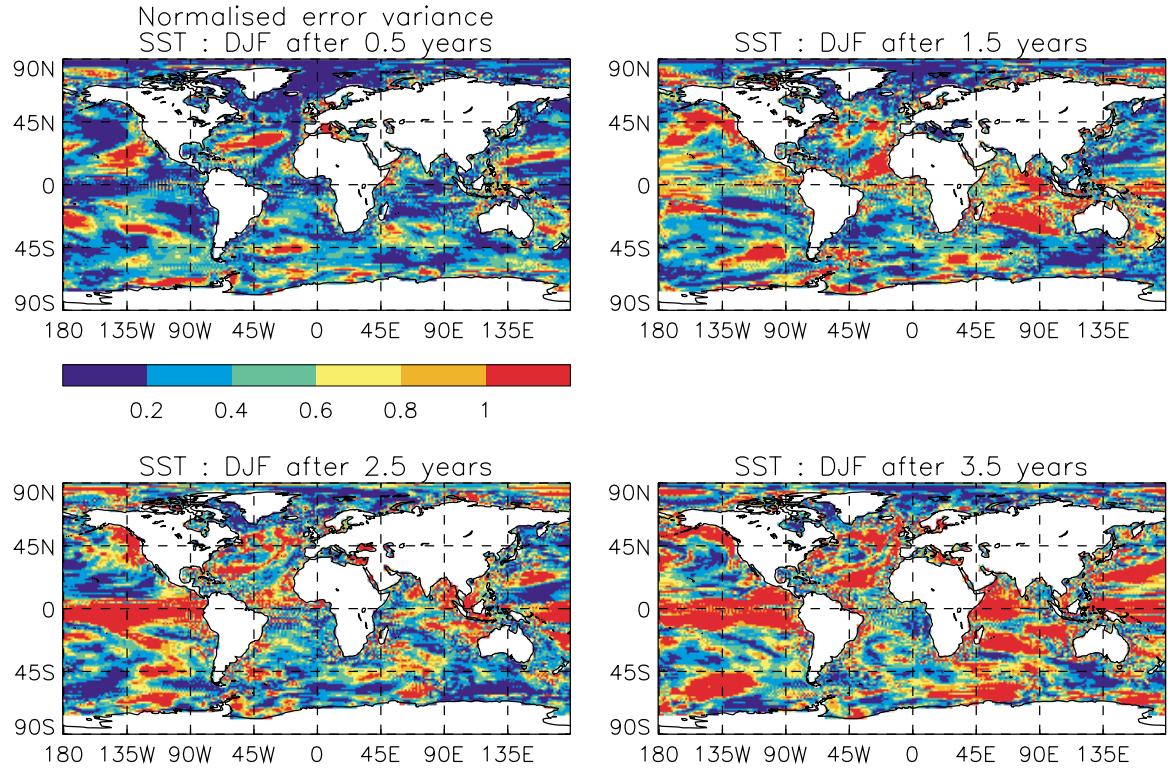


*Figure 3: Mean normalised SST error variance of ensemble mean (DJF).*

In order to asses potential predictability the normalised error variance, averaged over all four experiments, of the ensemble mean SST is shown in Figure 3 for DJF. Because the ensembles were started from very different atmospheric states these experiments would be expected to provide a lower bound of predictability. Furthermore, the weaker response to North Atlantic SST anomalies in HadCM3 than in reality would also be expected to degrade predictability. Nevertheless, SST is reasonably predictable over most of the ocean for at least 6 months. The tropical Pacific exhibits modest predictability for another year, but the error variance has saturated after 2.5 years. Except at high latitudes the error variance over most of the North Atlantic has also saturated after 2.5 years. There are reasonably large areas in the North and South Pacific, South Atlantic and south of Australia which are potentially predictable for 3.5 years.

The most predictable region is the high latitude North Atlantic. Further analysis of the HadCM3 control integration (not shown) reveals an oscillation of SST anomalies in the Labrador Sea with a period of about 20 years. This oscillation does not appear to be forced locally by the atmosphere since wind speed, heat flux, E - P and longwave radiation lag SST by about a year. This is consistent with the high degree of predictability exhibited by the ensemble experiments and suggests that ocean dynamics axe involved. This is further supported by the fact that vertical velocity at 165m leads SST by about 5 years, but the exact mechanism driving the oscillation has not yet been identified. Labrador Sea convection is highly correlated with SST and has been shown by Cooper and Gordon (2000) to cause slowly propagating SST anomalies along the path of the North Atlantic Current similar to those observed by Sutton and Allen (1997). Further understanding of the Labrador Sea oscillation might, therefore, help to explain the causes of SST anomalies over a wider area of the North Atlantic.

**References**


Cooper, C., and C. Gordon, 2000: North Atlantic oceanic decadal variability in the Hadley Centre coupled model. *J. Climate*, submitted.

Latif, M., K. Arpe, and E. Roeckner, 2000: Oceanic control of decadal North Atlantic sea level pressure variability in winter. *Geophys. Res. Lett*., **27**, 727-730.

Mehta, V.M., M.J. Suarez, J. Manganello, and T. L. Delworth, 2000: Oceanic influence on the North Atlantic Oscillation and associated Northern Hemisphere climate variations: 1959 -1993. *Geophys. Res. Lett*., **27**, 121-124.

Murphy, J.M., and D.M. Smith, 1999: Initialisation of HadCM3 for decadal climate predictions by assimilation of ocean observations, Report to DETR, Hadley Centre, Meteorological Office, Bracknell, UK.

Rodwell, M.J., and C.K. Folland, 1999: Atlantic air-sea interaction and seasonal predictability, submitted.

Rodwell, M.J., D.P. Rowell, and C.K. Folland, 1999: Oceanic forcing of the wintertime North Atlantic Oscillation and European climate. *Nature*, **398**, 320-323.

Smith, D.M., and J.M. Murphy, 1999: Experimental hindcast of the 1970s using HadCM3 initialised by assimilating ocean observations, Report to DETR, Hadley Centre, Meteorological Office, Bracknell, UK.

Smith, D.M., J.M. Murphy, and S.P. Murray, 2000: Experimental ensemble hindcasts of the 1970s using HadCM3 initialised by assimilating ocean observations, Report to DETR, Hadley Centre, Meteorological Office, Bracknell, UK.

Sutton, R. T., and M.R. Allen, 1997: Decadal predictability of North Atlantic sea surface temperature and climate. *Nature*, **388**, 563-567.

# PREDICATE: Mechanisms and Predictability of Decadal Fluctuations in Atlantic-European Climate

**Rowan Sutton**
**Centre for Global Atmospheric Modelling, University of Reading, Reading, UK**
**R.Sutton@reading.ac.uk**

Understanding fluctuations of the climate system on time scales from decades to centuries is one of the major topics of the CLIVAR programme. Five Principal Research Areas (PRAs) within the Initial CLIVAR Implementation Plan (WCRP, 1998) focus on aspects of decadal climate variability. In the Atlantic Sector the key topics are the North Atlantic Oscillation, the Thermohaline Circulation and Tropical Atlantic Variability. The problem of understanding and forecasting these aspects of decadal climate variability presents a major challenge to the scientific community. An adequate response is beyond the resources of any single organisation, and thus coordination of activities is essential. PREDICATE is a 3-year research programme, funded by the European Union under Framework 5, in which eight of the leading climate centres in Europe have come together to provide a focused effort in this vital area.

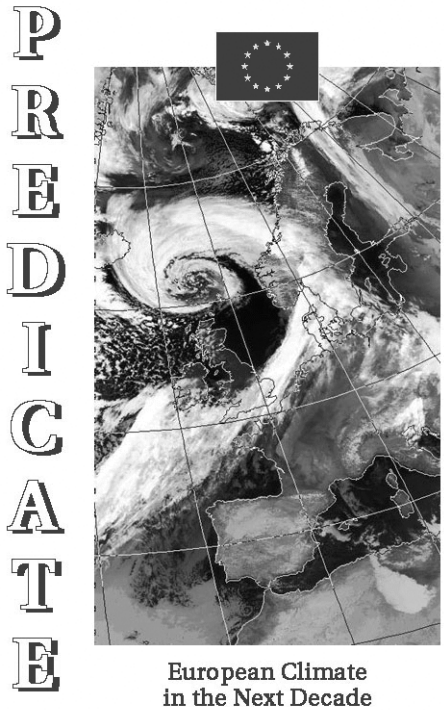


The objectives of PREDICATE are:

1. To assess the predictability of decadal fluctuations in Atlantic-European climate.
2. To improve understanding and simulation of mechanisms via which ocean-atmosphere interactions cause decadal fluctuations in Atlantic-European climate.
3. To improve the European capability for forecasting decadal fluctuations in Atlantic- European climate by developing forecasting systems based on coupled ocean-atmosphere models.
4. To work with targeted user groups to assess the potential benefits from possible future decadal forecasts for selected sensitive industries.

As can be seen, PREDICATE targets the role of ocean-atmosphere interactions rather than the response to external forcings. These aims are to be achieved through a coordinated programme of numerical experimentation, evaluation against observations, and development of prediction systems. The project has four principal themes, as follows.

**A) Mechanisms and Predictability of Decadal Fluctuations in the Atmosphere.**

The potential predictability of the North Atlantic Oscillation (NAO) has been a subject of considerable recent debate. It has been shown that atmosphere models forced with observed SST can simulate NAO variability that is highly correlated with the observed record (Rodwell et al., 1999). Because of large sampling fluctuations there is need for caution in the interpretation of these results (Mehta et to be fully explained. In some models there appears to be no significant skill (L. Terray, personal communication), and in those where skill exists it is not clear whether consistent features of the SST variability are responsible.

A major contribution of PREDICATE to this topic is a rigorous quantitative comparison of four different atmosphere GCMs to assess their skill in simulating the climate variability that was observed over the last century, with a particular focus on the North Atlantic region. The comparison includes the powerful technique of signal-to-noise optimised Principal Component Analysis (Venzke et al., 1999). This approach enables determination of which features in the SST field exert most influence.

**B) Mechanisms of Decadal Fluctuations in the Atlantic Ocean**

Prominent amongst the observational results of recent years has been the identification of persistent, often propagating, surface and subsurface anomalies in the North Atlantic ocean (e.g. Dickson et al., 1988; Sutton and Allen, 1997; Curry and McCartney, 1998). A major current challenge is to understand the mechanisms through which these anomalies form, propagate, and decay, and to understand how their life-cycles are related to fluctuations in the atmosphere and in the oceanic gyre and thermohaline circulations.

In PREDICATE these issues are being addressed through a coordinated programme of experimentation with six different ocean GCMs. PREDICATE partners are investigating the skill with which the variability observed in the Atlantic during the second half of the twentieth century is simulated in models forced with observed winds and air-sea fluxes. The sensitivity of simulations to model resolution and the representation of the Arctic ocean is being explored.

**C) Decadal Climate Prediction for the Atlantic European Region.**

The problem of decadal climate forecasting presents considerable scientific and technical challenges. Predictability on these timescales arises from two influences: that of the ocean, and that of external forcings such as the rising trend of greenhouse gases. Current climate change forecasts make no use of information about the present state of the oceans (see Figure 1). This approach is very unlikely to be optimal for forecasts with time horizons of a few years or decades. Thus work to incorporate ocean state information into climate forecasts is essential.

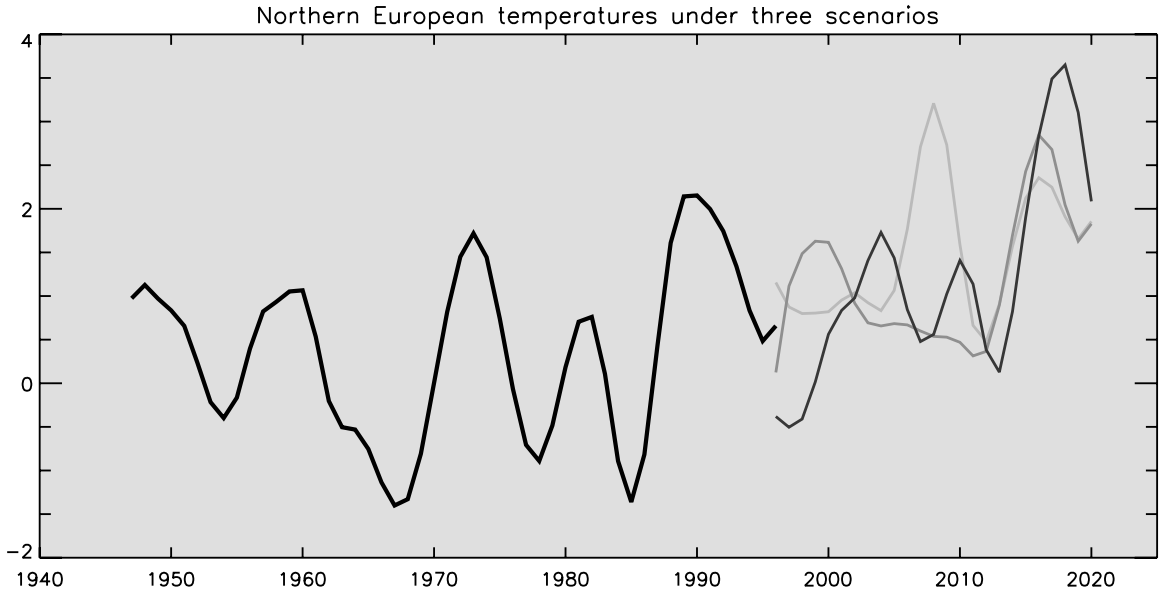


*Fig. 1: Observations of Northern European temperature anomalies (white line) and three forecasts demonstrating the large uncertainty in climate scenarios for the next 20 years. Note that the forecasts are not continuous with the observations because no information about the current ocean (and atmosphere) state is currently employed. This is a key issue that PREDICATE is addressing.*

Building on the understanding and evaluation of mechanisms achieved in other parts of the programme, a major part of PREDICATE is addressing the development of systems for decadal forecasting and the assessment of predictability on decadal timescales. The study of Griffies and Bryan (1997) was a pioneering step in this field. However, the coarse resolution of the model used brings into question the realism of the mechanisms it simulated. PREDICATE will take forward the work of Griffies and Bryan by performing experimental decadal predictions with four different coupled models, all of which have higher resolution than that used by Griffies and Bryan. The sensitivity of forecasts to initial conditions in both the ocean and the atmosphere will be investigated and a quantitative assessment of decadal predictability will be made for each of the models. The application to decadal forecasting of techniques (e.g. 'breeding') to generate initial perturbations for decadal forecasts will be investigated.

**D) Interactions with Users and Dissemination of Results.**

Decadal time horizons are of central concern for strategic planning in a wide range of industries. It is a high priority for PREDICATE that the needs of potential users are well understood and are taken into account throughout the programme. It is also essential that potential users begin to think seriously about how they could exploit future real-time decadal forecasts. To achieve these ends PREDICATE is promoting a dialogue between the climate prediction science community and business users in a wide range of sectors (for example, insurance, energy, water, construction). An example of the project activities is a workshop at The Royal Society London, 8-9 March 2002: 'Climate Risks to 2020: Business Needs and Scientific Capabilities'
The PREDICATE project began on 1 March 2000 and will end on 28 February 2003. The PREDICATE partners are:
CGAM: Centre for Global Atmospheric Modelling, University of Reading, UK, The Met Office, Bracknell, UK, MPI: Max Planck Institut für Meteorologie, Hamburg, Germany, LODYC: Laboratoire d'Oceanographie Dynamique et de Climatologie, Paris, France, NRSC: Nansen Environmental and Remote Sensing Research Centre, Bergen, Norway, ING: Istituto Nazionale di Geofisica, Bologna, Italy., DMI: Danmarks Meteorologiske Institut, Copenhagen, Denmark, CERFACS: The European Centre for Research and Advanced Training in Scientific Computation, Toulouse, France.
For further information see http://ugamp.nerc.ac.uk/predicate

**References**


Bretherton, C.S., and D.S. Battisti, 2000: An interpretation of the results from atmospheric general circulation models forced by the time history of the observed sea surface temperature distribution. *Geophys. Res. Lett.*, **27**, 767-770.

Curry, R.G., and M. S. McCartney, 1998: Oceanic transport of subpolar climate signals to mid-depth subtropical waters. *Nature*, **391**, 575-577.

Dickson, R. R., J. Meincke, S.-A. Malmberg, and A. J. Lee, 1988: The Great Salinity Anomaly in the northern North Atlantic 1968-1982. *Prog. Oceanogr.*, **20**, 103-151.

Griffies, S.M., and K. Bryan, 1997: A predictability study of simulated North Atlantic multidecadal variability. *Climate Dynamics*, **13**, 459-487.

Oceanic influence on the north atlantic oscillation and associated northern hemisphere climate variations. *Geophys. Res. Lett.*, **27**, 121-124.

Rodwell, M.J., D.P. Rowell, and C.K. Folland, 1999: Oceanic forcing of the winter North Atlantic Oscillation and European Climate. *Nature*, **398**, 320-323.

Sutton, R.T., and M. R. Allen, 1997: Decadal predictability of North Atlantic sea surface temperature and climate. *Nature*, **388**, 563-567.

Venzke, S., M. R. Allen, R. T. Sutton, and D. P. Rowell, 1999: The atmospheric response over the North Atlantic to decadal changes in sea surface temperature. *J. Climate*, **12**, 2562-2584.

# Climate Predictability in the Context of Global Warming: Preliminary Numerical Experiments

**G. Vallis, T. Delworth, S. Griffies and R.Stouffer GFDL/Princeton University**

## 1. Introduction

The predictability of climate on decadal timescales (i.e., timescales of a few years to a few decades) is not well understood. By this statement we mean the following. On the intraseasonal timescale, there is evidence that numerical forecasts can be made that improve on climatology (e.g., Shukla et al., 2000). Much of the source of this skill arises from predicting the conditions of the tropical ocean, and the effects this has on the global atmosphere. Forecasts at this timescale are in some ways well-posed initial-value problems. At much longer timescales, for example the multi-decadal, the response to greenhouse gases may dominate that of natural variability. That is to say, the difference between the climate of a century hence (given typical business-as-usual projections of the increase in greenhouse gas and aerosol concentrations) and that of today is likely to be much larger than the natural variability of climate itself, because the boundary/forcing conditions of the atmosphere have changed so much. Thus, if ones prior estimate is simply the climatology of today, one might say that predictability also resides at the multi-decadal–centennial timescales.

In contrast to both of these limits, on the decadal timescale the natural variability is likely to be roughly comparable with the forced change in climate over that time-period. Unless some aspects of this variability can be predicted, the useful predictability at this timescale may be limited. This situation is not unique to climate; an analogous situation exists in weather forecasting. Here, forecasts of a few days depend almost entirely on the initial conditions, and can be quite skillful. At the seasonal timescale (which we are now regarding as the long-time limit of weather forecasting), skill emerges by way of the influence of the slowly evolving sea-surface temperature, which provides a boundary condition on the atmosphere. But at the intermediate timescale useful skill is harder to define. Thus, for both climate and weather forecasts, the timescale that is long enough so that the memory of the initial conditions is partially lost, but not long enough for the slowly varying boundary conditions to have impressed themselves on the system, may provide the greatest challenge. It is this timescale we explore in this note.

## 2. Experimental Design

The main experiments we describe are performed with a standard GFDL coupled climate model at R30 horizontal atmospheric resolution and $2^{o}$oceanic resolution (Delworth and Knutson, 2000). A 900 year control integration with pre-industrial concentrations of forcing (greenhouse gases and aerosol concentrations) was performed to provide a stable climatology. Then, from three independent times in this integration (but each corresponding to a nominal year in terms of greenhouse gas concentrations of 1865) anthropogenic greenhouse gases were increased for a period of 136 years, so providing three different initial conditions that each correspond to January, 2001. We may thus expect, for example, that the thermohaline conditions of the ocean differ for each state.

From each of these three states we then create an ensemble of eight members by perturbing the atmospheric initial conditions, and continuing the integrations for an additional 30 years, each with projected increasing levels of greenhouse gases from anthropogenic emissions. The experiments are similar to those of Griffies and Bryan (1997), except that the model has higher resolution in both atmosphere and ocean, and anthropogenic greenhouse gases and aerosols increase through the integration.

## 3. Results

Fig. 1 shows the divergence of the thermohaline circulation in the North Atlantic in two of the ensembles. Evidently, the model thermohaline circulation can be predictable for a few decades. Furthermore, the natural variability of the thermohaline circulation over the next few decades dominates over the slow weakening expected because of global warming. (The weakening arises because of increased precipitation and runoff, and warming of the near-surface layer in the subpolar North Atlantic, all of which weaken the (negative) buoyancy forcing at high latitudes.)

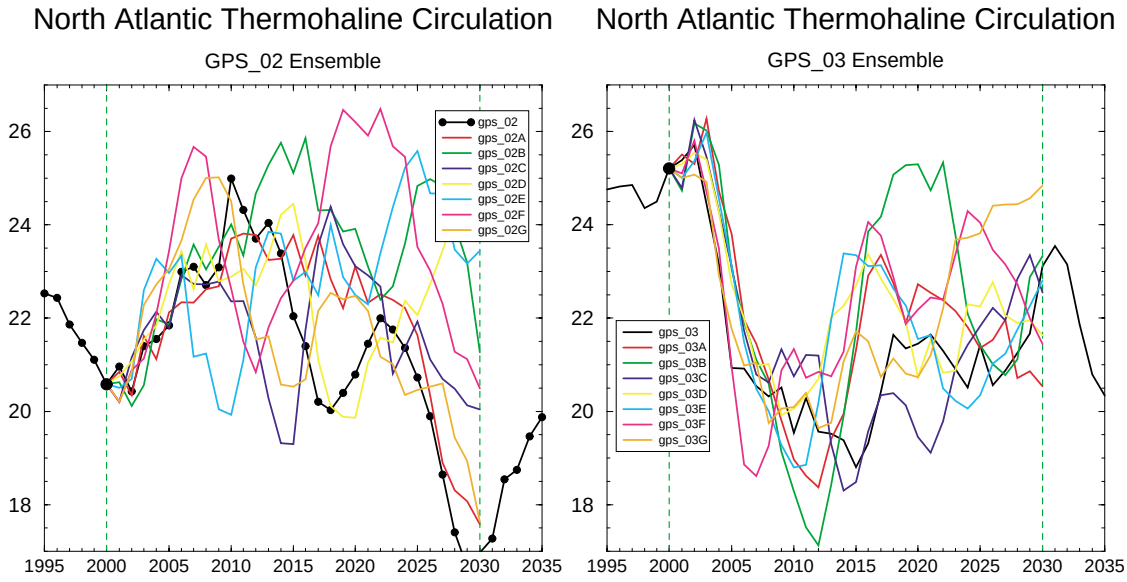


*Figure 1: Evolution of the North Atlantic overturning circulation (Sverdrups) in two of the ensembles. (The third is qualitatively similar.) Within each ensemble the atmospheric weather differs at day one, but the ocean conditions are identical.*

The predictability of the SST is assessed using EOFs, calculated from a 300 year segment of the control integration, and restricted to the North Atlantic. Typically, the first few EOFs have a dominant signal in the subpolar gyre. The divergence of the principal components of the first EOFs for two of the ensembles is illustrated in fig. 2. Predictability of the SST seems present for a decade or perhaps two, after which the variance of any one integration is comparable to the difference between integrations.

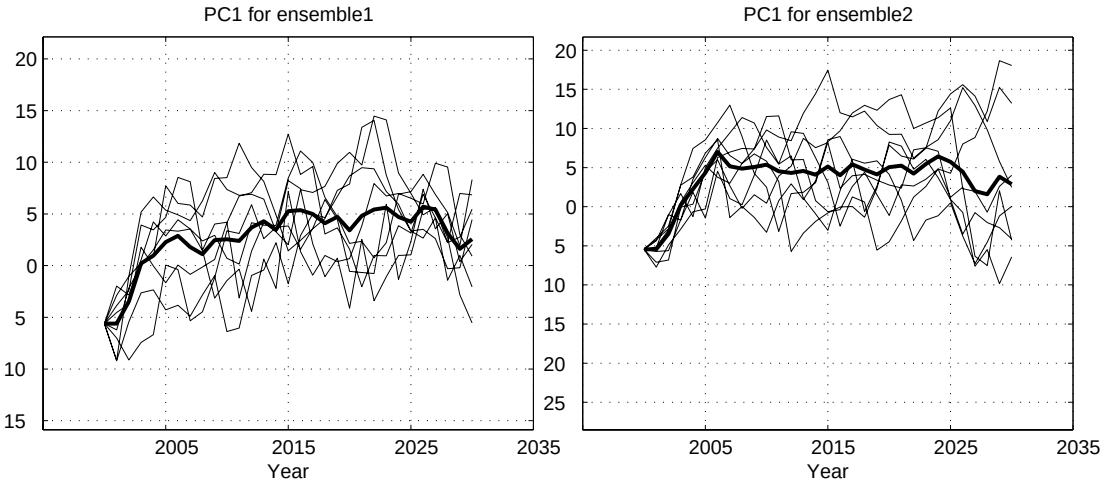


*Figure 2: As for fig. 1, but for the first principal component of the two ensembles.*

## 4. Discussion and Conclusions

The thermohaline circulation in this model undergoes fairly regular oscillations with a dominant period of about 50 years (Delworth et al., 1993), consistent with it being a damped oscillator driven by noise from the atmosphere (Griffies and Bryan, 1997). This circulation is, perhaps not unexpectedly, predictable on this timescale. The surface manifestation of these oscillations and the associated predictability appears to be mainly in the subpolar gyre, consistent with theory that suggests that the thermohaline circulation is at first order buffered from the subtropical sea-surface by an isothermal layer at the base of the ventilated thermocline (e.g., Vallis, 1999).

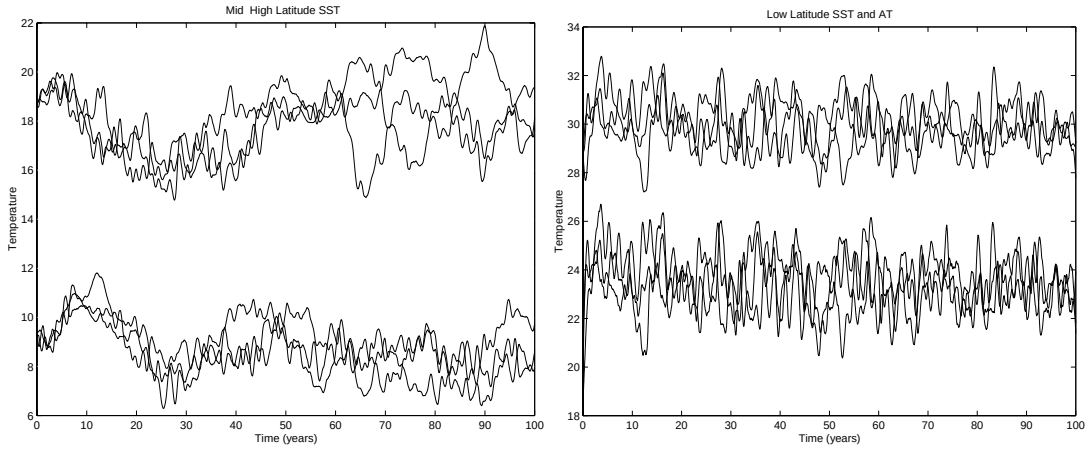


*Figure 3: Evolution of a small ensemble of experiments of an a sector ocean model coupled to an atmospheric EBM. The ensemble members have different realisations of atmospheric noise. Left, SST at two latitudes in the subpolar gyre. Right, evolution of SST and SAT in the subtropical gyre.*

Our results suggest that predictability of the SST of the subtropical gyres may be lower than that of the subpolar gyres. This may be because, even though the subtropical gyres may also have internal decadal-scale variability, their mixed layer is shallower and the SST is determined to a greater degree (than in the subpolar gyre) by the intrinsically unpredictable atmospheric dynamics. To explore this we performed similar predictability experiments with a sector ocean model coupled to an atmospheric energy balance model, plus noise whose variance is geographically uniform. Again the thermohaline circulation oscillates (in fact, sector models with flat bottoms typically oscillate more readily than models with realistic topography; Winton 1997) providing high latitude SST predictability, but the subtropical SST (and SAT) is less predictable (fig. 3). The predictability properties of the lower latitudes, and the predictability of the atmosphere in general, remain topics for future exploration.

## References

Delworth, T., and T. Knutson, 2000: Simulation of early 20th century global warming. *Science*, **287**, 2246–2250.

Delworth T.L., S. Manabe, and R. J. Stouffer, 1993: Multidecadal variations of the thermohaline circulation in a coupled ocean-atmosphere model. *J. Climate*, **12**, 1993–2011.

Griffies, S. M., and K. Bryan, 1997: A predictability study of simulated North Atlantic multidecadal variability. *Climate Dynamics*, **13**, 459–488.

Griffies, S. M., and E. Tziperman, 1995: A linear thermohaline oscillator driven by stochastic atmospheric forcing, *J. Climate*, **8**, 2440-2453.

Shukla, J. J. Anderson, D. Baumhefner, C. Brankovic, Y. Chang, E. Kalnay, L. Marx, T. Palmer, D. Paolino, J. Ploshay, S. Schubert, D. Straus, M. Suarez, and J. Tribbia, 2000: Dynamical seasonal prediction. *Bull. Amer. Meteor. Soc.*, **81**, 2593–2607.

Vallis, G. K., 2000: Large-scale circulation and production of stratification: effects of wind, geometry and diffusion. *J. Phys. Oceanogr.*, **30**, 933–954.

Winton, M., 1997: The damping effect of bottom topography on internal decadal-scale oscillations of the thermohaline circulation. *J. Phys. Oceanogr.*, **27**, 203–208.

# Decadal variability of the North Pacific upper ocean simulated by MRI ocean general circulation model

**Tamaki Yasuda and Yoshiteru Kitamura**
**Meteorological Research Institute, Tsukuba, Japan**
**tyasuda@mri-jma.go.jp**

## Introduction

On the decadal variability of the North Pacific, two major mechanisms have been proposed. One is a midlatitude-tropical linkage. Midlatitude temperature anomalies formed by the decadal shift of the atmospheric circulation are advected to the equatorial surface, and then atmospheric circulation over the North Pacific changes as a response to those altered SST and convection over the tropical Pacific. In this mechanism, subduction process in the thermocline brings the temperature anomalies from the midlatitude to the equator (Gu and Philander, 1997). From the analysis of the observed temperature data, Zhang and Liu (1999) claimed to obtain a mode associated with the subduction process, while Schneider et al. (1999) concluded that the subduction bridge from the midlatitude to the equator cannot be recognized. The other mechanism is a midlatitude air-sea interaction. According to Latif and Barnett (1994, 1996), the oceanic gyre responds baroclinically to the change in the wind stress fields, and then temperature variations in the northwestern part of the subtropical gyre caused by the gyre spinup/down change the atmospheric circulation through the surface heat flux. In the present study, decadal variability of the North Pacific is simulated by an OGCM, and the key oceanic processes for the mechanisms mentioned above are investigated.

## Model and boundary conditions

The ocean general circulation model used in this study is a z-coordinate primitive equation model developed in MRI (Yamanaka et al., 1998). The model spans from 120°E, 15°S to 70°W, 60°N with the horizontal grid resolution of 2 longitudes and 1 latitude, and has 30 levels in the vertical. The horizontal eddy viscosity is constant at $2.0 \times 10^4$ $m^2 s^{-1}$ and the isopycnal diffusion scheme of Gent and McWilliams (1991) is applied where the isopycnal and diapycnal diffusivities are $2.0 \times 10^3$ $m^2 s^{-1}$ and 0.1 $m^2 s^{-1}$ respectively. Vertical viscosity and diffusivity are determined by the level 2 turbulent closure scheme of Mellor and Yamada (1982). After 40-yr spinup integration, the interannual simulation for January 1960 through December 1993 is performed using COADS historical monthly data of wind stress, radiative uxes, and the atmospheric factors (da Silva et al., 1994). Salinity at the uppermost level is restored to the monthly climatology of sea surface salinity in WOA94.

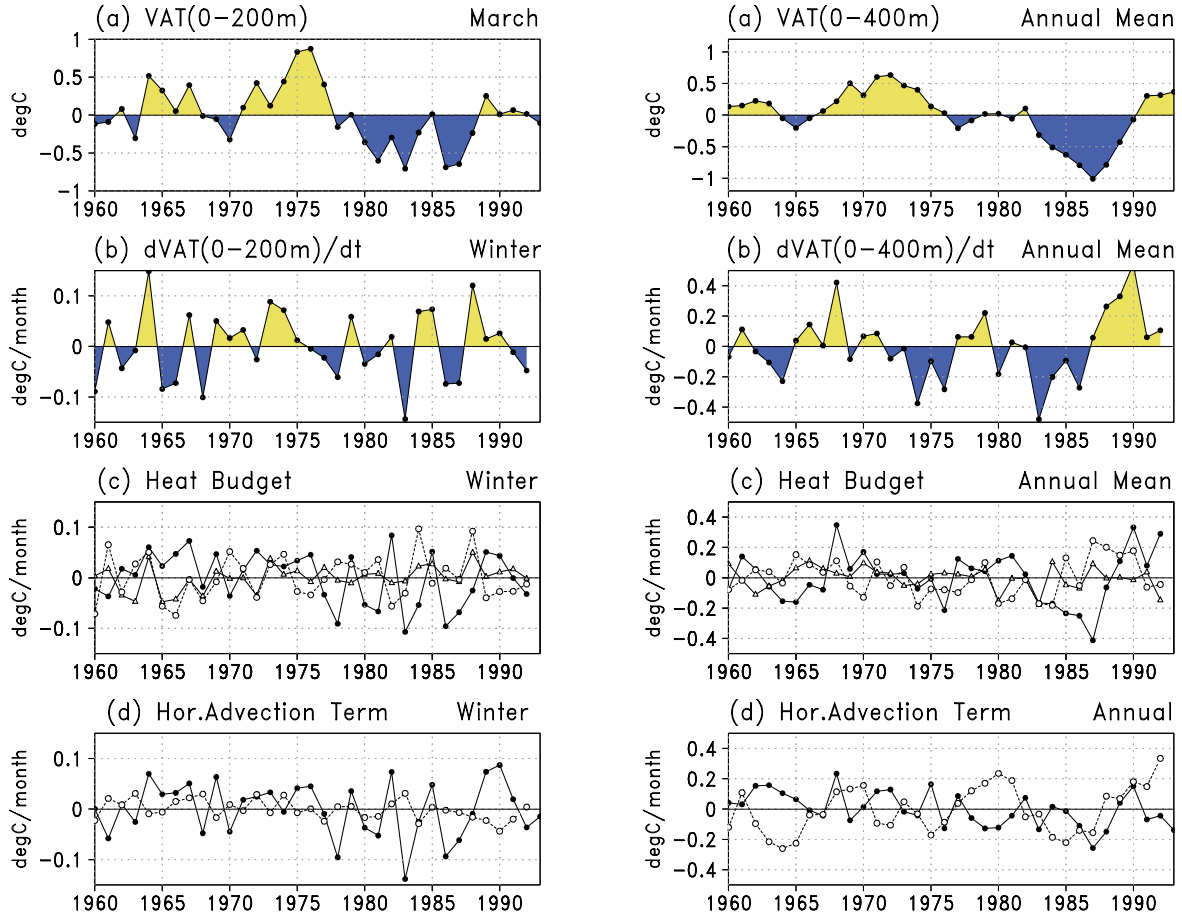


*Figure 1 (left): Heat budget of the wintertime 200m surface layer averaged in the Subtropical Front area (170°-150°W, 25°-35°N). (a) Temperature anomalies. (b) Temporal temperature change rate. (c) Anomalies of the horizontal advection (closed circle), the vertical advection (triangle), and the surface net heat flux (open circle). (d) Anomalies of the horizontal advections by Ekman (closed circle) and geostrophic (open circle) transports.*

*Figure 2 (right) : Heat budget of the annual mean 400m surface layer averaged in the Kuroshio Extension area (160°E-180°, 35°-45°N). (a) Temperature anomalies. (b) Temporal temperature change rate. (c) Anomalies of the horizontal advection (closed circle), the vertical advection (triangle), and the surface net heat flux (open circle). (d) Anomalies of the horizontal advections by Ekman (closed circle) and geostrophic (open circle) transports.*

**Heat budget of the midlatitude surface layer**

The first EOF mode of simulated SST reveals a cooling in the mid 1970s in the areas of the subtropical front and Kuroshio extension as seen in the observed SST (Nakamura et al., 1997). Figure 1 shows the heat budget of the wintertime 200m surface layer averaged in the subtropical front area (170°-150°W, 25°-35°N). Since the horizontal advection turns to negative in 1977 (closed circle in Fig. 1c), cooling occurs in the subtropical front area. The change in the divergence of the Ekman heat transport dominates in the horizontal advection term (closed circle in Fig. 1d). Figure 2 shows the heat budget of the annual mean 400m surface layer averaged in the Kuroshio extension area (160°E-180°, 35°-45°N). Although temperature anomalies remain positive in the early 1970s, temporal change rate becomes negative (Fig. 2b). The divergence of the geostrophic heat transport correlates well with the temperature change rate, but that of the Ekman heat transport does not (Fig. 2d).

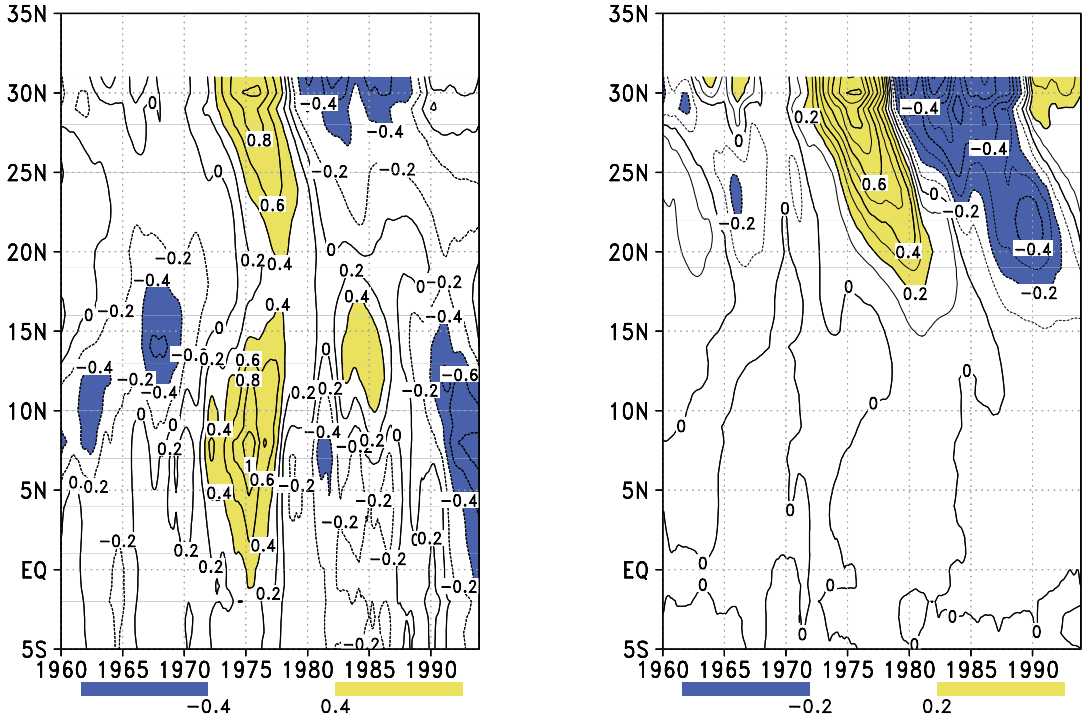


*Figure 3: Latitude-time plots of the zonally averaged temperature anomalies on the 25.2$\sigma_\theta$ climatological surface. Zonal average is taken in the area where the temperature variations related to the subduction processes are large. (a) Simulation forced by the wind stress in the whole area. (b) Simulation forced by the wind stress whose interannual anomalies are eliminated south of 20 $^o$N. Contour intervals are (a) 0.4 $^o$C and (b) 0.1 $^o$C.*

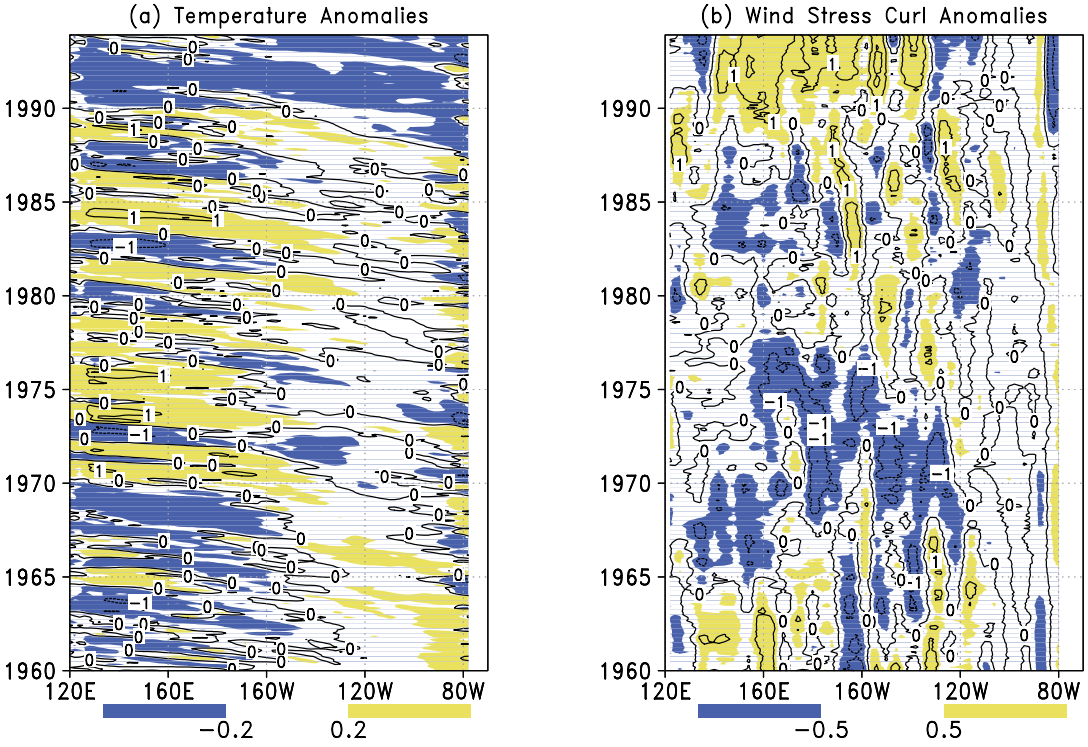


*Figure 4: Longitude-time plots of (a) temperature anomalies at 275m depth and (b) wind stress curl anomalies averaged in 5 $^o$-15$^o$N. Contour intervals are (a) 1 $^o$C and (b) $10^{-8}$ $Nm^{-3}$*

**Subduction signals**

The possibility of temperature advection from midlatitude to the equator by the subduction process is investigated. Figure 3a shows the latitude-time plots of zonally averaged the temperature anomalies on the $25.2\sigma_\theta$ climatological surface. Zonal average is taken in the area when the temperature variations related to the subduction processes are large. In the midlatitude, warm temperature anomalies subduct in 1974-1976, and cold anomalies subduct in 1977-1988. After 1989, warm anomalies subduct again. Those subducting temperature anomalies reach 15$^o$N along the subtropical gyre, but could not be traced furthermore to the equator nor to the northwestern part of the subtropical gyre. This coincides with the observed temperature fields in Schneider et al. (1999). Instead, temperature anomalies in the western tropical Pacific has a strong correlation with the wind stress curl anomalies averaged in 5$^o$to 15$^o$N (Fig. 4). Warm (cold) temperature anomalies correspond to negative (positive) wind stress curl anomalies. This implies that temperature anomalies in the western tropical Pacific are mainly determined by the zonal propagation of the Rossby waves generated by the wind stress curl. When the model is run by the wind stress whose interannual anomalies are eliminated south of 20$^o$N, tropical temperature changes associated with the wind stress curl anomalies disappear and the subduction signals from the midlatitude are more clearly seen. These signals, however, do not extend to the equator along the western boundary (Fig. 3b). The equatorial thermal structure could not be affected by the midlatitude temperature anomalies through the subduction process.

**Effect of the gyre intensification**

Surface temperature changes in the Kuroshio extension area due to the gyre spinup/down is important for the phase reversal in the mechanism of Latif and Barnett (1994, 1996). intensification of the westerlies associated with the Aleutian Low leads to an increase of the transport of both the sub- tropical and subpolar gyres after the mid 1970s. Simulated Kuroshio transport varies corresponding to the Sverdrup transport of the subtropical gyre. In the Kuroshio extension area (160$^o$E-180$^o$), the surface temperature anomalies are negative south of 36 $^o$N (the axis of the Kuroshio extension) and positive north of 36$^o$N before the mid 1970s, and vice verse after the mid 1970s. This represents that thermal structure of the subtropical gyre changes from a shallow one to a deep one in the mid 1970s, namely, the gyre becomes stronger. The gyre spinup/down influences the upper thermal structure in the Kuroshio extension area as shown in Fig. 2. Change in the surface heat flux in the Kuroshio extension area, however, is mainly caused by the observed air temperature. Consequently, it is difficult to estimate the contribution of the Kuroshio heat transport to the SST change in a quantitative sense.

**Concluding remarks**

It is concluded that the subduction process does not advect the midlatitude temperature anomalies strong enough to change the equatorial SST. It is also concluded that the change in the Kuroshio heat transport has a considerable influence on that in the heat budget of the surface layer. However, we cannot verify the decadal midlatitude air-sea interaction. Several mechanisms have been proposed recently on the midlatitude-tropical linkage in addition to the subduction process (Kleeman et al., 1999; Yukimoto et al., 2000). Their verification with an OGCM simulation is required. The influence of the variations in the South Pacific is not considered in the present model, but must be taken into account. Moreover, simulated variability in the Kuroshio extension area could depend on the model parameters (resolution, diffusivity, data using as boundary conditions at the sea surface, etc.). Therefore, further many numerical experiments with various model parameters are needed to understand mechanisms of the decadal variability of the North Pacific.

**References**


da Silva, A., A.C. Young, and S. Levitus, 1994: Atlas of surface marine data 1994. NOAA Atlas NESDIS.

Deser, C., M.A. Alexander, and M.S. Timlin, 1999: Evidence for a wind-driven intensification of the Kuroshio Current Extension from the 1970s to the 1980s. *J. Climate*, **12**, 1697-1706.

Gent, P.R., and J.C. McWilliams, 1990: Isopycnal mixing in ocean general circulation models. *J. Phys. Oceanogr.*, **20**, 150-155.

Gu, D.F., and S.G.H. Philander, 1997: Interdecadal climate fluctuations that depend on exchanges between the tropics and extratropics. *Science*, **275**, 805-807.

Kleeman, R., J.P. McCreary, and B.A. Klinger, 1999: A mechanism for generating ENSO decadal variability. *Geophys. Res. Lett.*, **26**, 1743-1746.

Latif, M., and T.P. Barnett, 1994: Cause of decadal climate variability over the North Pacific and North America. *Science*, **266**, 634-637.

Latif, M., and T.P. Barnett, 1996: Decadal climate variability over the North Pacific and North America: dynamics and predictability. *J. Climate*, **9**, 2407-2423.

Meller, G.L., and T. Yamada, 1982: Development of a turbulence closure model for geophysical fluid problems. *Rev. Geophys.*, **20**, 851-875.

Miller, A.J., D.R. Cayan, and W.R. White, 1998: A westward-intensified decadal change in the North Pacific thermocline and gyre-scale circulation. *J. Climate*, **11**, 3112-3127.

Nakamura, H., G. Lin, and T. Yamagata, 1997: Decadal Climate variability in the North Pacific during recent decades. *Bull. Amer. Meteor. Soc.*, **78**, 2215-2225.

Schneider, N.S., A.J. Miller, M.A. Alexander, and C. Deser, 1999: Subduction of decadal North Pacific temperature anomalies: Observation and dynamics. *J. Phys. Oceanogr.*, **29**, 1056-1070.

Yamanaka, G., Y. Kitamura, and M. Endoh, 1998: Formation of North Pacific Intermediate Water in an MRI ocean general circulation model, part 1: Subgrid-scale mixing and marginal sea fresh water. *J. Geophys. Res.*, **103**, 30885-30903.

Yukimoto, S., M. Endoh, Y. Kitamura, A. Kitoh, T. Motoi, and A. Noda, 2000: ENSO-like interdecadal variability in the Pacific Ocean as simulated in a coupled general circulation model. *J. Geophys. Res.*, **105**, 13945-13963.

Zhang, R. H., and Z. Liu, 1999: Decadal thermocline variability in the North Pacific Ocean: Two pathways around the subtropical gyre. *J. Climate*, **12**, 3273-3296.

# Multidecadal Rainfall Variability in the Sahel - the roles of SST, soil moisture and Vegetation

**Ning Zeng[1], J. D. Neelin, K.-M. Lau, and C. J. Tucker**

**[1]Department of Meteorology and Earth System Science Interdisciplinary Center University of Maryland,College Park, MD , USA**

**Email: zeng@atmos.umd.edu**

The roles of SST, land and naturally varying vegetation in influencing the climate variability in the Sahel are studied in a coupled atmosphere-land-vegetation model. The Sahel rainfall variability is influenced by sea surface temperature variations in the oceans. Land-surface feedback is found to increase this variability both on interannual and interdecadal time scales. Interactive vegetation enhances the interdecadal variation significantly, but can reduce year to year variability due to a phase lag introduced by the relatively slow vegetation adjustment time. Variations in vegetation accompany the changes in rainfall, in particular, the multi-decadal drying trend from the 1950s to the 1980s.

The rainfall over the West African Sahel region (Hulme, 1994) shows a multi-decadal drying trend from the 1950s to the 1980s and early 90s, as well as strong interannual variability (Figure A). Causes proposed to explain this dramatic trend include global sea surface temperature variations (Folland et al., 1986; Rowell, 1996; Semazzi et al., 1996) and land-use change, i.e., the desertification process (Xue and Shulka, 1993; Dirmeyer and Shukla, 1996). Since vegetation distribution tends to be controlled largely by climate, and surface property changes can impact climate by modifying the atmospheric energy and water budget (Charney, 1975; Claussen, 1998), it is reasonable to propose that dynamic vegetation-climate interaction might influence decadal climate variability substantially in a climatically sensitive zone like the Sahel. We test this hypothesis in a coupled atmosphere-land-vegetation model of intermediate complexity. The atmospheric component of the model is the Quasi-equilibrium Tropical Circulation Model (QTCM) (Neelin and Zeng, 2000; Zeng et al., 2000), which is coupled to the land-surface model Simple-Land (SLand) (Zeng et al., 2000). The QTCM simulates a seasonal climate over the Sahel that is close to observations and that compares favourably with current atmospheric general circulation models (GCMs).

We model the major effects on climate of a varying vegetation through its control of the evapotranspiration process and modification of surface albedo with SLand (Zeng et al., 1999). Vegetation dynamics is modelled by a biomass equation driven by photosynthesis and vegetation loss:

$$\frac{dL}{dt} = \alpha\beta(w)(1 - e^{-kL}) - V/\tau \qquad (1)$$

where $\alpha$ is a carbon assimilation coefficient, $\beta$ is the soil moisture dependence as used in the original SLand, $L$ is the plant leaf area index (LAI), and $k$ is the extinction coefficient of photosynthetically active sunlight taken as 0.75. The vegetation time scale $\tau$ is set to one year. This equation is similar to the biomass equations used in models with more explicit vegetation dynamics.

The original version of the land model was modified to account for the effects of leaf-to-canopy scaling (Sellers et al., 1996) so that the canopy conductance for evapotranspiration is:

$$g_c = g_{s_{max}}\beta(\omega)(1 - e^{-kL})/k \qquad (2)$$

where $g_{Smax}$ is a leaf-level maximum conductance. Note that photosynthesis and evapotranspiration are closely related in Eq. 1 and Eq. 2 (Sellers et al., 1996).

Besides modifying evapotranspiration through Eq. 2, vegetation also changes land-surface albedo $A$ as

$$A = 0.38 - 0.3\,(1 - e^{-kL}) \qquad (3)$$

This corresponds to an albedo of 0.38 at $V = 0$ (desert), and 0.09 at maximum vegetation $V = 1$ (dense forest). Thus, vegetation feeds back into the atmosphere by modifying evapotranspiration and surface albedo through Eq. 2 and Eq. 3. In order to identify the relative importance of oceanic forcing as represented by sea surface temperature (SST), land-surface and vegetation processes, we perform a series of model experiments, starting from a run in which both land and vegetation are interactive. In this realistic case, designated AOLV, the atmosphere, ocean, land and vegetation all contribute to variability. The monthly output from this run is then used to derive a vegetation climatology (with a seasonal cycle but which does not change from year to year) which issued as a model boundary condition for the second run AOL. The output of the run AOL is then used to derive a soil moisture climatology which is used to drive the third experiment AO. In all these three runs, the coupled atmosphere-land-vegetation model is driven by the observed monthly SST from 1950 to 1998 (Reynolds and Smith, 1994)). All three start from an initial condition taken from an interactive land/vegetation run forced by a climatological SST. The modelled annual rainfall over the Sahel from these experiments is shown in Fig. B-D.

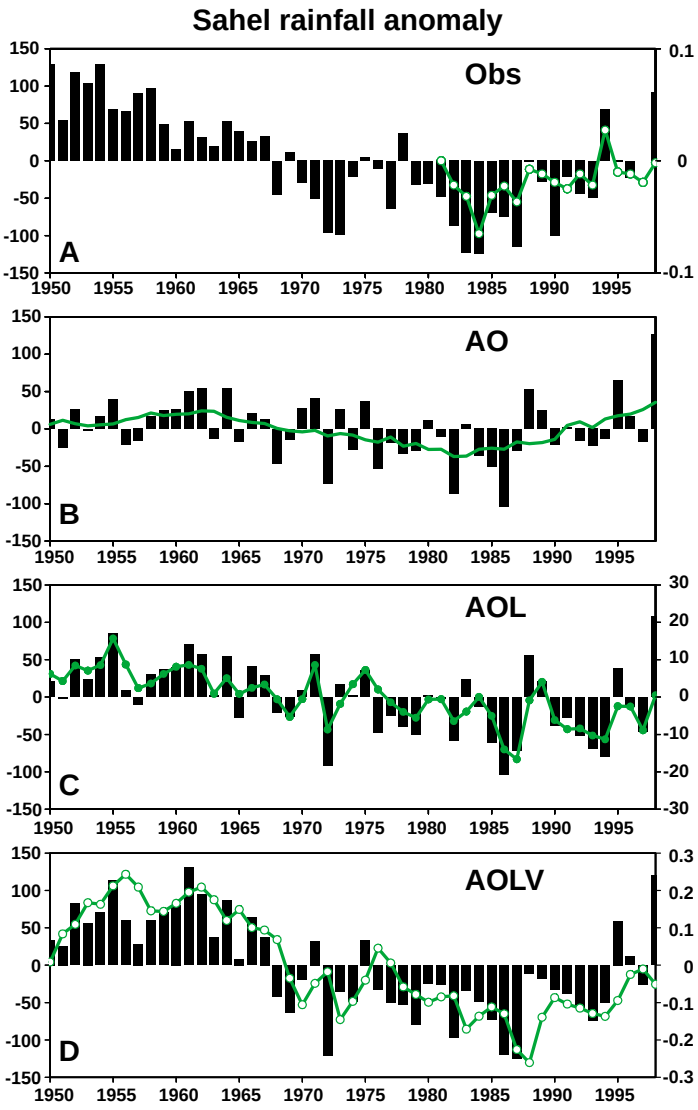


*Figure 1: Annual rainfall anomaly in mm $y^{-1}$ (vertical bars) over the West African Sahel ($13^0$N-$20^0$N, $15^0$W-$20^0$E) from 1950 to 1998: (A) observations from Hulme (1994); (B) model with non-interactive land-surface hydrology (fixed soil moisture) and non-interactive vegetation (SST in uence only, AO); smoothed line is a 9-year running mean showing the low-frequency variation; (C) model with interactive soil moisture but non-interactive vegetation (AOL); (D) model with interactive soil moisture and vegetation (AOLV). Also plotted (as connected circles; labeled on the right) are: (A) the Normalized Difference Vegetation Index (NDVI); (C) model simulated annual soil moisture anomaly (mm); (D) model simulated leaf area index (LAI) anomaly. All the anomalies are computed relative to the 1950-98 base period except that the NDVI data is relative to 1981.*

Compared to the observations in Fig. A, the AO run forced by interannually varying SST but with non-interactive soil moisture and vegetation (Fig. B) shows a weak interannual variation, and a much weaker interdecadal signal, although a drying trend can be seen from the 1950s to the 80s. The interactive soil moisture (Fig. C) appears to increase this interdecadal drying trend into the early 90s. The simulated soil moisture shows a high degree of correlation with precipitation. The amplitude of interannual variation is also larger in general, in agreement with other studies (Delworth and Manabe, 1993; Lau and Bua, 1998).

By allowing vegetation feedback to the atmosphere in AOLV, the decadal rainfall variability is enhanced significantly (Fig. D). The wet periods in the 1950s and the dry periods in the 1970s and the 80s stand out and are more like the observations. Compared to the non-interactive vegetation case, AOL, the interannual variability does not show enhancement. In some cases, the year to year change, such as from the dry 1987 to the relatively wet 1988, is actually reduced because the vegetation is still low from the previous drought due to its relatively slow response. This complicated, lagged relationship between vegetation and precipitation is also seen in the observations (Goward and Prince, 1995)), but our understanding of vegetation dynamics and the modelling tools available are not sufficient for a precise assessment of the reasons for this. Variation in rainfall drives a similar trend in vegetation through vegetation growth or loss (Fig. D). The vegetation lags slightly behind the rainfall and its variation is also smoother, although these tendencies are not very strong because the one-year vegetation time scale used in the model runs is comparable to the time resolution of the plot.

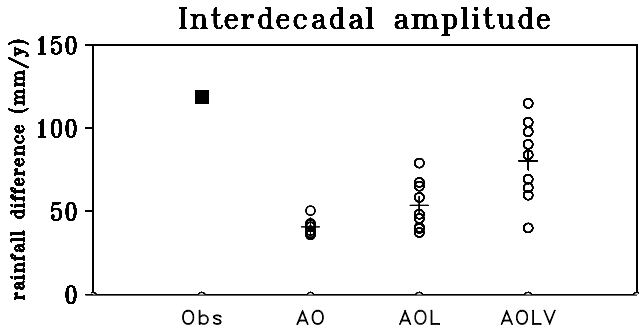


*Figure 2: Sahel rainfall difference between the period 1950-67 and the period 1968-87 for observations ( lled square) and three 9-member ensemble runs: AO-atmosphere model forced by observed SST, AOL-plus interactive soil moisture, AOLV- plus interactive vegetation. Open circles denote individual ensemble members, crosshairs denote ensemble means.*

To assess the internal climate variability in the model, additional three 9-member ensemble runs have been conducted corresponding to the cases above. The member runs in an ensemble differ only in their initial atmospheric and soil moisture conditions. We use the Sahel rainfall difference between the wet period 1950-67 and the dry period 1968-87 as an indicator of the amplitude of the interdecadal variation. Successive amplification of the decadal trend occurs with the inclusion of interactive soil moisture, and especially vegetation (Fig. 2). However, even the AOLV ensemble still tends to underestimate the observed decadal trend, and the case shown in Fig. D is on the high side of the distribution. Furthermore, the scatter among the ensemble members also increases when additional feedbacks are included. Interactive vegetation increases the variance even though vegetation initial conditions are identical in these runs.

The modelled Sahel rainfall in AOLV shows a correlation with observations of 0.67, a significant improvement from a 0.44 correlation in AOL. However, the year to year comparison with the observations is not as satisfactory. When we decompose the Sahel rainfall time series into low frequency (longer than 10 years) and high frequency (shorter than 10 years) components, the correlation with the observation is only 0.1 at high frequency and 0.94 at low frequency for the AOLV run. The discrepancy in the interannual simulation, both in our model and in the GCMs (Rowell, 1996; Sperber and Palmer, 1996), may have considerable contribution from chaotic atmospheric internal variability, for which model and observation can only be compared in a statistical sense.

While we focus on natural climate variations involving vegetation change, this does not exclude any role anthropogenic land-use change might play. It is possible that the anthropogenic factor might account for the remaining difference between the interactive vegetation run and observations in Fig. on decadal time scales, but because the vegetation feedback acts to amplify Sahel rainfall variability that originates from SST variations, significant effects can occur with relatively small vegetation changes. The change of surface albedo (not shown) on the interdecadal time scale is about 0.03 in the experiment with interactive vegetation (AOLV). This is a subtle change compared either to the albedo change values of 0.1 used in GCM desertification experiments (Xue and Shukla, 1993), or to what could be estimated from satellite observations in earlier decades. Current satellite systems will be capable of measuring this level of variation for future decadal fluctuations. The present results suggest the importance of such measurements, due to the role vegetation feedbacks can play ininterannual/interdecadal climate variability in climatically sensitive zones like the Sahel.

**References**


Charney, J.G., 1975: Dynamics of deserts and drought in the Sahel. *Quart. J. Roy. Meteor. Soc.*, **101**, 193-202.

Claussen, M. (1998): On multiple solutions of the atmosphere-vegetation system in present-day climate. *Global Change Biology*, **4**, 549-559.

Delworth, T., and S. Manabe, 1993: Climate variability and land-surface processes. *Advances in Water Resources*, **16**, 3-20.

Dirmeyer, P.A. and J. Shukla, 1996: The effect on regional and global climate of expansion of the world's deserts. *Quart. J. Roy. Meteor. Soc*., **122**, 451-482.

Folland, C.K., D.E. Parker, and T.N. Palmer, 1986: Sahel rainfall and worldwide sea temperatures 1901-85. *Nature*, **320**, 602-607.

Goward, S.N., and S. D. Prince, 1995: Transient effects of climate on vegetation dynamics—satellite observations. *J. Biogeogr*., **22**, 549-564.

Hulme, M., 1994: Validation of large-scale precipitation fields in General Circulation Models. In: Global precipitations and climate change, Eds.: M. Desbois and F. Desalmand, NATO ASI Series, Springer-Verlag, Berlin, 1994, pp. 466.

Koster, R.D., and J.J. Suarez, 1995: Relative contributions of land and ocean processes to precipitation variability. *J. Geophys. Res*., **100**, 13,775-13,790.

Lau, K.-M. and W. Bua, 1998: Mechanism of monsoon-Southern Oscillation coupling: insights from GCM experiments. *Climate Dynamics*, **14**, 759-780.

Neelin, J. D., and N. Zeng, 2000: The first quasi-equilibrium tropical circulation model-formulation. *J. Atmos. Sci*., **57**, 1741-1766.

Reynolds, R.W., and T. M. Smith, 1994: Improved Global Sea Surface Temperature Analyses Using Optimum Interpolation. *J. Climate*, **7**, 929-948.

Rowell, D.P., 1996: Further analysis of simulated interdecadal and interannual variability of summer rainfall over tropical north Africa. Reply to Y.C. Sud and W.K.-M. Lau. *Quart. J. Roy. Meteor. Soc*., **122**, 1007-1013.

Sellers, P.J., G.J. Collatz, D.A. Randall, D.A. Dazlich, C. Zhang, J.A. Berry, C.B. Field, G.D. Collelo, and L. Bounoua, 1996: A Revised Land Surface Parameterization (SiB2) for Atmospheric GCMS. Part I: Model Formulation. *J. Climate*, **9**, 676-705.

Semazzi, H F M, Burns, B, Lin, N H, and Schemm, J E, 1996, A GCM study of teleconnections between the continental climate of Africa and global sea surface temperature anomalies, *J. Climate*, **9**, 2480-2497.

Sperber, K.R., and Palmer, T.N. 1996: Interannual tropical rainfall variability in GCM simulations associated with AMIP. *J. Climate*, **9**, 2727-2749.

Xue, Y. and J. Shukla, 1993: The influence of land-surface properties on Sahel climate. Part I. Desertification. *J. Climate*, **5**, 2232-2245.

Zeng, N., J. D. Neelin, and C. Chou, 2000: The first quasi-equilibrium tropical circulation model-implementation and simulation. *J. Atmos. Sci.*, **57**, 1767-1796.

Zeng, N., J. D. Neelin, K.-M. Lau, and C. J. Tucker, 1999: Enhancement of interdecadal climate variability in the Sahel by vegetation interaction. *Science*, **286**, 1537-1540.